HIGH PERFORMANCE AND ULTRA HIGH PERFORMANCE CONCRETE WITH LOCALLY AVAILABLE MATERIALS FROM SASKATCHEWAN

A Thesis Submitted to the College of Graduate Studies and Research in Partial Fulfillment of the Requirements for the Degree of Master of Science in the Department of Civil, Geological and Environmental Engineering

University of Saskatchewan, Saskatoon, Canada

By

Zhe Song

Permission to Use

In presenting this thesis in partial fulfilment of the requirements for a Postgraduate degree from the University of Saskatchewan, I agree that the Libraries of this University may make it freely available for inspection. I further agree that permission for copying of this thesis in any manner, in whole or in part, for scholarly purposes may be granted by the professor or professors who supervised my thesis work or, in their absence, by the Head of the Department or the Dean of the College in which my thesis work was done. It is understood that any copying or publication or use of this thesis or parts thereof for financial gain shall not be allowed without my written permission. It is also understood that due recognition shall be given to me and to the University of Saskatchewan in any scholarly use which may be made of any material in my thesis.

Requests for permission to copy or to make other use of material in this thesis in whole or part should be addressed to:

Head of the Department of Civil, Geological and Environmental Engineering
University of Saskatchewan
57 Campus Drive
Saskatoon, Saskatchewan, Canada, S7N 5A9

Abstract

Reinforced concrete structures exhibit various durability problems, such as the corrosion of reinforcing steel, sulfate attack, etc., when exposed to harsh environments. This type of damage often leads to very serious technical and economic problems, such as a short lifetime of infrastructure and high costs associated with their long term maintenance and repair. High performance concrete (HPC) and ultra-high performance concrete (UHPC) could play key roles in solving or in mitigating these problems.

The main research goal of this thesis was to determine whether it is possible to produce high performance concrete (HPC), very-high performance concrete (VHPC) and ultra-high performance concrete (UHPC) that have unique combinations of strength, freeze-thaw durability and self-placeability at competitive costs using materials locally available in Saskatchewan.

To develop HPC and VHPC/UHPC, a statistical experimental design was used to perform experimental designs, analyze the fitting models and optimize multiple responses. The procedure was implemented using the Design-Expert Version 9.0 software.

Seven materials were researched in this project to make concrete, namely: water, cement, silica fume, silica flour, fine sand, steel fiber, and superplasticizer (SP). Four different properties were measured, including the compressive strength, splitting tensile strength, air content of hardened concrete and flow cone test.

After analyzing the results of these tests, it was found that the goal of developing a HPC material with the specified properties was achieved (flow cone spread value = 274 mm and, after 28 days, the obtained properties were: compressive strength = 82 MPa, splitting tensile strength = 23 MPa and air content = 6%.). The goal of making VHPC with the specified properties was obtained (flow cone spread value = 274 mm and, after 28 days, the obtained properties were: compressive strength

= 102.4 MPa and splitting tensile strength = 23 MPa) regardless of air content. Nevertheless, the results of the analysis clearly showed that it would be impossible to produce a UHPC with a 28 day compressive strength greater than 150 MPa using the mix ingredients and fabrication processes adopted in this study.

Acknowledgements

I would like to thank my supervisor, Professor Mohamed Boulfiza for his guidance, patience and support throughout this work without which it would have been impossible to complete this work. I would like to thank my temporary supervisor, Professor Bruce Sparling for his time and help in the last stage of my thesis. I would also like to thank Professor Leon Wegner and Professor Lisa Feldman, the members of my advisory committee, for their constructive criticism and valuable comments during this research.

I appreciate Gang Li for his help on the knowledge of concrete. I would like to thank Ming Zhu for his good suggestions and discussions on the concrete mixture making. I would like to thank my wife, Qiulan Zhu, my son, Ethan Song and my daughter Nina Song. Their love supported me throughout all my academic work. I would also like to thank all the others whom I may have missed, who have contributed to my research.

Table of Contents

List of Tables

List of Figures

List of Symbols and Abbreviations

Symbols

a	volume of air
b	a factor depending on the size and shape of pores
c	volume of cement
d_i	desirability functions for each response
D	overall desirability function
f_0'	intrinsic compressive strength at zero porosity
f_c	compressive strength of concrete cylinders at 28 days
f_c'	compressive strength of the material containing porosity p
H	the variation of the relative viscosity of a monodispersed suspension
k	a constant depending on the type of cement
K_g	a parameter depending on the aggregate type
l	length of concrete cylinder, mm
m	a factor depending on the bonding
n_C	the number of center runs in central composite design (CCD)
p	volume fraction porosity
P	maximum applied load, N
r_i	importance in desirability function
R_c	the strength of cement at 28 days
S	tensile strength of the material which contains a volume fraction porosity p

S_0	intrinsic tensile strength at zero porosity
T	splitting tensile strength, MPa
w	volume of water
x_i	independent variables in response function
X_{Actual}	independent variable in actual unit
X_{Coded}	independent variable in coded unit
X_{Hi}	independent variable at the high level in central composite design (CCD)
X_{low}	independent variable at the low level in central composite design (CCD)
y	response function
$\hat{Y}_{7\,Com.}$	compressive strength at 7 days
$\hat{Y}_{28\,Com.}$	compressive strength at 28 days
$\hat{Y}_{28\,splitting}$	splitting tensile strength at 28 days
$\hat{Y}_{air\,content}$	air content (in %) at 28 days
α	the axial distance in central composite design (CCD)
β_i	the components of the vector of unknown parameters in response function
ε_i	the components of the vector of unobserved disturbances
Φ_0	the volume of the liquid
Φ_i	the volume occupied by the i – class in a unit volume of the mix
η	viscosity of polydispersed suspensions
η_0	viscosity of the liquid

Abbreviations

ACI	American Concrete Institute
ACM	advanced cementitious material
ANOVA	analysis of variance
ASTM	American Society for Testing and Materials
CCD	central composite design
CPCA	Canadian Portland Cement Association
C-S-H	calcium silicate hydrate
DOE	design of experiments
df	degree of freedom
FRC	fiber reinforced concrete
GSD	grain size distribution
HPC	high performance concrete
HPFRCC	high performance fiber reinforced cement composite
NC	normal concrete
RC	reinforced concrete
R/D	research and development
RPC	reactive powder concrete
RSM	response surface method
SCM	supplementary cementitious materials
SP	superplasticizer
TS	tensile strength

UHPC	ultra high performance concrete
UHPFRC	ultra high performance fiber reinforced concrete
UTS	ultimate tensile strength
VHPC	very high performance concrete
W/C	water-cement ratio by mass
W/CM	water-cementitious material ratio by mass

1. Introduction

1.1 Background Information

Under relatively mild service environments, properly designed reinforced concrete (RC) structures show excellent performance in terms of durability and structural behavior. However, this is no longer the case when they are subjected to severe mechanical or aggressive environmental conditions. Premature deterioration of reinforced concrete structures, such as bridges, has been a persistent and frustrating problem to those responsible for maintaining those structures as well as to those using them. The deterioration typically consists of concrete delamination and spalling due to various mechanisms, including corrosion of embedded steel reinforcement, deicing salt–induced scaling, freezing and thawing cycles, or reactive aggregates. The rate of this deterioration is mainly dependent on the permeability of the concrete to moisture and aggressive substances. This decay shortens the lifetime of infrastructure and increases the costs of their long term maintenance. High performance concrete (HPC), very high performance concrete (VHPC) and ultra high performance concrete (UHPC) could play important roles in mitigating the effects of this problem and be utilized in the rehabilitation of structures (Graybeal 2014; Tayeh et al. 2013) because HPC and VHPC/UHPC have high strength and durability.

One way to minimize durability problems in RC structures is to make the concrete less permeable. This reduced permeability is usually achieved by using lower water–cementitious materials ratio (W/CM) and supplementary cementitious materials (SCMs), such as silica fume, ground granulated blast furnace slag, fly ash, or metakaolin. However, if the concrete cracks, aggressive agents may reach the interior of the concrete and the reinforcing steel regardless of how low the concrete permeability is. Hence, the attributes of any good method for the rehabilitation or strengthening of this kind of deteriorating structures should include reliability, effectiveness and economy.

The low porosity and permeability characteristics of HPC give it its enhanced durability properties, thus making it potentially suitable for the rehabilitation and retrofitting of reinforced concrete structures. The advantages of utilizing the technology of HPC in repairing works include (i) decreasing the working time needed for the rehabilitation works; and (ii) increasing the serviceability and durability to an extent where the repaired structures can meet the expected design life of the structures, with minor preventative measures.

The pursuit of high performance concrete goes back to 1960s and can be attributed to the "pioneering spirit" of a small group of designers and producers. The first application where high-strength concrete was used in significant quantities took place in the early 1960s (Freedman 1971).

UHPC, also known as reactive powder concrete (RPC), is a very high-strength, ductile material formulated by combining Portland cement, silica fume (or metakaolin), quartz flour, fine silica sand, high-range water reducer, water, and steel or organic fibers. The material provides compressive strengths up to 200 MPa (29000 psi) and flexural strengths up to 50 MPa (7000 psi). These materials are usually supplied in a three-component premix: powders (Portland cement, silica fume, metakaolin, quartz flour, and fine silica sand) pre-blended in bulk-bags; superplasticizers; and organic fibers. The ductile behavior of this material is a first for concrete, with the capacity to deform and support flexural and tensile loads, even after initial cracking. The use of this material can also simplify construction by the elimination of reinforcing steel. Therefore, it can help to solve the degradation of reinforced concrete infrastructures due to corrosion of the embedded reinforcing steel.

HPC and VHPC/UHPC can be used in many construction fields, such as repair materials (Muñoz and Ángel 2012), bridges (FHWA 2011; Graybeal 2005; Hartwell 2011; Shann 2012), pavements, tunnels, high buildings and so on. This is because both of these materials can offer

advantages over normal concrete, including greater strength, lower permeability and longer service life. HPC and VHPC/UHPC formulations that include Supplementary Cementing Materials (SCMs) derived from industrial waste products are also more environmentally sustainable.

It is also worth noting that the compressive strength is not the only criterion used to classify a material as HPC or VHPC/UHPC. For example, a normal strength concrete with very high durability and very low permeability is considered to have high-performance properties (Bickley and Fung 2006). Not all properties can be achieved at the same time. Therefore, HPC and VHPC/UHPC specifications are purpose oriented. In other words, they are designed according to the specific requirements of a specific project.

The first UHPC highway bridge in the U.S.A. is the Mars Hill bridge (Figure 1.1, left), Wapello County, Iowa, and the world's first Light Rail Transit (LRT) system to be constructed with UHPC is the Shawnessy LRT Station (Figure 1.1, right) in Calgary, Canada.

Figure 1.1. Mars Hill bridge in Wapello County, Iowa, the first UHPC bridge in U.S. (2006, left (FHWA 2013)) and Shawnessy LRT Station in Calgary, Canada, the world's first UHPC canopy (2004, right(Perry and Zakariasen 2004)).

Conventional Portland cement based concrete mixture proportioning methods, such as that described in ACI 211 (ACI Committee 211 1991), which is an absolute volume method, are not

suitable for making HPC and VHPC/UHPC. Several published documents contain the methods of proportioning HPC. (ACI Committee 363 1992) recommends that many trial batches should be cast before one could come up with an optimal mixture. (Kumar Mehta and Aitcin 1990) proposed a step by step method to make HPC. To keep the drying shrinkage and creep low, the cement paste-aggregate volume ratio is fixed at 35:65. The strength enhancement is achieved by reducing the water content with the help of a superlasticizing admixture. The LCPC (De Larrard 1990; De Larrard and Belloc 1997) method is based on Féret's formula (Féret 1892) and the Farris model which is a classical rheological model for the prediction of viscosity of polydispersed suspensions. The idea behind the Farris model is that each granular class has the same interaction with the mix of liquid plus finer classes as with a homogenous fluid. Then the different viscosities are computed by a recurrence method, starting with the finer class and adding the subsequent class at each step. However, it is important to point out that any mixture proportioning method only provides a starting mix design that will have to be modified to satisfy all the requirements. These methods are either too complicated or need too many trial batches. Simon used a statistical mix design method to optimize HPC (Simon et al. 1999; Simon 2003; Simon et al. 1997; Simon et al. 1999). This method reduces the number of trial batches dramatically and can also be applied with UHPC.

A single universal approach to concrete mixture design does not currently exist in the open literature. This is mainly because it would not achieve the goal of maximizing long-term durability given that the quality of local available materials used to produce the concrete strongly influence mixture properties and performance. Large variability within the concrete raw materials would typically influence the short-term properties and long-term durability of the concrete. Hence, without testing locally available materials, concrete mixtures cannot be truly optimized. It is worth

remembering that concrete mixtures are usually designed to achieve minimum specification requirements; optimization is rarely performed.

A great deal of research has been performed on properties of concrete containing one or more supplementary cementitious materials. The present study was conducted to propose a statistically based experimental methodology, the response surface method (RSM), for determining the best possible mixture proportions of HPC and VHPC/UHPC using locally available materials in Saskatchewan. This methodology relies on well-established methods of statistical design and analysis of experiments. It provides a framework for obtaining useful information about the impact of relatively large numbers of mix parameters on the performance of the produced concrete while testing a small number of the possible combinations of variables that describe the full test range.

Saskatchewan is rich in natural resources, such as oil sand, potash and uranium, and its economy, as well as its concrete infrastructure, will have to grow in the future. Given the known durability problems of reinforced concrete infrastructure, there is a stronger and stronger demand for materials that can guarantee superior performance in various service conditions. For example, there are many repairs of bridges in Saskatoon due to reinforcing problems. Hence, it is believed that through a wider use of HPC and VHPC/UHPC, Saskatchewan could mitigate a significant number of the durability problems experienced by RC structures. However, this has not been the case so far because the costs of HPC, as well as UHPC, are much higher than the average national costs in Canada. The main reason behind this difference in costs has to do with the fact that the locally available ingredients (especially the aggregates) have not been successfully used to produce this kind of material.

Eneray Sustainable Structures Inc. is a company based in Moose Jaw, Saskatchewan, that specializes in the use of high performance and ultra-high performance fiber reinforced concretes

to conduct projects with concrete that have not been easy, and sometimes even impossible using traditional technology. One major problem that the company faced is that the production of HPC, VHPC, and UHPC requires very high quality ingredients which often need to be purchased from other parts of North America, making it very hard for their products to be available in Saskatchewan at competitive costs. Recognizing that those costs would be significantly reduced if they could produce some of their products with materials that were locally available in Saskatchewan, they teamed up with the University of Saskatchewan in a collaborative research project to determine the possibility of producing HPC and UHPC using locally available materials.

1.2 Research Goal

To address the aforementioned research needs, the main goal of this research was to investigate the possibility of developing HPC and VHPC/UHPC using locally available materials in Saskatchewan while minimizing production costs. For this purpose, the following target properties were established:

a) High Performance Concrete (HPC)

- Compressive strength at 28 days: 70 to 100 MPa
- Splitting tensile strength at 28 days: over 20 MPa
- Air-content in hardened concrete: 4 to 6%
- Flow cone spread values: 270 to 330 mm

b) Very/Ultra High Performance Concrete (VHPC/UHPC)

- Compressive strength at 28 days: over 100 MPa for VHPC, over 150 MPa for UHPC
- Splitting tensile strength at 28 days: over 20 MPa
- Air-content in hardened concrete: 4 to 6%
- Flow cone spread values: 270 to 330 mm

The above goal was accomplished by fulfilling the following research objectives:

i) Review the literature concerning concrete mixture design and the RSM method;
ii) Investigate the influences of water-cement ratio (by mass), silica fume, silica flour, sand and steel fiber on concrete properties; and
iii) Determine the optimized designs that maximized 28 day compressive strength or had minimum cost.

1.3 Scope and Methodology

This research employed the RSM statistical method to design the experiments using locally available materials. The RSM is a well-established optimization method in the realm of concrete technology and other construction materials, as can be found in many documents in the published literature (report FHWA-RD-03-060, NCHRP report 566). Compressive strength, splitting tensile strength, air-content and flow cone tests were conducted.

The rationale for using the splitting tensile strength is because it provides an indirect measure of the tensile strength that is easier to carry out than the corresponding flexural test or direct tensile test. Typically, it provides estimates of tensile strength that are about 10–15% higher than those determined from a direct tensile strength. An air-content test of hardened concrete was used because concrete freeze-thaw durability can be estimated from it. The freeze-thaw resistance of hardened concrete is mainly affected by the capillary porosity and air content in the concrete mixture. These parameters can be controlled in the concrete production process.

2. Literature Review

Over the last few decades, concrete technology has experienced substantial advances, resulting in innovative uses and unconventional applications of concrete. The use of supplementary cementitious materials and additives has allowed the development of new generations of concrete with enhanced properties, which can be used in areas that were traditionally dominated by metals and ceramics. These new generations of concrete can be categorized based on compressive strength development. Categories include normal concrete (NC) (20 to 60 MPa), high performance concrete (HPC) (60 to 100 MPa), very high performance concrete (VHPC) (100 to <150 MPa), and ultra high performance concrete (UHPC) ($\geqslant$ 150 MPa), the last of which represents a major leap in concrete technology.

Up to the present time, progress in the field of HPC and VHPC/UHPC has been mostly the fruit of an empirical approach rather than a fundamental and scientific theory. Although it is not yet possible to explain every aspect in detail, it is still possible to explain the better performance of HPC and VHPC/UHPC on the basis of scientific principles. As a consequence, the selection of concrete-making materials and their mix proportions are no longer governed by pure empiricism.

Recent research (Vandamme and Ulm 2009) on the nanogranular origin of concrete creep makes it possible to slow the creep rate, increase concrete's durability and prolong the life of structures from a nanoscopic perspective. Creep is time dependent deformation under load that may cause cracks inside concrete which will decrease concrete's durability. That research was done through monitoring creep rates which are determined from packing density distributions of nanoscale particles. This is likely to lead to concrete structures capable of lasting hundreds of years rather than tens by slowing the creep rate, which in turn will bring enormous cost-savings.

From a fracture mechanics stand point, concrete can be considered as a non-homogeneous material composed of three separate phases:

1. the hydrated cement paste;
2. the transition zone between aggregate and hydrated cement paste;
3. the aggregates.

Concrete failure will always initiate in the weakest part of one of these three phases. Therefore, in order to increase the compressive strength of concrete, great care must be taken to strengthen all these three phases (Aïtcin and Mehta 1990).

UHPC is characterized by a very specific mixture design, which gives it a superior performance compared to that of conventional concrete. The main concept behind UHPC mixture is to minimize the number of defects, such as voids and internal micro-cracks, and to achieve a greater percentage of the ultimate load capacity of its components (Acker and Behloul 2004). This can be reached by enhancing homogeneity and increasing the packing density through optimization of the granular mixture and elimination of coarse aggregates (Holschemacher et al. 2005), producing a very dense and strong structure of the hydration products using very low water-cement ratio (W/C, about 0.20 to 0.25) (Schmidt and Fehling 2005).

The main characteristics of UHPC include very high compressive strength, a relatively high tensile strength and enhanced durability compared even with that of HPC. These outstanding properties make it a promising material for different concrete applications (Tang 2004). Recently, UHPC has been used for producing special pre-stressed and precast concrete members (Yazici 2007). Applications include the production of nuclear waste storage facilities (Yazıcı et al. 2009), precast pre-stressed concrete highway bridge girders (Garas 2009), pedestrian footbridges (Shah and Weiss 1998), inner wedges and the outer barrel of nonmetallic anchorage systems (Reda et al.

1999), rehabilitation and retrofitting of concrete structures (e.g. the waterproofing layer in bridge decks, a protection layer on crash barrier walls and strengthening of industrial floors) (Brühwiler and Denarié 2008). Although there are only a few applications for these concretes due to its high production cost, some economic advantages do exist in UHPC applications (Yazıcı et al. 2009). For instance, it is possible to reduce maintenance costs relative to steel and conventional concrete bridge girders (Garas 2009). Moreover, due to superior mechanical performance, the thickness of UHPC elements can be reduced, which results in materials and cost savings (Yazıcı et al. 2009) and increased useful space in buildings.

The targeted use of high performance materials like advanced cementitious materials (ACM) in new structures or conservation projects leads to enhanced performance and durability. ACM such as ultra high performance fibre reinforced concretes (UHPFRC) are promising in structures. UHPFRC belongs to the group of high performance fiber reinforced cement composites (HPFRCC). HPFRCC are fiber reinforced concretes (FRC) that exhibit strain-hardening under uniaxial tension. In addition, UHPFRC are characterized by a dense matrix and have consequently a very low permeability when compared to HPFRCC and normal strength concretes.

UHPFRC have exceptional material properties. However, their costs are significantly higher than those of normal strength concretes. Therefore, it is proposed to combine normal strength concretes and UHPFRC in composite structures in order to exploit the advantages of the two materials in an optimal way. UHPFRC are used in the parts of a structure subjected to attack by detrimental substances and/or where high strengths or stiffness are required. The other parts are made of normal strength reinforced concrete. This concept of composite “UHPFRC-concrete” structures can be applied to new structures and to conservation projects.

2.1 Improving the Strength of Hydrated Cement Paste

As a first approximation, hydrated cement paste (C-S-H) can be considered to be a single-phase material to which the fundamental principles governing the behavior of brittle solids can be applied. The porosity dependence of the tensile strength of a single-phase crystalline material can be expressed as

$$S = S_0 e^{-bp} \ , \tag{2.1}$$

where S is the tensile strength of the material which contains a volume fraction porosity p, S_0 is the intrinsic tensile strength at zero porosity, and b is a factor depending on the size and shape of pores (Aïtcin and Mehta 1990). Assuming the compressive strength to be several times the tensile strength, the Griffith tensile fracture theory and concepts of continuum mechanics can be used to predict that the compressive strength of a homogeneous ceramic is about eight times its tensile strength. This ratio between compressive and tensile strengths applies quite well to concrete.

From empirical compressive strength studies, many researchers have reported that the experimental data can be fitted to the equation (Aïtcin 2004)

$$f_c' = f_0'(1-p)^m \ , \tag{2.2}$$

where f_c' is the compressive strength of the material containing the volume fraction porosity p, f_0' is the intrinsic compressive strength at zero porosity, and m is a factor depending on the bonding in the solid, the shape and size of pores or flaws, grain size and the presence of impurities. In general, the compressive strength decreases with increasing pore size and increases with decreasing grain size. In conclusion, the strength can be improved by manipulating the microstructure of hydrated cement paste with parameters such as porosity, grain size and inhomogeneity .

2.2 Féret's Formula

In 1892, Féret found that the main factors affecting the porosity of the hydrated cement paste are the ratio of the volume of water available, the volume of the silicate phase to be hydrated and the amount of air entrapped during mixing. This relation can be expressed as:

$$f_c' = k\left(\frac{c}{c+w+a}\right)^2 \tag{2.3}$$

where f_c' is the compressive strength of the hydrated cement paste, *c*, *w*, and *a* are the volumes of cement, water and air, respectively, and *k* is a constant depending on the type of cement (Féret 1892). It can be rewritten as:

$$f_c' = k\left(\frac{1}{1+w/c+a/c}\right)^2 \tag{2.4}$$

The term a/c can be neglected because the volume of entrapped air is usually less than 1 or 2%. Therefore, Féret's formula can be rewritten as:

$$f_c' = k\left(\frac{1}{1+w/c}\right)^2 \tag{2.5}$$

From equation (2.5), it is very clear that in order to increase the compressive strength, the water-cement ratio must be reduced. Thus, from a theoretical point of view, when making HPC and VHPC/UHPC, one of the key factors is the maximum possible reduction of the water-cement or water-binder ratio. It is interesting to note that, when superplasticizers first started to be used as high-range water reducers, they were never used in such a way that the water-binder ratio would be reduced below the 'psychological barrier' of about 0.30. However, (Bache 1981) made a concrete with a compressive strength of 270 MPa using a very strong aggregate, a high dosage of superplasticizer (5 to 20 liters per cubic meter of concrete relative to 1 to 3 liters per cubic meter of concrete) and silica fume in a 0.16 water-binder ratio mixture.

2.3 Improving the Strength of the Transition Zone

Compared with the bulk cement paste, the microstructure of the transition zone is characterized by the presence of large pores and large crystalline hydration products. These characteristic microstructural inhomogeneities have serious implications for concrete strength. Microstructural differences between the hydrated cement paste and the transition zone play an important role in determining the strength characteristics of concrete. When concrete is subjected to a given stress, the cracks first begin to develop in the transition zone.

Generally speaking, in the 0.50 to 0.70 water-binder ratio range, it can be said that the inherently weak microstructure of the transition zone prevents concrete from behaving like a true composite material. As long as large pores and microcracks continue to be present in the transition zone, the strength of aggregate particles play no part in determining the strength of the concrete, since there is little effective stress transfer between the bulk cement paste and the aggregate. Reducing the water-binder ratio and using silica fume and silica flour tend to reduce the thickness and weakness of the transition zone (Aïtcin 2004).

2.4 Strong Aggregates

The selection of particularly strong aggregates is not necessary when producing normal concrete. When selecting aggregates for UHPC, the selection of very strong aggregates is necessary. This is because the hydrated cement paste and the transition zone can be made so strong in UHPC that the aggregates become the weakest component. The aggregates typically used to make high-performance concrete are natural sand and gravel or crushed aggregate (Aïtcin 1989). Detailed geological and petrographic studies can help in the search for a strong aggregate (Aïtcin and Mehta 1990).

2.5 Placing, Consolidation and Curing

Delays in delivery and placing must be eliminated to avoid early setting of the mix. For instance, the batch sizes should be reduced if placing procedures are slower than anticipated. Consolidation is very important in achieving the potential strengths of high-performance concrete (Kosmatka et al. 2003). Concrete must be vibrated as quickly as possible after placement in the forms. Curing of high-performance concrete is even more important than curing normal concrete. Providing adequate moisture and favorable temperature conditions is strongly recommended. Fog curing or evaporation retarders maybe used. Figure 2.1 shows the influences of different curing on compressive strength. It can be seen that the compressive strength for most samples treated with steam curing are higher than the strengths created by other methods. Therefore, steam treated curing is recommended. For this project, curing at room temperature (20°C) will be used as the basis for comparison of all trail mixes.

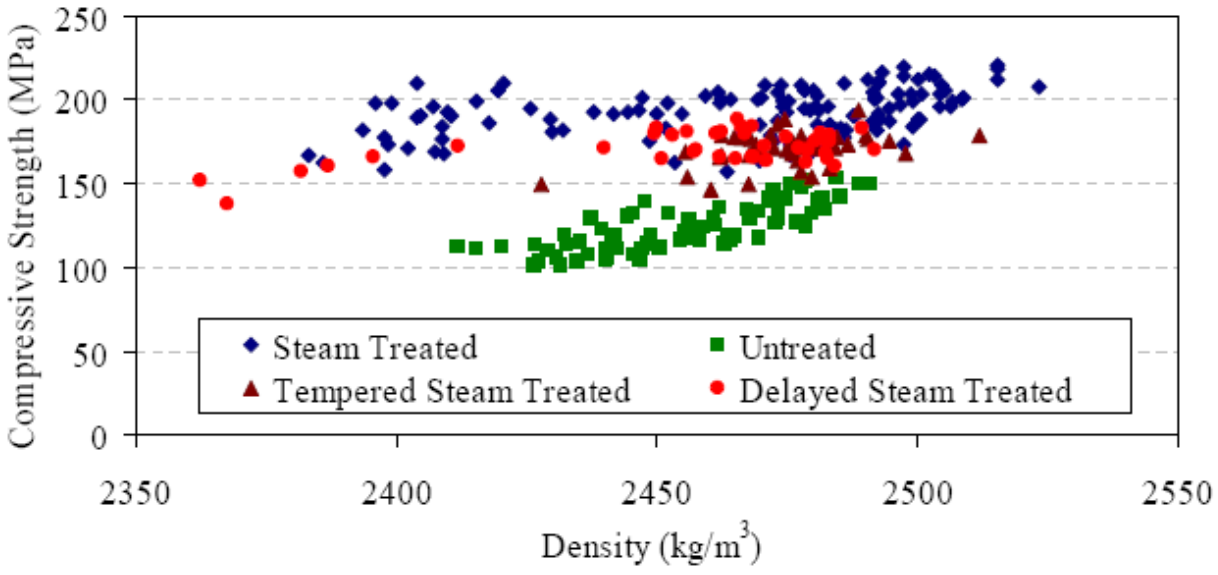

Figure 2.1. Compressive strength and density of control cylinders (FHWA 2006).

2.6 Mixture Proportioning

The goal of concrete mixture proportioning is to obtain an appropriate combination of concrete constituents which can be used to produce a concrete that satisfies various design specifications. These specifications can include: fresh concrete properties; required mechanical properties of hardened concrete such as strength together with durability provisions; and inclusion, exclusion, or limits on some ingredients. What is an appropriate concrete mix? Most people agree with the following qualities: good workability of freshly mixed concrete; acceptable properties of hardened concrete and lower cost.

The first thing required for mixture proportioning is to set up a list of specifications. Knowing concrete specifications and materials characteristics, mix design becomes feasible. With new components appearing such as silica fume, silica flour, superplasticizer and so on, the concrete mixture proportioning problem becomes more and more complicated compared to the normal concrete. The major concrete mixture proportioning methods will be reviewed in the following sections.

2.6.1 ACI 211.1 Standard Practice for Selecting Proportions for Normal, Heavy Weight, and Mass Concrete

Concrete mixtures can be proportioned by masses or volumes. The ACI 211.1 method (ACI Committee 211 1991) is based on an absolute volume approach. The absolute volume method provides a means for calculating the yield of concrete on the basis that the volume of compacted concrete equals the sum of the absolute volumes of the aggregates, cement and water. It is the most common concrete mix method in North America. The Canadian Portland Cement Association (CPCA) also adopted this method. Some background data should be gathered before starting the mixing process when using ACI 211.1. These data are:

i) Sieve analysis of fine and coarse aggregate; fineness modulus

ii) Dry-rodded unit weight of coarse aggregate

iii) Bulk specific gravity of materials

iv) Absorption capacity or free moisture in the aggregate

v) Variations in the approximate mixing water requirement with slump, air content, and grading of the available aggregates

vi) Relationship between strength and water-cement ratio

vii) Job specifications such as slump, strength at 28 day, maximum size of aggregate, air content and so on.

There are nine steps that need to be followed when using the ACI 211.1 method.

1. Slump selection.

   Different construction jobs need different slump values which can be found in a special table. Mixes with the stiffest possible consistency that can be easily placed and compacted without segregation should be used. The value of slump for pumping concrete is typically from 100 mm to 150 mm.

2. Choice of maximum size of aggregate.

   The maximum size that can be used depends on factors such as the size and shape of the concrete member to be cast, the amount and distribution of reinforcing steel in the member, and the thickness of slabs. For the same volume of coarse aggregate, using a large maximum size of a well-graded aggregate will produce less void space than a smaller size, thereby reducing the mortar requirement and cost.

3. Estimation of the mixing water content and air content.

Given a maximum size of aggregate and slump values, the amount of mixing water can be checked from a table (air-entrained or non-air-entrained table). The data in the table also show the approximate amount of air content needed for frost resistance.

4. Choice of water-cement or water-cementitious materials ratio.

   The water-cementitious materials ratio is simply the mass of water divided by the mass of cementitious material (portland cement, blended cement, fly ash, slag, silica fume, and natural pozzolans). This ratio must be the lowest value required to meet anticipated exposure conditions. When durability does not control, the water-cementitious materials ratio should be selected according to concrete compressive strength. These can be done from some tables in ACI 211.1.

5. Calculation of cement content.

   The required cement content is fixed by the above step 3 and step 4. It can be calculated from the estimated mixing water content divided by the water-cement ratio. In case the minimum amount of cement specification is given, the mixture must be based on whichever criterion leads to the larger amount of cement.

6. Estimation of coarse aggregate.

   The bulk volume of dry-rodded coarse aggregate per unit volume of concrete is determined from a table for a given fineness modulus of sand and a given maximum size of aggregate. For less workable concrete, such as required for concrete pavement construction, they may be increased by about 10%. For more workable concrete, such as may be required when placement is by pump, they may be reduced by up to 10%.

7. Estimation of fine aggregate content.

So far, all components of the concrete have been estimated except the fine aggregate. The amount of fine aggregate can be determined by calculating the difference between the total weight or volume and the sub total of all the other components.

8. Moisture adjustments.

   The mass of aggregates obtained in this procedure are for aggregate in a saturated surface-dry (SSD) state. To take into account the actual moisture of the aggregates, their mass, along with that of the mixing water, is adjusted.

9. Trial batches.

   The calculated mixture proportions should be checked by means of trial batches prepared and tested in accordance with ASTM C192. Sufficient water should be used to produce the specified slump regardless of the amount assumed in selecting the trial proportions.

2.6.2 ACI 363 Committee on high-strength concrete

High-strength concrete mix proportioning is more difficult than the design of normal concrete mixtures. Besides water, cement and aggregates, more ingredients are added into the concrete mixture such as specially selected pozzolanic and chemical admixtures (ACI Committee 363 1992). Moreover, the water-cement ratio is lower than that of normal concrete mixes. Usually, many trial batches are needed to obtain the optimal mix. There are 9 steps for this method as follows:

1. Choice of water-cement or water-cementitious ratio.

   When concrete includes pozzolanic materials, a water-cement plus pozzolan ratio by weight is considered in place of the traditional water-cement ratio by weight. Water-cementitious ratio for high-strength concrete typically have ranged from 0.27 to 0.50.

2. Choice of slump and specified strength.

   The value of slump is decided according to different applications. 0-50 mm slump concrete has been produced in precast operations. Specified slumps for cast-in-place concretes not containing high-range water reducers have ranged from 64 to 114 mm. Field-placed nonplasticized concrete have had measured slumps averaging as high as 121 mm. The high-range water reducer is proven to obtain lower water-cementitious ratio and higher slump. Strength can be found by using a figure representing the compressive strength as a function of water-cementitious ratio.

3. Estimation of cement content.

   The optimal cement quantity can be determined by trial batches.

4. Choice of the maximum size of the coarse aggregate.

   A table suggests maximum size of the coarse aggregate according to fineness modulus of sand.

5. Estimation of coarse aggregate volume.

   The same table from step 2 can be used to estimate the volume of coarse aggregate.

6. Estimation of free water and air content.

   Water can be computed from water-cementitious ratio.

7. First trial mixture with cement.

8. Other trial mixtures with partial cement replacements.

   Part of cement will be replaced with at least two different cementitious materials, such as fly ash, blast-furnace slag, silica fume and so on.

9. Trial batches.

The masses of aggregates and mixing water are adjusted for actual moisture conditions. The concretes made with no cement replacement and others using fly ash or blast-furnace flag are then adjusted to meet the desired physical and mechanical characteristics.

2.6.3 De Larrard method

The De Larrard method (De Larrard 1990) deals with the problem of proportioning high-strength concrete mixtures. It is based on two semi-empirical mix-design tools: Féret's formula is used to predict the strength of concrete from a limited number of mix-design parameters, while the viscosity of the mix, which is closely related to workability, is estimated using a rheological model known as the Farris model. Two assumptions are made when using these tools: (1) the strength of a concrete is mainly controlled by the nature of the binding paste and (2) the workability of a concrete, whose strength grading is fixed, is to be determined by a combination of the binding paste concentration and paste fluidity.

De Larrard proposed equation (2.6) for the 28 day compressive strength, which is actually an extension of the original Féret's formula (Féret 1892):

$$f_c = \frac{K_g \times R_c}{\left[1 + \frac{3.1 w/c}{1.4 - 0.4\exp(-11 s/c)}\right]} \tag{2.6}$$

where

f_c = the compressive strength of concrete cylinders at 28 day,

w, c, s = the mass of water, cement, and condensed silica fume for a unit volume of fresh concrete, respectively,

K_g = a parameter depending on the aggregate type (a value of 4.91 applies to common river gravels),

R_c = the strength of cement at 28 day (e.g., the strength of ISO mortar containing three parts of sand for each part of cement and one-half part of water).

The Farris model can be expressed as:

$$\eta = \eta_0 H\left(\frac{\Phi_1}{\Phi_1 + .. \Phi_n + \Phi_0}\right) H\left(\frac{\Phi_2}{\Phi_2 + .. \Phi_n + \Phi_0}\right) \ldots H\left(\frac{\Phi_n}{\Phi_n + \Phi_0}\right) \tag{2.7}$$

where

Φ_i = the volume occupied by the $i-$ class (*i*th class in a mix containing n classes of monodispersed grains) in a unit volume of the mix,

Φ_0 = The volume of the liquid,

η_0 = Viscosity of the liquid,

H = The variation of the relative viscosity of a monodispersed suspension, as a function of its solid concentration.

Farris' model is a classical rheological model for the prediction of viscosity of polydispersed suspensions. The idea behind it is that each granular class has the same interaction with the mix of liquid plus finer classes as with a homogenous fluid. Many model materials tests need to be performed: grout is used for rheological tests and mortar is used for mechanical tests. Eight steps are needed in this method (De Larrard 1990), as follows:

1. Proportioning a control concrete containing a large amount of superplasticizer together with the amount of cement corresponding to the least water demand. The water content of this control concrete must be adjusted to obtain the right workability.
2. Measuring the flow time of the paste of the control concrete. The W/C ratio of this paste must be computed taking the moisture in aggregates into account: when fresh concrete is flowing, a part of the mixing water is absorbed by the granular materials and does not lubricate the mix.
3. Arbitrarily choosing the percentages of binders for several grouts.
4. For each grout, adding a small amount of superplasticizer, adjusting the water content to obtain a sticky paste. With the W/C ratio temporarily fixed, adding superplasticizer until the flowing time does not decrease anymore. This amount of superplasticizer represents the saturation value and remains fixed.
5. Adjusting the water content to obtain the same flowing time as the control grout. Therefore, the W/C ratio is fixed for each paste.
6. Measuring the change in the flow characteristics with time for the duration of high strength concrete (HSC) casting. If the flow time increase too much, a retarding agent must be added to maintain it under the reference value.
7. Predicting the strength of HSC made up with the different grouts. This can be done by the proposed Féret's formula. A better precision will be achieved with compression tests performed on the different mortars.
8. Manufacturing the HSC using the same granular materials and the same volume of paste as for the control concrete, but modified with additional water for aggregate moistening.

2.6.4 Mehta and Aitcin simplified method

Mehta and Aïtcin proposed a simplified mixture proportioning procedure that is applicable for normal weight concrete with strength values of between 60 and 120 MPa (Mehta and Aïtcin 1990). It assumes that non-air-entrained high-performance concrete has an entrapped air volume of 2% which can be increased to 5-6% when concrete is air-entrained.

The steps for this method are as follows:

1. Strength determination.

   The 60 to 120 MPa strength range is arbitrarily divided into five strength grades, namely 65, 75, 90, 105, and 120 MPa, average strength of standard cured concrete specimens at 28 day.

2. Choice of water content.

   A table is provided to estimate the maximum content of mixing water from a given strength.

3. Volume fraction of cement paste components.

   The volume of binder can be calculated by subtracting the volume of aggregates and that of air (entrapped or entrained).

4. Estimation of aggregate content.

   The total aggregate volume is equal to 65% of the concrete volume. For strength grades 65, 75, 90, 105 and 120 MPa, the volume ratios of fine to coarse aggregates are suggested to be 2.00:3.00, 1.95:3.05, 1.90:3.10, 1.85:3.15, and 1.80:3.20, respectively.

5. Batch weight calculation.

   The weights per unit volume of concrete can be calculated using the volume fractions of the concrete and specified gravity values of each of the concrete constituents.

Usually, the specific gravity values are 3.14, 2.5, 2.9 and 2.1 for Portland cement, Type C fly ash, blast-furnace slag and silica fume, respectively.

6. Superplasticizer Dosage.

   For the first trial mixture, the use of 1% superplasticizer by weight of binder is suggested. The mass and volume of a superplasticizer solution are then calculated taking into account the percentage of solids in the solution and the specific gravity of the superplasticizer.

7. Moisture adjustment.

   The volume of the water included in the superplasticizer is calculated and subtracted from the amount of initial mixing water.

8. Trial batch correction.

   The first batch has to be modified to meet the desired workability and strength criteria because of many assumptions. A lot of trial batches are needed due to many parameters involved.

2.7 Response Surface Methods (RSM)

As the previous sections show, classically, research and development (R/D) work in concrete technology involves a fair amount of trial and error experimentation, empirical techniques which often lead to poor understanding of concrete and a low chance of finding an optimum solution. The most common test plan is to evaluate the effect of one parameter on product performance. This is what is typically called a one factor experiment. This type of experiment evaluates the effect of one parameter while holding everything else constant. The simplest case of testing the effect of one parameter on performance would be to run a test at two different conditions of that parameter. The methodology for this approach consists of the following steps:

1. Isolate what is believed to be the most important factor;
2. Investigate this factor by itself while ignoring all others;
3. Make recommendations on changes to this crucial factor;
4. Move on to the next factor and repeat.

The one factor experiment approach has several drawbacks: it takes much longer and uses up more resources than other available approaches, the optimum combination of all variables may never be found, and the interaction between factors may never be revealed. The statistical methods of experimental design provide much better tools for coming up with set-ups of experiments to obtaining the most information on all the variables in the shortest period of time. In contrast to one factor experiment designs, factorial designs involve simultaneous optimization of many factors at once and, hence, offer a simple, efficient, and statistically valid method for optimizing mixture proportioning. The theory of Experimental Design began with Ronald A. Fisher (1880-1962) in England in the 1920's, when he wanted to find out how much rain, sunshine, fertilizer, and water would produce the best crop (Box et al. 2005). The design of experiments (DOE) can be defined as a statistical technique that studies the effects of multiple variables simultaneously, and determines the factor combination for optimum result.

Statistical experiment design methods are very mature and rigorous techniques for optimizing products that are combinations of several components, such as concrete, to meet a number of performance criteria simultaneously, at minimum cost. For concrete, these performance criteria could include mechanical properties such as strength, creep, and shrinkage; fresh concrete properties such as yield stress, viscosity, setting time, and temperature; and durability-related properties such as permeability, frost resistance, or abrasion. In other words, they provide a

systematic approach for setting up of experiments to obtain the most information out of all the variables in the shortest period of time.

Response surface methodology (RSM) which dates back to the 1950's is basically a set of statistical methods that can be used to optimize products in situations where several factors influence one or more performance characteristics (Box and Wilson 1951). Typically, RSM involves experimental design, regression models, and optimization. Many parameters will be considered in the current mixture proportioning study. Therefore, many experiments would be needed if traditional mix design approaches are used. Given the limited time and cost constraints, only a limited number of tests can be conducted. RSM is particularly useful for the modeling and analysis of problems in which a response of interest is influenced by several parameters. For example, a chemist wants to find the amount of catalyst (x_1) and the levels of temperature (x_2) that maximize the yield (y) of a process. In this case, the yield (y) is the response variable, and it is a function of catalyst and temperature. It can be expressed as

$$y = f(x_1 + x_2) + \varepsilon \tag{2.8}$$

where ε represents the noise or error observed in the response. The variables x_1 and x_2 are independent variables. If we denote the expected response by $E(\mathrm{y}) = f(x_1 + x_2) = \eta$, then the surface

$$\eta = f(x_1 + x_2) \tag{2.9}$$

is called a response surface. The response surface can be illustrated graphically as shown in Figure 2.2.

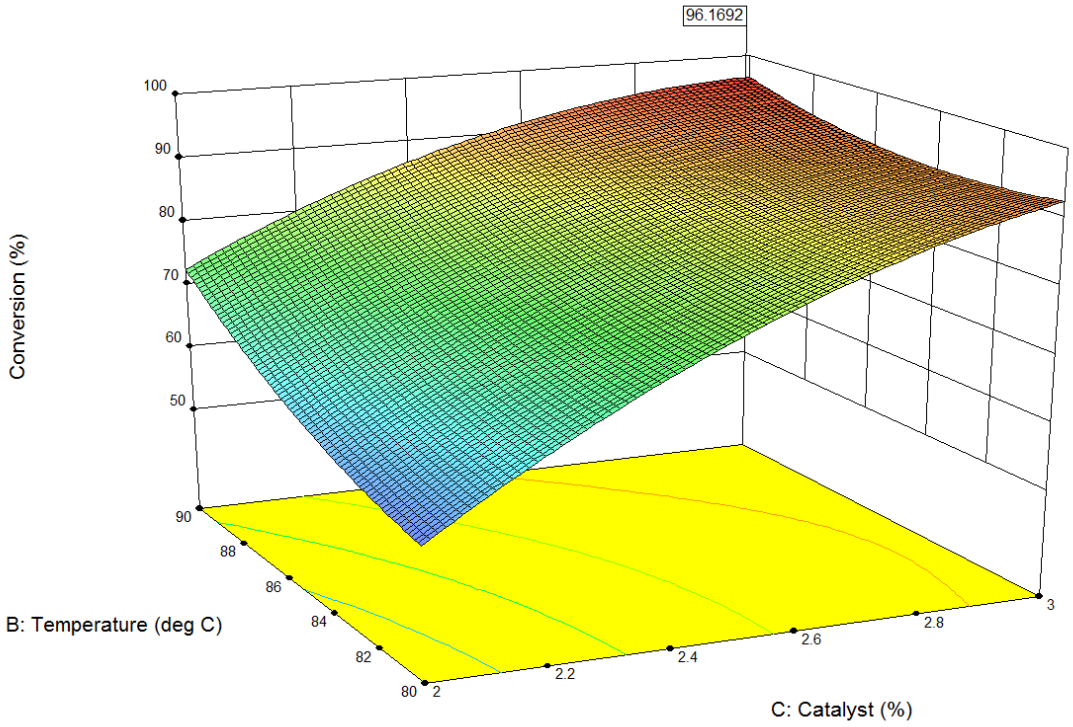

Figure 2.2. A three-dimensional response surface with a contour plot.

Clearly, if the graphical display in Figure 2.2 can be constructed, the optimization of this process would be very straightforward by inspecting the plot. Unfortunately, in most practical problems, the true response function is unknown. Thus, the first step in RSM is to find a suitable approximation for the true functional relationship between *y* and the set of independent variables. Low-order polynomials are typically employed when approximating the response function. A first-order function is given by

$$y = \beta_0 + \beta_1 x_1 + \beta_2 x_2 + \cdots + \beta_k x_k + \varepsilon \tag{2.10}$$

This representation is used when the response can be well modeled by a linear function. In the presence of some curvature in the system, then a polynomial of higher degree must be used. Usually, a second-order model is used.

$$y = \beta_0 + \sum_{i=1}^{k} \beta_i x_i + \sum_{i=1}^{k} \beta_{ii} x_i^2 + \sum_{i<j} \sum \beta_{ij} x_i x_j + \varepsilon \tag{2.11}$$

where

$$\sum_{i=1}^{k} \beta_{ii} x_i^2 \tag{2.12}$$

is called quadratic term and

$$\sum_{i<j} \sum \beta_{ij} x_i x_j \tag{2.13}$$

is called 2 factor interaction (2FI) term. The first order and second order functions are two important models which almost all RSM problems use. In order to get the most efficient result in the approximation of polynomials, the proper experimental design must be used to collect data. The Least Square technique is used after the data is collected. The response surface analysis is performed by using the fitted surface. Designs for fitting the response surface are called response surface designs.

Models that have interaction terms or quadratic terms can still be analyzed by multiple linear regression method. For example, using the model:

$$y = \beta_0 + \beta_1 x_1 + \beta_2 x_2 + \beta_{11} x_1^2 + \beta_{22} x_2^2 + \beta_{12} x_1 x_2 + \varepsilon \ , \tag{2.14}$$

and letting $x_3 = x_1^2, x_4 = x_2^2, x_5 = x_1 x_2, \beta_3 = \beta_{11}, \beta_4 = \beta_{22},$ and $\beta_5 = \beta_{12}$, then *y* becomes

$$y = \beta_0 + \beta_1 x_1 + \beta_2 x_2 + \beta_3 x_3 + \beta_4 x_4 + \beta_5 x_5 + \varepsilon \tag{2.15}$$

which is a linear model.

The main idea of RSM is to use a sequence of designed experiments to obtain an optimal response (Box et al. 2005; Lawler et al. 2007; Simon 2003), as shown in Figure 2.3. Therefore, the final goal of RSM is to find the region where the optimal response occurs. Though RSM is only an approximation, it still can be used because it is easy to estimate and apply, even

when little is known about the process. The main steps include experiment design, modeling, and optimization.

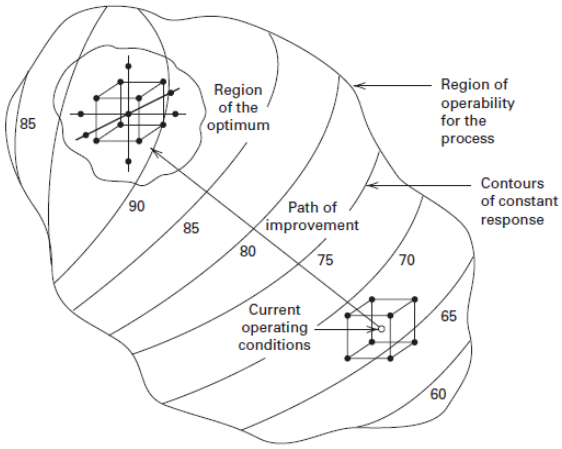

Figure 2.3. The sequential procedure of RSM (Montgomery 2013).

2.7.1 Analysis of First-Order Model

To estimate the coefficients of a linear model (equation (2.10)) with k independent variables, $n > k$ experimental runs are needed. The data of corresponding responses is

Table 2.1. Data for Multiple Linear Regression

y	x_1	x_2	$\cdots$	x_k
y_1	x_{11}	x_{12}	$\cdots$	x_{1k}
y_2	x_{21}	x_{22}	$\cdots$	x_{2k}
M	M	M	M	M
y_n	x_{n1}	x_{n2}	$\cdots$	x_{nk}

where x_{ij} denotes the ith observation of variable x_j . The coefficients can be determined by a mathematical model, regression model. This can be expressed as

$$\begin{aligned} y_i &= \beta_0 + \beta_1 x_{i1} + \beta_2 x_{i2} + \mathrm{L} \ + \beta_k x_{ik} + \varepsilon_i \\ &= \beta_0 + \sum_{j=1}^{k} \beta_j x_{ij} + \varepsilon_i, \qquad i = 1, 2, ..., n \end{aligned} \tag{2.16}$$

Here β_i are the components of the vector of unknown parameters and ε_i are the components of the vector of unobserved disturbances. The above formula can be re-written in matrix notation as

$$\mathbf{y} = \mathbf{X}\boldsymbol{\beta} + \boldsymbol{\varepsilon} \tag{2.17}$$

where

$$\mathbf{y} = \begin{bmatrix} y_1 \\ y_2 \\ \mathrm{M} \\ y_n \end{bmatrix}, \quad \mathbf{X} = \begin{bmatrix} 1 & x_{11} & x_{12} & \mathrm{L} & x_{1k} \\ 1 & x_{21} & x_{22} & \mathrm{L} & x_{2k} \\ \mathrm{M} & \mathrm{M} & \mathrm{M} & \mathrm{M} & \mathrm{M} \\ 1 & x_{n1} & x_{n2} & \mathrm{L} & x_{nk} \end{bmatrix}, \quad \boldsymbol{\beta} = \begin{bmatrix} \beta_0 \\ \beta_1 \\ \mathrm{M} \\ \beta_k \end{bmatrix}, \quad \text{and} \quad \boldsymbol{\varepsilon} = \begin{bmatrix} \varepsilon_1 \\ \varepsilon_2 \\ \mathrm{M} \\ \varepsilon_n \end{bmatrix} \tag{2.18}$$

Through the analysis of least square method, the unique solution of $\boldsymbol{\beta}$ can be shown to be given by

$$\hat{\boldsymbol{\beta}} = (\mathbf{X}'\mathbf{X})^{-1}\mathbf{X}'\mathbf{y} \tag{2.19}$$

where $\mathbf{X}'$ denotes the transpose of matrix $\mathbf{X}$ and $(\mathbf{X}'\mathbf{X})^{-1}$ the inverse of matrix $\mathbf{X}'\mathbf{X}$. Then the fitted regression model is

$$\hat{\mathbf{y}} = \mathbf{X}\hat{\boldsymbol{\beta}} \ . \tag{2.20}$$

It can also be represented in scalar notation as

$$\hat{y}_i = \hat{\beta}_0 + \sum_{j=1}^{k} \hat{\beta}_j x_{ij}, \quad i = 1, 2, ..., n \ . \tag{2.21}$$

The residual is defined as the difference between the actual observation y_i and the corresponding fitted value $\hat{y}_i$, i.e.

$$e_i = y_i - \hat{y}_i \ . \tag{2.22}$$

Then the $(n \times 1)$ vector of residuals can be expressed as:

$$\mathbf{e} = \mathbf{y} - \hat{\mathbf{y}} = \mathbf{y} - \mathbf{X}\hat{\boldsymbol{\beta}} . \tag{2.23}$$

The sum of squares of residuals, SS_E, can be calculated as:

$$SS_E = \sum_{i=1}^{n} (y_i - \hat{y}_i)^2 = \sum_{i=1}^{n} e_i^2 = \mathbf{e'e} \tag{2.24}$$

where $\mathbf{e'}$ is the transpose of matrix **e**.

Substituting equation (2.21), SS_E can be re-calculated as:

$$\begin{aligned} SS_E &= (\mathbf{y} - \mathbf{X}\hat{\boldsymbol{\beta}})'(\mathbf{y} - \mathbf{X}\hat{\boldsymbol{\beta}}) \\ &= \mathbf{y}'\mathbf{y} - \hat{\boldsymbol{\beta}}'\mathbf{X}'\mathbf{y} - \mathbf{y}'\mathbf{X}\hat{\boldsymbol{\beta}} + \hat{\boldsymbol{\beta}}'\mathbf{X}'\mathbf{X}\hat{\boldsymbol{\beta}} \\ &= \mathbf{y}'\mathbf{y} - 2\hat{\boldsymbol{\beta}}'\mathbf{X}'\mathbf{y} + \hat{\boldsymbol{\beta}}'\mathbf{X}'\mathbf{X}\hat{\boldsymbol{\beta}} \end{aligned} . \tag{2.25}$$

Because

$$\mathbf{X}'\mathbf{X}\hat{\boldsymbol{\beta}} = \mathbf{X}'\mathbf{y} , \tag{2.26}$$

the final sum of squares of residuals becomes:

$$SS_E = \mathbf{y}'\mathbf{y} - \hat{\boldsymbol{\beta}}'\mathbf{X}'\mathbf{y} \tag{2.27}$$

where $\mathbf{y}'$ is the transpose of **y**.

The total sum of squares is defined as:

$$SS_T = \sum_{i=1}^{n} (y_i - \bar{y})^2 \tag{2.28}$$

where $\bar{y}$ is average of *y* with

$$\bar{y} = \frac{1}{n}\sum_{i=1}^{n} y_i . \tag{2.29}$$

The total sum of squares can be derived as:

$$
\begin{aligned}
SS_T &= \sum_{i=1}^{n}(y_i - \bar{y})^2 \\
&= \sum_{i=1}^{n}(y_i^2 - 2y_i\bar{y} + \bar{y}^2) \\
&= \sum_{i=1}^{n}(y_i^2 - 2y_i(\frac{1}{n}\sum_{i=1}^{n}y_i) + (\frac{1}{n}\sum_{i=1}^{n}y_i)^2) \\
&= \sum_{i=1}^{n}y_i^2 - 2\frac{1}{n}(\sum_{i=1}^{n}y_i)^2 + \frac{1}{n}(\sum_{i=1}^{n}y_i)^2) \\
&= \sum_{i=1}^{n}y_i^2 - 2\frac{1}{n}(\sum_{i=1}^{n}y_i)^2 + \frac{1}{n}(\sum_{i=1}^{n}y_i)^2) \\
&= \sum_{i=1}^{n}y_i^2 - \frac{1}{n}(\sum_{i=1}^{n}y_i)^2
\end{aligned}
\tag{2.30}
$$

The final total sum of squares is:

$$
SS_T = \mathbf{y}'\mathbf{y} - \frac{1}{n}(\sum_{i=1}^{n}y_i)^2 \tag{2.31}
$$

The regression sum of squares is defined as:

$$
\begin{aligned}
SS_R &= SS_T - SS_E \\
&= \mathbf{y}'\mathbf{y} - \frac{1}{n}(\sum_{i=1}^{n}y_i)^2 - (\mathbf{y}'\mathbf{y} - \hat{\boldsymbol{\beta}}'\mathbf{X}'\mathbf{y}) \\
&= \hat{\boldsymbol{\beta}}'\mathbf{X}'\mathbf{y} - -\frac{1}{n}(\sum_{i=1}^{n}y_i)^2
\end{aligned}
\tag{2.32}
$$

2.7.2 Experimental Design For Fitting a First-Order Model

Factorial designs are most efficient when the experiments at hand involve the study of the effects of two or more factors. They are designed to obtain maximum information from the least amount of experimental runs. In a full factorial design, all possible combinations of the levels of the factors are investigated in each replication. If there are a levels of factor A, and b levels of factor B, then each replicate contains all ab treatment combinations. Obviously, the number of experimental runs required for a full factorial design depends on the number of factors being

studied and is equal to 2x, where x represents the number of factors. For example, a full factorial design for three factors would require 2^3 or eight runs. The advantage of this design is that maximum information regarding the factors is obtained. However, the main disadvantage of this design is that as the number of factors increases, the number of experiments required increases very rapidly. As a consequence, this type of design becomes impractical when more than four factors need to be evaluated. For example, a design for four factors requires only sixteen runs, whereas a full factorial for five factors requires a total of thirty-two runs.

When more than four factors need to be considered, other factorial designs with a reduced number of runs, such as fractional factorial designs are preferred. The most common form of factorial designs involves studying each factor at two levels. Although possible, designs with more than two levels are complicated, and hence, less commonly used.

In some experiments we may find that the difference in response between the levels of one factor is not the same at all levels of the other factors. When this occurs, there is an interaction between the factors. A factorial design is necessary when interactions may be present to avoid misleading conclusions. Factorial designs allow the effects of a factor to be estimated at several levels of the other factors, yielding conclusions that are valid over a range of experimental conditions.

For first order problems, as described in the previous section, there is a unique design that minimizes the variance of the regression coefficients $\left\{\hat{\beta}_i\right\}$.

2.7.2.1 The 2^k Factorial Design

In a 2^k factorial design, each control variable is measured at two levels, i.e. low and high, which can be coded to take the values -1 and 1. Here *k* is the number of independent variables.

The statistical model for this design includes k main effects, $\binom{k}{2}$ two-factor interactions, $\binom{k}{3}$ three-factor interactions, …, and $\binom{k}{k}=1$ k-factor interaction. Thus, the model would contain 2^k-1 effects. For example, the standard order for a 2^3 design is (1), a, b, ab, c, ac, bc, abc.

To analyse a 2^k design, several procedures should be followed:

1. Estimate factor effects through computing contrast.
2. Obtain initial model.
3. Perform analysis of variables (ANOVA).
4. Refine model.
5. Analyze residuals.
6. Check and interpret results.

The effect here is defined as the difference in the means between the high and the low level of a factor or variable. It is notated as corresponding capital letter(s). The contrast is defined as the sum of each group mean multiplied by a coefficient for each group where coefficients add up to zero. The contrast can be calculated by using the equation (2.20):

$$Contrast_{AB\cdots K}=(a\pm1)(b\pm1)\cdots(k\pm1) \tag{2.33}$$

A negative sign "$-$" will be taken if the factor is included in the effect. Otherwise, a positive sign "$+$" will be kept if the factor is not included in the effect. For example, in a 2^3 factorial design, the contrast for AC would be

$$\begin{aligned} Contrast_{AC} &= (a-1)(b+1)(c-1) \\ &= abc+ac-bc-c-ab-a+b+(1) \end{aligned} \tag{2.34}$$

Then, the effects and sum of squares can be calculated according to

$$AB\cdots K = \frac{2}{n2^k}\left(Contrast_{AB\cdots K}\right) \tag{2.35}$$

and

$$SS_{AB\cdots K} = \frac{1}{n2^k}\left(Contrast_{AB\cdots K}\right)^2 \tag{2.36}$$

respectively, where n represents the number of replicates.

2.7.2.2 The One-Half Fraction of 2^k Factorial Design

With the increasing of k values, the number of experiments will go up rapidly. For $k=6$, $k=7$, $k=8$, $k=9$, and $k=10$, there are 64, 128, 256, 512, and 1024 experiments respectively. Most experimenters cannot afford these larger numbers due to limited time, cost and other resources. Among these experiments, only some are actually needed to estimate the main effects and some are used to estimate two-factor interactions; the rest of them are for higher interactions. For example, in a 2^6 design, there are 64 runs where only 6 of 63 degrees of freedom are for the main effects while 15 degrees of freedom are for two-factor interactions. The remaining 42 degrees of freedom are used to estimate three-factor or higher interactions. If certain higher interactions can be negligible, then only a fraction of the complete factorial experiment is needed to estimate the main effects and low-order interactions. This will decrease the number of experiments dramatically.

In a 2^3 design, there are eight treatment combinations. If four of them are picked to estimate the model, this design is called 2^{3-1} design or a one-half fraction of a 2^3 design.

2.7.2.3 The Simplex Design

The simplex design is an orthogonal design consisting of $N = k + 1$ design points, where k is the number of variables in the first-order model. These design points are located at the vertices of a *k*-dimensional regular-sided figure, or a simplex, and characterized by the fact that the angle θ which any two points make with the origin is such that $\cos\theta = -\frac{1}{N-1} = -\frac{1}{k}$ (Box 1952). For $k = 2$, the $\cos\theta = -\frac{1}{k} = -\frac{1}{2}$, then $\theta = 120°$. The simplex design points are the vertices of an equilateral triangle. Hence, for $k = 3$, the design points are the vertices of a tetrahedron which can be illustrated as in Figure 2.4.

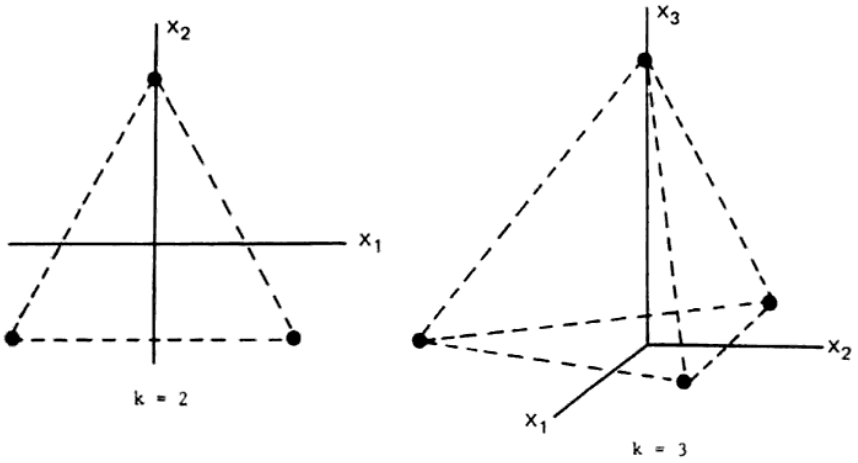

Figure 2.4. The simplex design in $k = 2$ and $k = 3$ dimensions.

2.7.3 Analysis of the Second-Order Model

When there is a curvature in the response surface, the first-order model is not suitable. In this case, the second-order model should be employed to analyze the problem. The second-order model would be the following form

$$y = \beta_0 + \sum_{i=1}^{k} \beta_i x_i + \sum_{i=1}^{k} \beta_{ii} x_i^2 + \sum_{i<j} \sum \beta_{ij} x_i x_j + \varepsilon \qquad (2.37)$$

If an experimenter wants to find the optimal conditions for a response with maximum or minimum values, the first step is to find the stationary points and then characterize them. The point for which the response is optimized is the point at which all the partial derivatives of y with respect to x_i are equal to zero as shown in equation (2.25).

$$\frac{\partial \hat{y}}{\partial x_1} = \frac{\partial \hat{y}}{\partial x_2} = \cdots = \frac{\partial \hat{y}}{\partial x_k} = 0 \tag{2.38}$$

The stationary point may be a point of maximum response, minimum response or a saddle point. These three different conditions are shown in the following a, b and c in Figure 2.5, respectively.

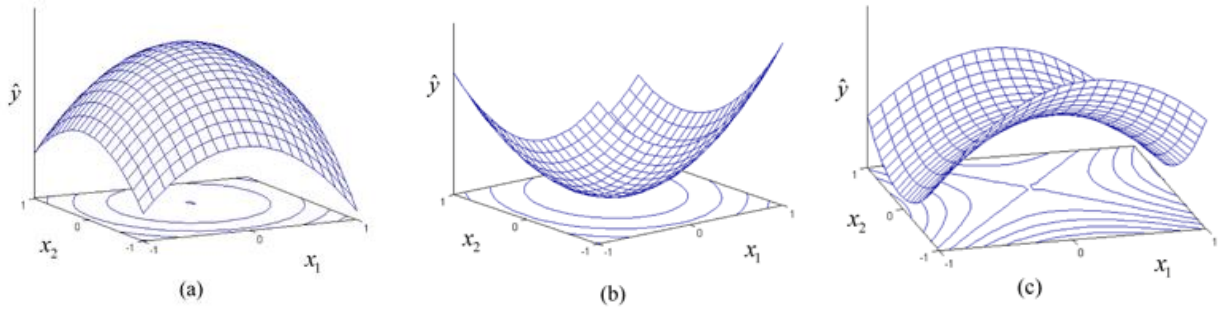

Figure 2.5. Types of second-order response surfaces. (a) maximum point; (b) minimum point; (c) saddle point (ReliaSoft 2015).

These conditions are easy to identify from the observation of Figure 2-5 with two factor experiments. However, if more than two factors exist in an experiment, the general mathematical solution for the location of the stationary point has to be used. The Matrix notation of second-order model is

$$\hat{y} = \hat{\beta}_0 + \mathbf{X'b} + \mathbf{X'BX} \tag{2.39}$$

where

$$\mathbf{X} = \begin{bmatrix} x_1 \\ x_2 \\ \vdots \\ x_k \end{bmatrix} \quad \mathbf{b} = \begin{bmatrix} \hat{\beta}_1 \\ \hat{\beta}_2 \\ \vdots \\ \hat{\beta}_k \end{bmatrix} \quad \text{and} \quad \mathbf{B} = \begin{bmatrix} \hat{\beta}_{11}, \hat{\beta}_{11}/2, \ldots, \hat{\beta}_{1k}/2 \\ \hat{\beta}_{22}, \ \ldots, \hat{\beta}_{1k}/2 \\ \ddots \\ sym. \qquad\qquad \hat{\beta}_{22} \end{bmatrix} \tag{2.40}$$

Then the stationary point can be determined as follows:

$$\frac{\partial \hat{y}}{\partial \mathbf{X}} = \mathbf{b} + 2\mathbf{B}\mathbf{X} = 0 \tag{2.41}$$

Thus, the stationary point is:

$$\mathbf{X}_s = -\frac{1}{2}\mathbf{B}^{-1}\mathbf{b} \tag{2.42}$$

Furthermore, the predicted response at the stationary point is

$$\hat{y} = \hat{\beta}_0 + \mathbf{X}_s'\mathbf{b} + \mathbf{X}_s'\mathbf{B}\mathbf{X}_s = \hat{\beta}_0 + \frac{1}{2}\mathbf{X}_s'\mathbf{b} \tag{2.43}$$

2.7.4 Experimental Design For Fitting a Second-Order Model

The number of parameters in the second-degree model is $p = 1 + 2k + \frac{1}{2}k(k-1)$. Therefore, the number of distinct design points of a second order design must be at least equal to *p*. There are many designs for fitting a second-order model. The most popular one is the central composite design (CCD) first introduced by Box and Wilson (Box and Wilson 1951). CCD was developed through a sequential experimentation. It contains the use of two-level factorial (2^k) or fraction (2^{k-q}) design combined with the following 2*k* axial or star points (Table 2.2):

Table 2.2. Axial or star points in CCD design

x_1	x_1	⋯	x_1
$-\alpha$	0	⋯	0
α	0	⋯	0
0	$-\alpha$	⋯	0
0	α	⋯	0
⋮	⋮	⋮	⋮
0	0	⋯	$-\alpha$
0	0	⋯	α

Thus, CCD design consists of 2^k factorial or fractional factorial of resolution V with n_F runs, $2k$ axial or star runs, and n_C center runs. CCD designs for $k = 2$ and $k = 3$ are shown in Figure 2.6. α is the axial distance which is defined as the distance from center to the end of that axis. The number of center runs n_C and the axial distance α are the two parameters in CCD design.

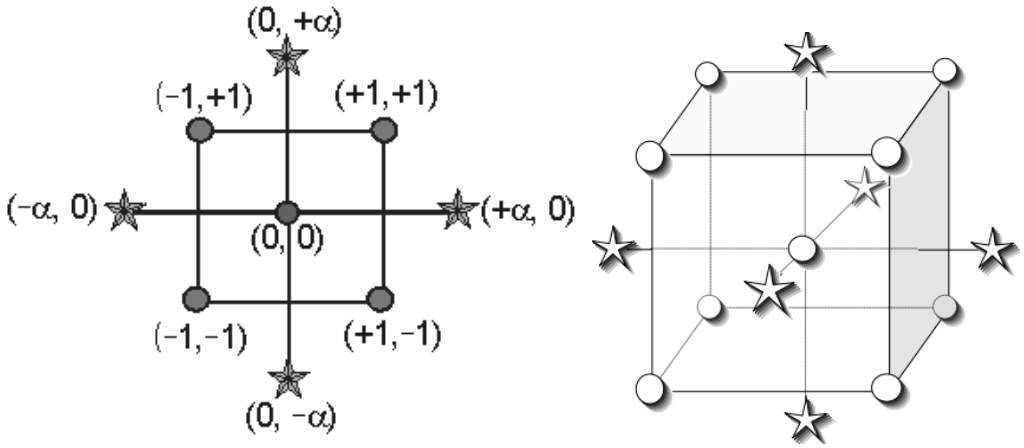

Figure 2.6. CCD designs for $k = 2$ and $k = 3$ (Stat-Ease 2014).

The factorial points represent a design for a first-order model or a first-order + two-factor interaction model. Curvature information can be obtained for center points. If curvature is found in a system, the addition of axial points or star points provide efficient estimation of the pure quadratic terms, i.e. x_i^2.

2.7.4.1 Rotation of CCD

An experimental design is said to be rotatable if $Var\left(\hat{y}\left(\mathbf{x}\right)\right)$ is constant at all points *x* equidistant from the design center (del Castillo 2007). $Var\left(\hat{y}\left(\mathbf{x}\right)\right)=\sigma^2\mathbf{x}'(\mathbf{X}'\mathbf{X})^{-1}\mathbf{x}$ is the variance of the predicted response at some point **x**. The contours of constant standard deviation $\sqrt{Var\left(\hat{y}\left(\mathbf{x}\right)\right)}$ of predicted response are shown in Figure 2.7.

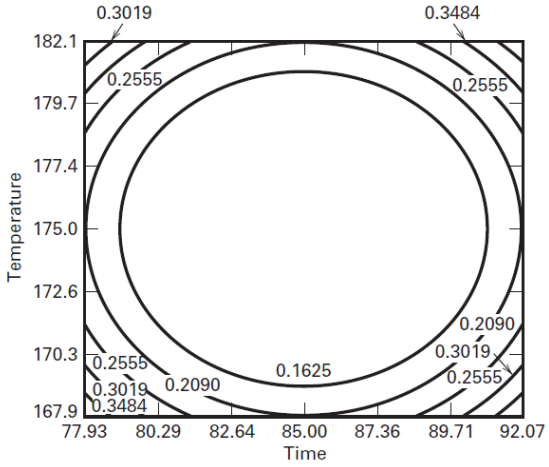

Figure 2.7. Contours of constant standard deviation of predicted response (Montgomery 2013).

The rotatable design is a desirable choice which can provide equal precision of estimation of the surface in all directions (Box and Hunter 1957). The choice of α will make the CCD design rotatable. The value of α depends on the number (n_F) of points in the factorial portion of the design. In fact, $\alpha=(n_F)^{1/4}$ will obtain a rotatable CCD design. α equals $\left(2^k\right)^{1/4}$ for the full factorial design and α equals $\left(2^{k-p}\right)^{1/4}$ for a fractional factorial design. In case of one-half fractional factorial design, n_F equals $\left(2^{k-1}\right)^{1/4}$.

2.7.5 Optimization of Multiple Response Processes

In practical life, most processes need to be optimized with respect to several criteria simultaneously. Usually, operating conditions need to satisfy several conditions or constraints on *m* responses, $y_1, y_2, \cdots, y_m$. A simple method to do optimization is to plot contours and overlay them on the space of controllable factors. Then the experimenter searches a region of operating conditions which optimize all responses. This is very useful provided the number of controllable factors is $k = 2$ or $k = 3$. Even with $k = 3$, interpreting the graphs is already complicated because the experimenter has to search on three different $x_i - x_j$ planes where the contours are projected. For *k* factors, there are $\binom{k}{2}$ such planes. With the increasing of *k*, the number of these planes will get bigger and bigger.

2.7.5.1 Desirability Approach

Since the contour plots way is not appropriate to optimize a process when $k > 3$. Another approach has to be developed. This is so-called desirability approach originally proposed by (Harrington 1965) and later refined by (Derringer and Suich 1980). This is the most common use in practice today. It is based on the idea that the quality of a product or process that has multiple quality characteristics, with one of them out of some desired limits, is completely unacceptable. The method finds operating conditions *x* that provide the most desirable response values.

For each response y_i, a desirability function d_i assigns numbers to the possible values of y_i with

$$0 \le d_i \le 1 \tag{2.44}$$

$d_i = 0$ represents a completely undesirable value of y_i and $d_i = 1$ represents a completely desirable or ideal value. Then the design variables are chosen to maximize the overall desirability *D*:

$$D = \left(d_1 d_2 \cdots d_m\right)^{1/m} \tag{2.45}$$

where *m* is the number of responses. From the above formula, it is very obvious that the overall desirability *D* is zero if any response y_i is completely undesirable, i.e. $d_i = 0$. Let *L*, *T*, *U* be the lower, target and upper values desired for response *y*, where $L \le T \le U$. If the object for the response y is a maximum value, the individual desirability function (Montgomery 2013) is:

$$d = \begin{cases} 0 & y < L \\ \left(\dfrac{y-L}{T-L}\right)^r & L \le y \le T \\ 1 & y > T \end{cases} \tag{2.46}$$

If the weight $r = 1$, the desirability function *d* is linear. If $r > 1$, the function gives more attention on being close to the target value. But if $0 < r < 1$, the function makes this less important. If the target for the response is a minimum value, the individual desirability function is:

$$d = \begin{cases} 1 & y < T \\ \left(\dfrac{U-y}{U-L}\right)^r & T \le y \le U \\ 0 & y > U \end{cases} \tag{2.47}$$

If the object is between *L* and *U*, the individual desirability function is:

$$d = \begin{cases} 0 & y < L \\ \left(\dfrac{y-L}{T-L}\right)^{r_1} & L \le y \le T \\ \left(\dfrac{U-y}{U-T}\right)^{r_2} & T \le y \le U \\ 1 & y > U \end{cases} \tag{2.48}$$

Figure 2.8 shows the individual desirability functions. Usually, the optimization will be done by software. In this project, Design-Expert 9 software was used to optimize the responses.

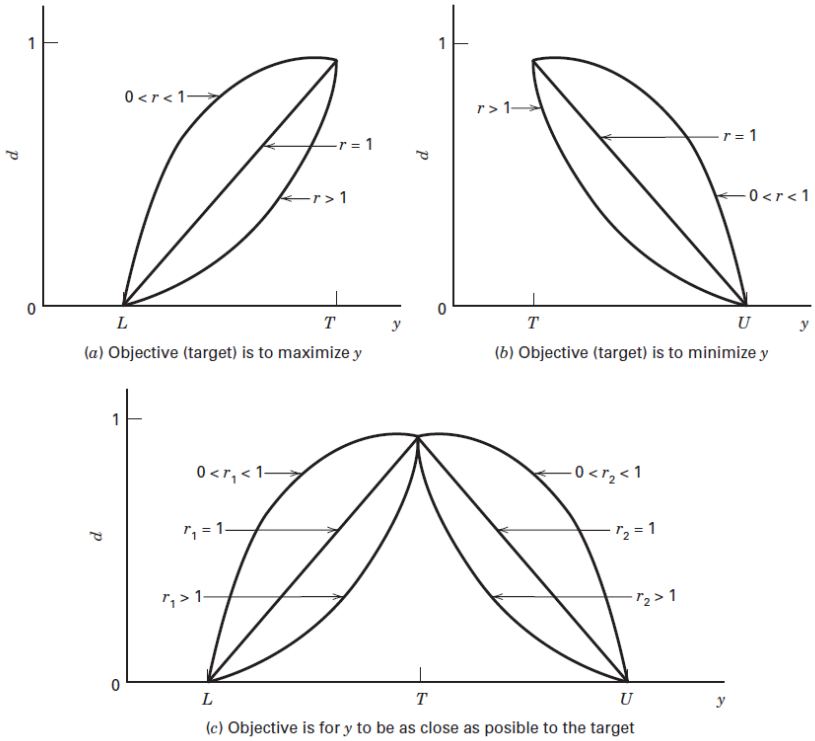

Figure 2.8. Individual desirability functions for simultaneous optimization (Montgomery 2013).

2.8 Splitting Tensile Test

The ultimate tensile strength (UTS) (often shortened to tensile strength (TS) or ultimate strength) is the maximum stress that a material can withstand while being stretched or pulled before failing or breaking. It is one of the basic and important properties of the concrete. The concrete is not usually expected to resist the direct tension because of its low tensile strength and brittle nature. However, the determination of the tensile strength of concrete is necessary to determine the load at which the concrete members may crack. Cracking is a form of tension failure.

Apart from the flexure test, the other methods to determine the tensile strength of concrete can be broadly classified as direct and indirect methods. The direct method suffers from a number of difficulties related to holding the specimen properly in the testing machine without introducing stress concentrations, and to the application of uniaxial tensile load which is free from eccentricity to the specimen. As the concrete is weak in tension, even a small eccentricity of load will induce a combined bending and axial force condition, and the concrete will fail at an apparent tensile stress that is lower than the actual tensile strength.

Since there are many difficulties associated with the direct tension test, a number of indirect methods have been developed to determine the tensile strength. The splitting tensile test is a well-known indirect test for determining the tensile strength of concrete (Melis et al. 1985). The test consists of applying a compressive line load over the entire length of the cylindrical specimen.

Due to this compressive loading, an element lying along the vertical diameter of the cylinder is subjected to a vertical compressive stress and a horizontal tensile stress (see Figure 2.9).

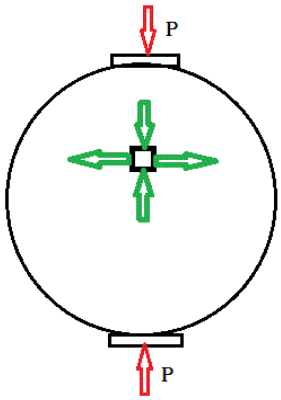

Figure 2.9. Compressive loading in splitting tensile test.

The splitting tensile strength of the specimen can be calculated (ASTM C496 / C496M-11 2004) as follows:

$$T = 2P / \pi ld \tag{2.49}$$

where

T = splitting tensile strength, MPa
P = maximum applied load indicated by the testing machine, N
l = length of concrete cylinder, mm, and
d = diameter, mm.

2.9 Air Content Test for Hardened Concrete

The air content is defined as the total air content in a sample of fresh or hardened concrete. Air void analysis in fresh concrete can be evaluated easily by the pressure method (ASTM C231 / C231M-14 2014). Air void analysis for hardened concrete, on the other hand, is more difficult to conduct using the traditional methods. Since the freeze-thaw resistance of concrete is mainly affected by the capillary porosity and air content in its hardened state, an air void analysis was carried out for hardened concrete. Entrained and entrapped air-voids are important for the continuum of pores present in hardened concrete. The interaction between entrained air-voids and the surrounding capillary pore system of the hardened paste is the key to freeze-thaw durability. From this test, the resistance to freezing and thawing can be evaluated. Usually, the optimal air-content with good resistance to freezing and thawing is 6.0% (Kosmatka et al. 2003).

Traditional air-content test for hardened concrete can be done either by recording individual lengths of intercepts through air-voids, aggregates, and hardened paste along a test line (Procedure A Linear Traverse Method) or recording the number of intersections between air-voids, aggregates, and hardened paste within a grid of test points, along with the number of intercepts through air-voids by a test line (Procedure B Modified Point-Count Method) according to ASTM C457. The accuracy of these measurements mainly relies on the microscopist. The microscopist may have to conduct this test for long periods of time and the results from this analysis will usually vary from

person to person, even when carried out by skilled technicians. Hence, this method was not adopted in this project. Alternatively, a relatively recent method, known as the Flatbed Scanner Method for air-void characterization of hardened concrete (Peterson et al. 2001), was employed in this study, as shown in Figure 2.10.

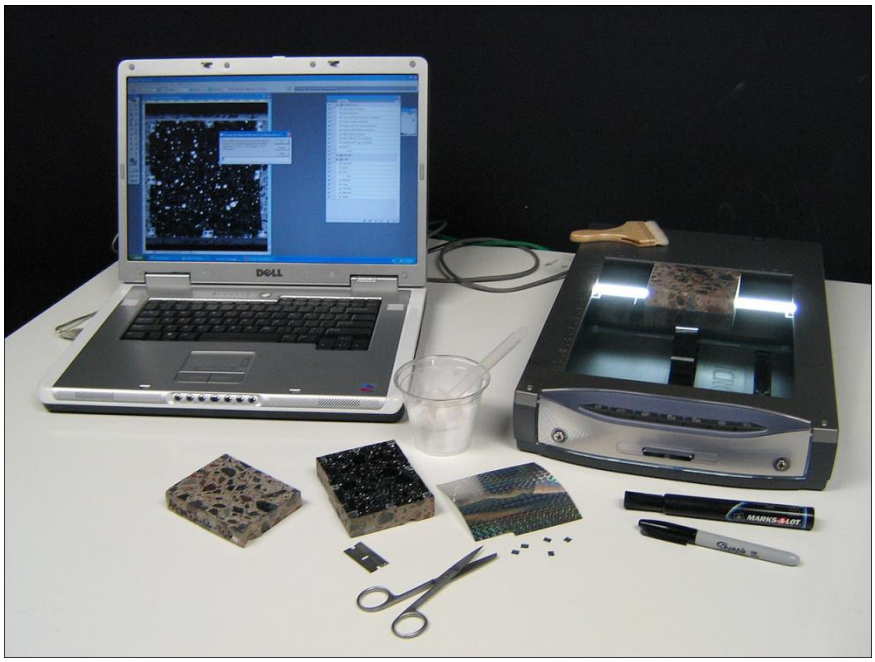

Figure 2.10. Flatbed scanner method for air-void characterization of hardened concrete (Jana 2007).

The system used in Figure 3.7 replaces the microscope and mechanical stage with a high definition flat scanner, and replaces the microscopist and tally counter with a personal computer. Both the scanner and computer are widely available and very economical.

These automated systems are based on the method developed by (Chatterji and Gudmundsson 1977). They and other researchers (Laurencot et al. 1992; Peterson et al. 2001; Roberts and Scali 1987; Zhang et al. 2005) proposed that the polished surface of a sample should be painted black, and white powder (such as wollastonite powder) forced into the depressions of air-voids. This is called contrast enhancement. The high contrast between regions of white powder and black paint

allows for easy visualization of the air-voids present in the concrete. Then the surface of the specimen is scanned by a high definition scanner, as illustrated in Figure 2.11. To categorize the

Figure 2.11. Scanned surface of specimen before and after contrast enhancement.

pixels that represent the air-voids, most procedures begin with a choice of threshold. Pixels in the digital image darker than the threshold level are classified as non-air and pixels brighter than the threshold level are classified as air. Automated systems based on contrast enhancement often require the manual darkening of pores in aggregate with a black marker prior to collecting the digital images. The last step is the analysis of the scanned surfaces using some commercially available software.

3. Materials and Experimental Procedures

Although numerous regulations and guidelines cover the composition and properties of concrete and its components, the actual process of concrete production, i.e. mixing, is, for all intents and purposes, left to the user. Due to the low water content with respect to the content of fines (<0.125 mm) and the high dosage of admixtures, the production of HPC and VHPC/UHPC requires more mixing energy to homogenise the concrete components. It has to be pointed out that the traditional mix design methods that have been developed over the years for normal concrete cannot be used for HPC and VHPC/UHPC.

The response surface methodology (RSM) was employed in this experimental design using Design-Expert Version 9.0 software. Seven components were considered in this project, namely: water, cement, silica fume, silica flour, fine sand, steel fiber, and superplasticizer (SP). As discussed below, the amount of superplasticizer was fixed, so only five independent parameters had to be determined: water-cement ratio (by mass), silica fume, silica flour, fine sand and steel fiber. The main reason that the amount of superplasticizer was fixed is because the number of experiments was decreased to a relatively small number. There were 31 batches including 16 factorial points, 10 axial points, and 5 center points.

3.1 Selection of Materials, Proportions, and Constraints

To design experiments using RSM, the ranges of water-cement ratio, silica fume, silica flour, fine sand and steel fiber had to be determined. The selection of these ranges was mainly done based on results found in the public literature, as elucidated in the following sections.

Recently, researchers (Habel et al. 2008) in Polytechnique of Montreal and University of Toronto proposed two optimized UHPC mixtures by conducting many trial tests on different

cements, sands, silica fumes, and superplasticizers (SP). One of those two mixtures is shown in Table 3.1.

Table 3.1. Mixture proportions by mass from (Habel et al. 2008).

	Cement	**Silica Fume**	**Sand**	**Steel Fibers**	**SP**	**Water**
Kg in 1 m^3	1087	163	652	390	46	250
Mass Ratio to Cement	1	0.15	0.60	0.36	0.04	0.23

From Table 3.1, it is observed that the volume of steel fiber is around 5%. However, from the work of (Orange et al. 1999)， (Acker and Behloul 2004) and (Wille et al. 2011), 2 to 2.5% of steel fiber by volume is strongly recommended. A test with 5% of steel fiber by volume was also performed as part of the current study. However, the mixture from that was very sticky with very poor workability.

Table 3.2 shows a recommended mixture where proportions are by mass, except for steel fibers, where the content is specified as 2.5% by volume. For this particular mixture, the steel fiber-cement mass ratio equals 0.25/1 without considering air content in the materials. If air content is considered to be 3% by volume, the steel fiber-cement mass ratio is 0.24/1. This mass ratio of 0.24/1 was chosen in this study as the upper bound of steel fiber content in the mix. For the minimum amount of steel fiber in this experimental design, 2.0% of steel fiber by volume was chosen, which is about 0.20/1 for the steel fiber-cement mass ratio.

Table 3.3 shows Orange's optimal mixture for DUCTAL®, a mixture by mass. DUCTAL® is a trademark for Lafarge's UHPC. Acker and Behloul (2004) conducted research on DUCTAL® at Lafarge Company. They proposed that a content of 2% by volume of 13-15 mm long fiber with a

diameter of approximately 0.2 mm was the optimum, based on the results of thousands of tests (Acker and Behloul 2004).

Table 3.2. Mixture proportions by mass from (Wille et al. 2011).

	Cement	Silica Fume	Silica Flour	Sand	Steel Fiber	SP	Water
Mass Ratio to Cement	1	0.25	0.25	1.29	2.5% by volume	0.0054	0.22

NYCON-SF TYPE I was the steel fiber that was used to satisfy the above requirements, having a length of 13 mm and a diameter of 0.2 mm. Therefore, it was chosen as a component in this project.

Table 3.3. Mixture proportions by mass from (Orange et al. 1999).

Cement	Silica Fume	Silica Flour	Sand	Steel Fiber	Microfiber	SP	Water
1	0.15	0.1	1.25	0.22	0.2	0.016	0.21

The water-cement ratios (by mass) from Table 3.1 to 3.3 are 0.23, 0.22, and 0.21, respectively. Therefore, the range for the water-cement ratio in this project was taken to be from 0.19 to 0.23. Wille and his co-authors (Wille et al. 2011) obtained good results with Type I Portland cement (Type I in US, and GU for Canada). Thus, Lafarge Portland cement GU was used in this project given its low cost and wide availability.

The content of silica fume from Table 3-1 to 3-3 are 15%, 25%, and 15% of cement content by mass. Hence, a range from 14% to 26% of cement content by mass was chosen for silica fume.

BASF RHEOMAC SF 100 silica fume was used as a concrete component. It is well known that the particle size of silica fume is less than 1 μm.

The optimal sand to cement ratio by mass has been reported in previous studies to be between 1.25 and 1.36 (Orange et al. 1999). Therefore, the range for the mass ratio of fine sand has been assumed to lie between 1.24 and 1.39. All previous studies recommended that the particle size of sand should be less than 0.5 mm, i.e. 500 μm. To satisfy this requirement, Granusil 4030 fine sand was used with 53 μm < particle size < 500 μm. Table 3.4 from Granusil technical data sheet shows the particle size analysis of 4030 sand.

Table 3.4. Particle size analysis of 4030 sand.

	Mesh Size		
	ASTM	**Microns (μm)**	**4030 Sand**
Typical Mean % Retained on Individual Sieves	20	850	---
	30	600	3.3
	40	425	36.4
	50	300	34.5
	70	210	16.2
	100	150	7.2
	140	106	2.1
	200	75	0.3
	270	53	---
	PAN	PAN	---

In the mixture of (Wille et al. 2011), one more material was used: silica flour. The reason it was used is because it is finer than fine sand and coarser than silica fume. Hence, it can fill the gaps between fine sand and silica fume. This will increase the compactness of concrete which is the key to HPC and VHPC/UHPC. The optimal amounts of silica flour from Table 3.2 and 3.3 are 25%

and 10% of cement content by mass, respectively. Based on this, 7% to 25% of cement content by mass was the content range for silica flour considered in this study. AGSCO A7 silica flour was used in this project with median particle size = 1.6 μm. Thus, the particle size of 1.6 μm of silica flour is just between the sizes of silica fume and fine sand. Typical percent passing of AGSCO A7 silica flour from AGSCO technical data sheet is shown in Table 3.5.

Table 3.5. Particle size analysis of AGSCO A7 silica flour.

Microns (μm)	**AGSCO A7 Silica Flour**
25	---
15	100.00
10	99.90
8	99.10
5	90.00

Using the mixture in Table 3.2 from the work of Wille et al.(2011), two tests were performed with the only difference being the type of superplasticizer. Three 50×100 mm cylinders for each superplasticizer were made. The results for the compressive strength tests are shown in Table 3-6.

Table 3.6. 7 day compressive strength for different superplasticizers.

		7 day Compressive Strength (MPa)	**SP Type**
SP 1	Rheobuild 1000	51±4	Non-polycarboxylate
SP 2	Chryso Premia 150	78±10	Polycarboxylate

Since the 7 day compressive strength produced using SP2 was much larger than that of SP1, the polycarboxylate-based Chryso Premia 150 superplasticizer was used. The amount of superplasticizer was determined such that the spread value of the mixture was 300 $\pm$ 30 mm

(Wille et al. 2011). By trial and error, the amount of superplasticizer was determined to be 75 ml / (kg of cement). This test is explained in more detail in Section 3.4.3.

Once the amount of superplasticizer was fixed, only five variables remained, namely: water-cement ratio, silica fume, silica flour, sand, and steel fiber. Table 3.7 provides a summary of the various mix variables selected in this project together with range of variation.

Table 3.7. Materials with ranges, specific gravities and related standards in this project.

Components	Mass Ratio to Cement	Specific Gravity	Source	Standard
Portland Cement	1	3.15	Lafarge GU	ASTM C150 CSA A3000-08
Water	0.19 – 0.23	1.00	Tap Water	N/A
Silica Fume	0.14 – 0.26	2.20	BASF RHEOMAC SF 100	ASTM C1240
Silica Flour	0.07 – 0.25	2.65	AGSCO A7	N/A
Sand	1.24 – 1.39	2.65	Granusil 4030	N/A
Steel Fiber	0.20 – 0.24	7.85	NYCON-SF TYPE I	ASTM A820
Superplasticizer	(75 ml) / (kg of cement)	1.06	Chryso Premia 150	ASTM C494 ASTM C1017

3.2 Central Composite Design

A central composite design (CCD) with fraction 2^{k-q} was chosen for this project. There were five variables to consider in this case, thus $k=5$. Here, one-half fraction design, i.e. $q=1$, was considered to be a relatively economical choice because it could generate 31 runs with 16 factorial points, 10 axial points, and 5 center points. On the other hand, full factorial design with 5 center points will generate 47 runs. The number of center runs, n_C, and the axial distance α are the two parameters needed in a CCD design. The number of center runs n_C was set to 5 in this experiment

because a value for n_C of 3 to 5 for can usually give enough information and simultaneously limit the number of required experiments (Montgomery 2013). The parameter α can then be calculated as follows:

$$\alpha = \left(2^{k-p}\right)^{1/4} = \left(2^{5-1}\right)^{1/4} = 2 \tag{3.1}$$

This way one can obtain a rotatable CCD design. The commercially available software, Design-Expert Version 9.0, was used to implement the design of this study. Table 3.8 shows the mixture proportions used for the 31 batches tested in terms of mass ratio to cement.

3.3 Specimen Preparation

As shown in Table 3.8, 31 designs were prepared. Ten 50×100 mm cylinders were made for each design. Three of these 10 samples (from the same pot) were used for 7 day compressive strength tests, 3 (from the same pot) were used for 28 day compressive strength tests, 1 (from the same pot as 28 day compressive strength samples) was used to measure the air-content of the hardened concrete, and the last 3 samples were used for 28 day splitting tensile strength tests. The reason why three pots were made for one batch or mixture was because a food type concrete mixer (see Figure 3.1) was used to conduct the experiments. The amount of concrete that could be produced from this mixer was very small. Only four or five 50×100 mm cylinders could be obtained from each batch.

Figure 3.1. High energy food type concrete mixer.

Table 3.8. Mixture proportions for CCD design (mass ratio to cement).

Design Number	Water	Silica Fume	Silica Flour	Sand (4030)	Steel Fiber
1	0.220	0.230	0.115	1.278	0.230
2	0.200	0.170	0.115	1.353	0.210
3	0.200	0.170	0.205	1.353	0.230
4	0.200	0.230	0.205	1.278	0.230
5	0.210	0.200	0.160	1.315	0.220
6	0.220	0.230	0.115	1.353	0.210
7	0.210	0.200	0.160	1.315	0.220
8	0.200	0.230	0.115	1.278	0.210
9	0.220	0.170	0.115	1.278	0.210
10	0.210	0.200	0.160	1.315	0.220
11	0.220	0.230	0.205	1.278	0.210
12	0.200	0.170	0.115	1.278	0.230
13	0.220	0.170	0.205	1.353	0.210
14	0.220	0.170	0.115	1.353	0.230
15	0.200	0.230	0.205	1.353	0.210
16	0.200	0.170	0.205	1.278	0.210
17	0.220	0.230	0.205	1.353	0.230
18	0.200	0.230	0.115	1.353	0.230
19	0.220	0.170	0.205	1.278	0.230
20	0.210	0.200	0.250	1.315	0.220
21	0.210	0.260	0.160	1.315	0.220
22	0.210	0.200	0.160	1.240	0.220
23	0.210	0.200	0.160	1.315	0.220
24	0.210	0.200	0.160	1.315	0.200
25	0.210	0.200	0.160	1.390	0.220
26	0.210	0.200	0.070	1.315	0.220
27	0.210	0.200	0.160	1.315	0.220
28	0.210	0.200	0.160	1.315	0.240
29	0.210	0.140	0.160	1.315	0.220
30	0.190	0.200	0.160	1.315	0.220
31	0.230	0.200	0.160	1.315	0.220

The experiments were conducted in the order shown in Table 3.8. For each pot, a fixed mass of 700 g of Portland cement was used and the other components were prepared in accordance with the mass ratio to cement. As described before, the amount of superplasticizer was fixed at 75 ml / (kg of cement). Hence, the amount of superplasticizer for each pot was $0.7 \times 75 = 52.5 \approx 53$ ml.

Cement, silica fume, silica flour and sand were placed into the pot and all mixed together for 5 minutes using the low speed of the food type mixer. The pot was then emptied by putting all those ingredients into another container. Superplasticizer was then injected into tap water using a syringe and the mixture was put into an empty pot. At that moment, the mixed cement, silica fume, silica flour, and sand were put into the pot gently. Following this, all the ingredients were mixed for 1 minute with the low speed of mixer and another 3 minutes at high speed of the mixer. Finally, steel fibers were added into the mixture and mixed for another 2 minutes. Concrete samples were made from this mixture, taking care to rod for proper consolidation.

Room temperature curing was followed by placing plastic sheet on the top of the cylinder moulds for the first 24 hours. After demoulding the samples, all the cylinders were submerged into lime saturated water (see Figure 3.2) for curing. With this curing, the lime inside the concrete cylinders can be prevented from leaching out.

Figure 3.2. Concrete cylinders curing in lime saturated water.

3.4 Material Tests

Several tests were conducted on the prepared concrete following standard procedures to obtain the required properties. The details of the tests are presented in Table 3.9.

Table 3.9. Outline of concrete tests.

Test	Description	Relevant Standard
Compressive strength	To obtain the capacity of concrete to withstand axially directed pushing forces	ASTM C39
Splitting tensile strength	To estimate the tensile strength	ASTM C496
Air-content test for hardened concrete	To evaluate the resistance to freezing and thawing and chemical attack	ASTM C457
Flow cone test	To obtain the spread value of paste	ASTM C1437 ASTM C230

3.4.1 Compressive Strength Test

Before conducting compressive strength test, the concrete cylinders were capped to make the surfaces on both ends of samples planar and parallel according to ASTM C617. Cylinders were capped with sulphur and placed between the bearing platens of the testing machine as illustrated in Figure 3.3. The cylinders were placed on the center of the platen. Three cylinders were tested for the 7 day compressive strength for each batch and another three for the 28 day compressive strength.

3.4.2 Splitting Tensile Strength Test

Two bearing strips were utilized in the splitting tensile test. The strips used for this project were plywood, free of imperfections, with a nominal 3.0 mm thickness, approximately 25 mm wide, and of a length equal to, or slightly longer than that of the specimen. They were placed between

the specimen and both the upper and lower bearing blocks of the testing machine and were not reused. Great care was taken when placing the concrete cylinder on the upper and lower of platens to make sure it was placed on the center of the platen. Figure 3.4 illustrates the splitting tensile test.

Figure 3.3. Concrete compressive strength test.

Figure 3.4. Concrete splitting tensile test

In this project, only a small amount of concrete could be made in every batch, making it very difficult to manufacture a specimen suitable for a flexural test. Therefore, the spitting tensile test was selected as the best alternative. Apart from this, the splitting tensile test also has the following advantages:

1. The test is simple to perform and gives more uniform results than that given by other tests.
2. The splitting tensile strength determined is slightly greater than direct tensile strength and lower than flexural strength (ASTM C496 / C496M-11 2004). This conclusion was obtained mainly based on large-scale data comparisons (Popovics 1998). Therefore, it was concluded that flexural strength can be deduced from the result of splitting tensile strength.
3. The same moulds and testing machine can be used for compressive strength and splitting strength tests.

The splitting tensile tests were performed on three cylinders for each batch.

3.4.3 Flow Cone Test

According to (Wille et al. 2011), the spread value of flow cone test is a quick test indicator to optimize the packing density of the paste. Flow cone tests were conducted to evaluate the rheological behavior. The spread value of 300 $\pm$ 30 mm was considered as an optimal value (Wille et al. 2011).

Figure 3.5 shows the flow cone test as well as the specification of a flow cone (ASTM C230 / C230M-14 2014). Before the test, the flow cone was placed on a plane plate. After mixing, the concrete was poured into the flow cone to full capacity. The cone was then removed, allowing the paste to spread on the plate while the plate remained steady. After 30 seconds, the spread was measured. The diameter of the spread is called spread value. The main difference between the test

here and ASTM 1437 is that a flow plate was used in this project instead of flow table described in ASTM 1437 and C230. The main reason for this difference was that the diameter of the prescribed flow table is 254 mm which was not suitable for this project.

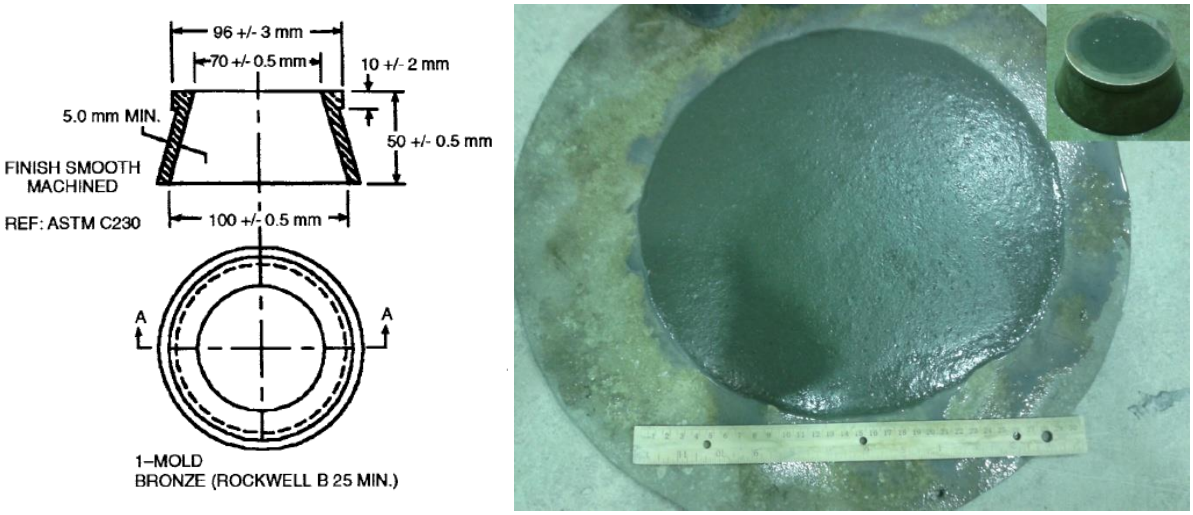

Figure 3.5. Concrete flow test and the specification of flow cone (left side from (ASTM C230 / C230M-14 2014)).

3.4.4 Air Content Test for Hardened Concrete

Bubble Counter (Peterson et al. 2012), freely avaialble available software coded by a group at Michigan Technological University, was adopted to estimate the air content in the hardened concrete in this research. Rapid Air 457 software (include manufacturer information) is a widely used alternative to Bubble Counter, but it is very expensive.

The system using Bubble Counter consists of a high definition scanner (Epson V750 PRO in this project), and three software packages (Bubble_Counter, Adobe Photoshope CS5, and Microsoft Office 2007). This system is a semi-automated approach to the ASTM C457 method.

3.4.4.1 Calibration of Threshold Value

The threshold value is an important parameter for automated systems because it has a profound effect on the test results. This value should be calibrated for each specific flatbed scanner system. To perform this, concrete slab samples are needed and these slabs are manually analyzed by using traditional procedures A or B as outlined in ASTM C457 to obtain the air content and void frequency. Void frequency is defined as:

$$n = \frac{N}{T_t} \tag{3.2}$$

where

$N =$ total number of air void intersected, and

$T_t =$ total length of traverse.

Two round consistent concrete slabs (19 mm thick and 100 mm diameter) were sent to Michigan Technological University to conduct manual analysis per ASTM C457. When running "optimization" in Bubble Counter software, the results of the air content and void frequency tests from Michigan Technological University were input to the package. The calibrated threshold value of 139 was then obtained and kept for the future analyses.

3.4.4.2 Sample Preparation

Thirty one 19 mm (or ¾ inch) thick slabs were cut using a water-cooled diamond saw from the middle of cylinders (50 × 100 mm). After cutting, one face of each slab was polished flat and smooth. A BG 20 single belt water-cooled grinder (see Figure 3.6 for the grinder located at the University of Saskatchewan) with nominal 190 μm grit size (No. 80) was first used to do the basic polishing with hand pressure. After this, a series of polishing steps were performed through nominal grit sizes of 150, 75, 35, 17.5, and 12.5 μm (No. 100, 220, 320, 600 and 800, respectively).

This was done using hand pressure on a water-cooled cast iron rotating lap topped with a magnetic platen (see Figure 3.7 for the unit located at the University of Saskatchewan).

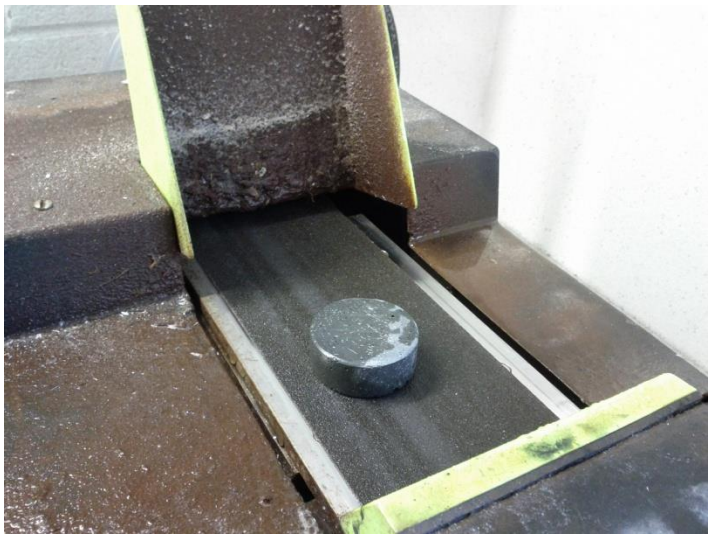

Figure 3.6. BG 20 single belt grinder.

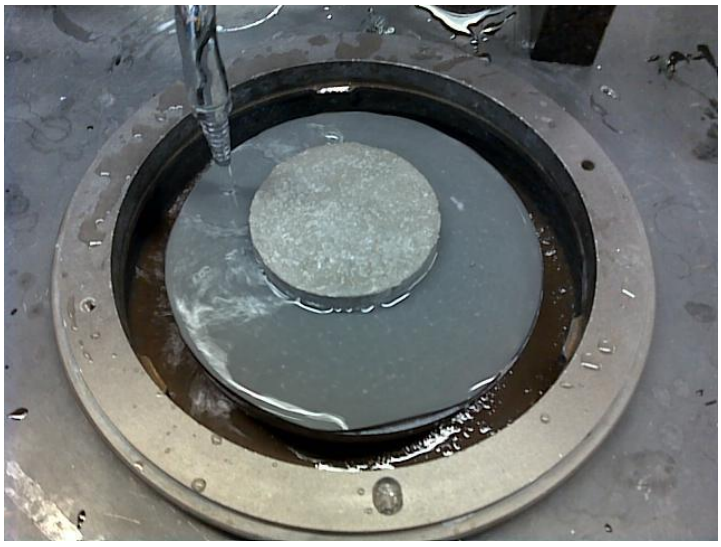

Figure 3.7. Rotatable magnetic polisher.

Once the polishing was finished, contrast enhancement was carried out as follows:

i) A series of slightly overlapping parallel lines were drawn across the entire sample surface using a wide tipped black permanent marker. This was done in 3 coats, rotating the sample 90 degrees between coats.

ii) The ink was allowed to dry. A 2 µm NYAD 1250 wollastonite white powder was put on the surface of the sample and pressed into the voids using the plane side of a card.

iii) A razor blade was used to scrape away the excess powder. Residual powder after scraping was removed by wiping the surface with a clean and lightly oiled fingertip.

iv) A fine tipped black permanent marker was used to darken locations wherever lighter areas were deemed not be be due to air voids.

3.4.4.3 Scanning the Slabs

A high definition scanner with at least 3,175 dpi resolution was needed to discriminate an air void of 10 µm. Four prismatic mosaic stickers were put on the polished surfaces of samples to protect the glass surface of the scanner. Prior to conducting contrast enhancement, polished slabs were scanned at a resolution of 3,175 dpi in 24 bit RGB color and saved in TIFF format. The contrast enhanced slabs, as well as a white balance card, were then scanned at a resolution of 3,175 dpi in 8 bit grayscale and saved in TIFF format.

3.4.4.4 Analyzing Images

All the required images were obtained. The image to be analyzed was opened in Photoshop software. The area of interest was then selected and analyzed by running Bubble Counter scripts. Finally, the results were saved as .csv files which could be opened by Microsoft Excel for further processing.

4. Results and Discussion

This chapter presents the results obtained from different tests as well as costs that were described in Chapter 3. The air-content for hardened concrete, spread values for flow cone tests, average values for 7 day compressive strength, 28 day compressive strength and 28 day splitting tensile strength are shown in Table 4.1. Except for spread value and cost, each response was analyzed individually by examining various plots of the data, fitting a model using ANOVA and least-squares techniques. An optimization was performed based on the mix design criteria listed in Chapter 1. Design-Expert Version 9.0 was used to carry out the statistical analyses and Origin Pro 8 (supplier information) was used to generate the related plots. All the tables in this chapter except for Table 4.1, 4.3, 4.15, 4.16 and 4.17 were generated from Design-Expert Version 9.0 software.

4.1 Spread Values for Flow Cone Tests

A spread value of 300 $\pm$ 30 mm for flow cone test was recommended according to (Wille et al. 2011). Figure 4.1 shows a plot of spread value vs. design number. From this plot, it is evident that all the spread values except the value from the 30th run were between 270 and 330 mm (the blue lines). Values below 300 mm (represented by the green line) imply that more superplasticizer may have been added. Since there is only one measurement for each batch due to the small volume of concrete made for each batch, no error bars are displayed in Figure 4.1.

4.2 28 day Compressive Strength

A standard deviation bar plot was constructed for average values of 28 day compressive strength, as shown in Figure 4.2. This plot gives a graphical representation of the variability of data and can be used to indicate the uncertainty in a reported measurement. From Figure 4.2, one can see that

the uncertainty of the recorded 28 day compressive strength was acceptable, as indicated by the fact that all the data are within the range between (average value – 2×standard deviation) and (average value + 2×standard deviation). This standard deviation bar was calculated according to the expression:

$$Standard\ \ Deviation = \sqrt{\frac{\sum \left(x_i - \overline{x}_i \right)^2}{N}} \tag{4.1}$$

and N is the number of repeated measurements. In this case, $N = 3$. From Figure 4.2, it is observed that the maximum 28 day compressive strength was 100 MPa which was obtained for design #27, and the minimum value was 48 MPa which corresponded to occurred at design #1. This shows the large differences between properties of the different mixtures.

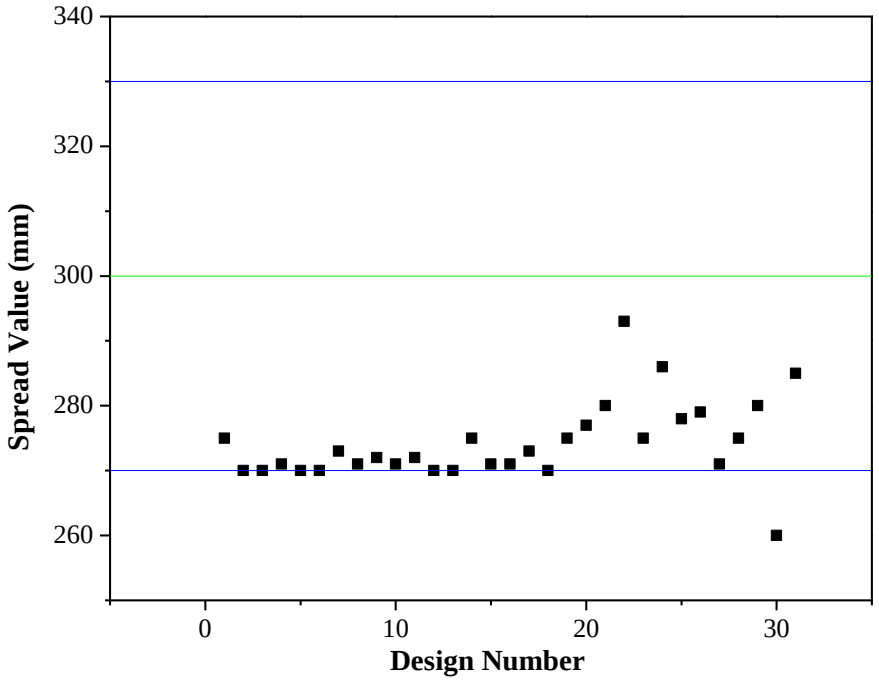

Figure 4.1. Spread values for flow cone tests.

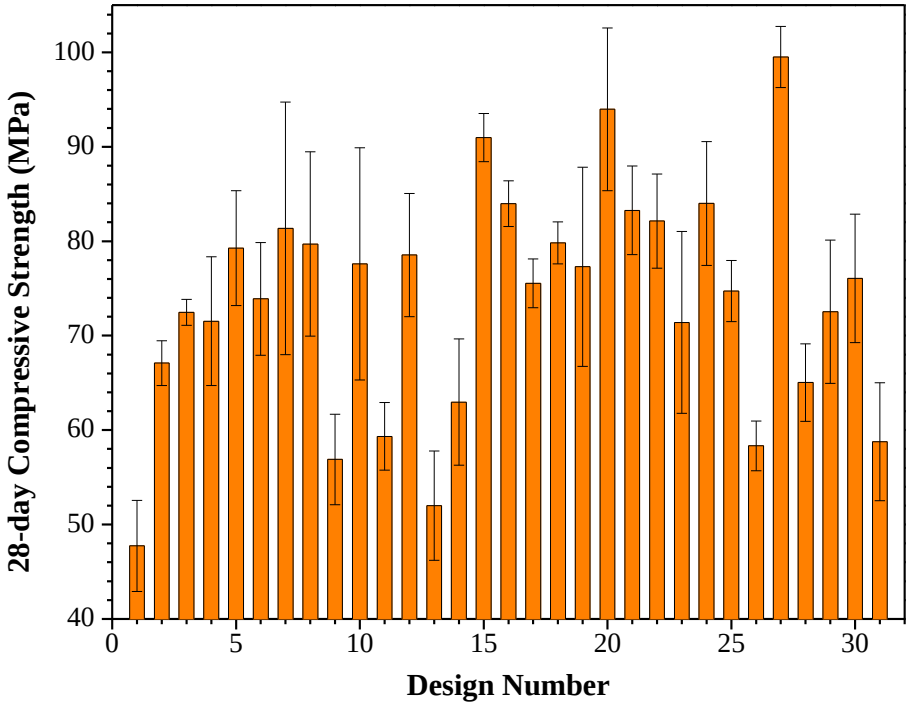

Figure 4.2. 28 day compressive strength with standard deviation bars.

Table 4.1. Summary of all results.

design number	7 day com. strength (MPa)	28 day com. strength (MPa)	28 day splitting tensile strength (MPa)	Air content (%)	spread value (mm)	Cost (dollars/m^3)
1	36±3	48±5	23±2	5.3	275	2534
2	53±3	67±2	22±1	6.9	270	2441
3	55±4	72±1	29±4	2.9	270	2613
4	60±3	72±7	23±4	4.1	271	2662
5	55±5	79±6	30±2	2.7	270	2533
6	39±4	74±6	19±3	3.9	270	2422
7	51±7	81±13	20±2	1.8	273	2533
8	58±1	80±10	23±5	4.9	271	2492
9	43±6	57±5	24±2	5.0	272	2434
10	41±3	78±12	24±3	3.6	271	2533
11	41±4	59±4	24±4	2.8	272	2543
12	49±7	79±7	29±2	3.3	270	2558
13	40±1	52±6	20±4	6.5	270	2494
14	45±3	63±7	27±2	6.2	275	2484
15	58±1	91±3	20±0	6.7	271	2549
16	43±1	84±2	24±4	5.0	271	2566
17	49±6	76±3	19±1	5.9	273	2588
18	59±2	80±2	26±4	4.5	270	2541
19	46±3	77±11	22±3	5.3	275	2607
20	56±3	94±9	22±3	4.9	277	2621
21	48±5	83±5	22±4	5.6	280	2550
22	45±6	82±5	22±4	4.2	293	2567
23	50±2	71±10	20±2	5.3	275	2533
24	50±3	84±7	27±3	6.1	286	2452
25	50±5	75±3	23±1	3.8	278	2501
26	39±3	58±3	26±4	5.5	279	2442
27	52±3	100±3	23±4	4.8	271	2533
28	51±4	65±4	22±1	5.4	275	2614
29	40±2	73±8	22±2	4.0	280	2516
30	62±5	76±7	19±0	3.0	260	2574
31	40±0	59±6	23±2	6.1	285	2494

The question as to whether compressive strength has some correlation with water-cement ratio by mass (W/C), silica fume, silica flour, sand and steel fiber can be studied by analyzing the scatter plots. The scatter plot of 28 day compressive strength vs. W/C is shown in Figure 4.3, along with the equation and root mean squared error (RMSE) for the linear fit to the data (denoted by the blue line on the graph). The RMSE is determined by

$$RMSE = \sqrt{\frac{1}{n}\sum_{i=1}^{n}(y_i - y_i)^2} \tag{4.2}$$

where n is number of designs, y_i is test value and y_i is predicted value from fitting equation. It can be seen that there is a general trend of decreasing strengths with increasing W/C.

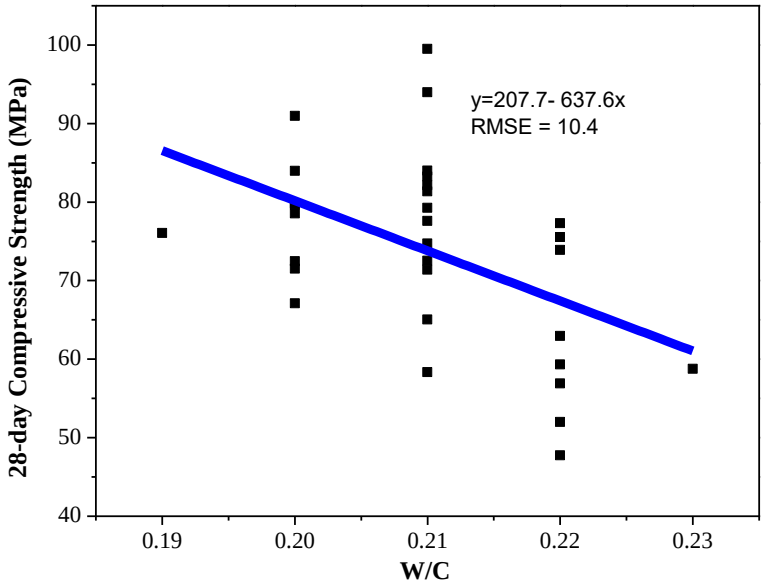

Figure 4.3. 28 day compressive strength vs. W/C ratio.

Figures 4.4 to 4.7 show the plots of 28 day compressive strength vs. silica fume, silica flour, sand, and steel fiber by mass ratio to cement, respectively. Upward trends are observed in Figure 4.4 and 4.5. Figure 4.6 shows very light upward trend. These suggest that 28 day compressive

strength increases with increasing mass ratios relative to cement of silica fume, silica flour and sand. However, a downward trend is shown in Figure 4-7 which implies that 28 day compressive strength decreases with an increasing steel fiber – cement ratio by mass. If *A*, *B*, *C*, *D* and *E* represent the mass ratio of water, silica fume, silica flour, sand and steel fiber, respectively, the linear model of 28 day compressive strength $Y_{28\,Com.}$ can be expressed in the form of

$$Y_{28\,Com.} = a_0 - aA + bB + cC + dD - eE \tag{4.3}$$

where a_0 is the intercept of the function, and *a* , *b*, *c*, *d*, and *e* are positive or zero values. This was confirmed through the analysis of data by Design-Expert Version 9.0.

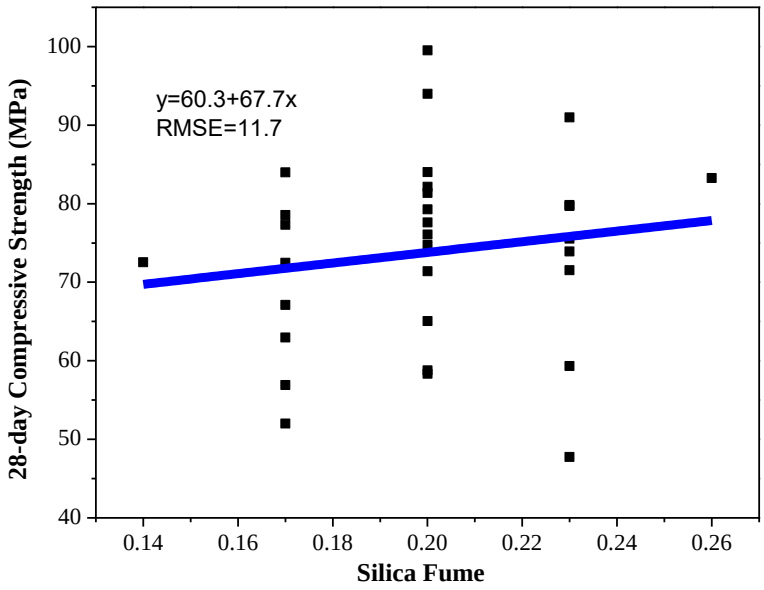

Figure 4.4. 28 day compressive strength vs. silica fume to cement ratio.

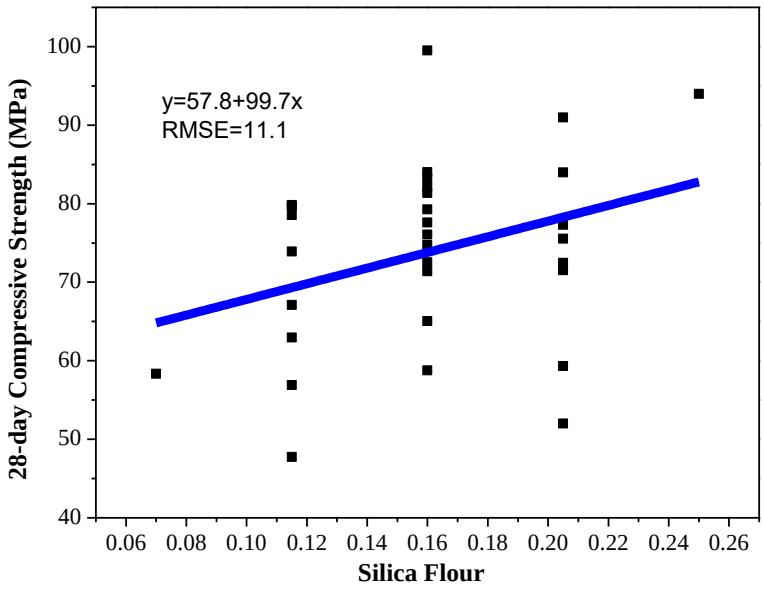

Figure 4.5. 28 day compressive strength vs. silica flour to cement ratio.

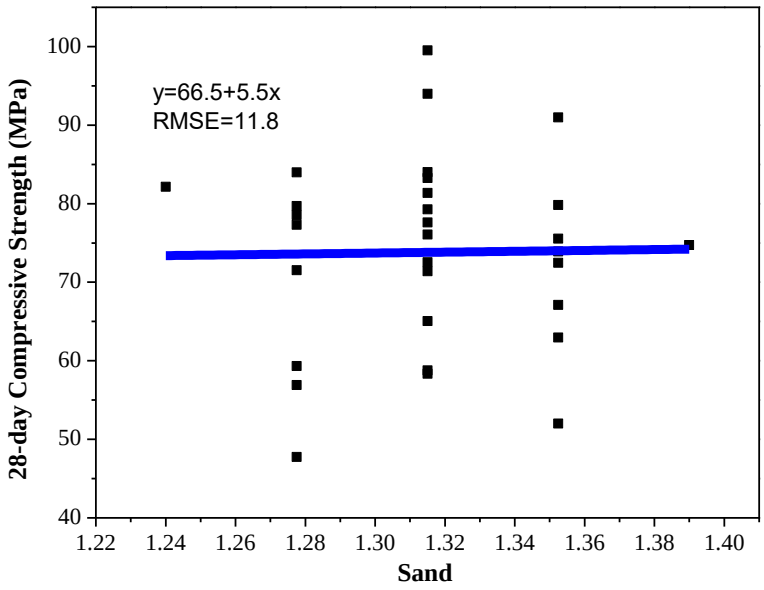

Figure 4.6. 28 day compressive strength vs. sand to cement ratio.

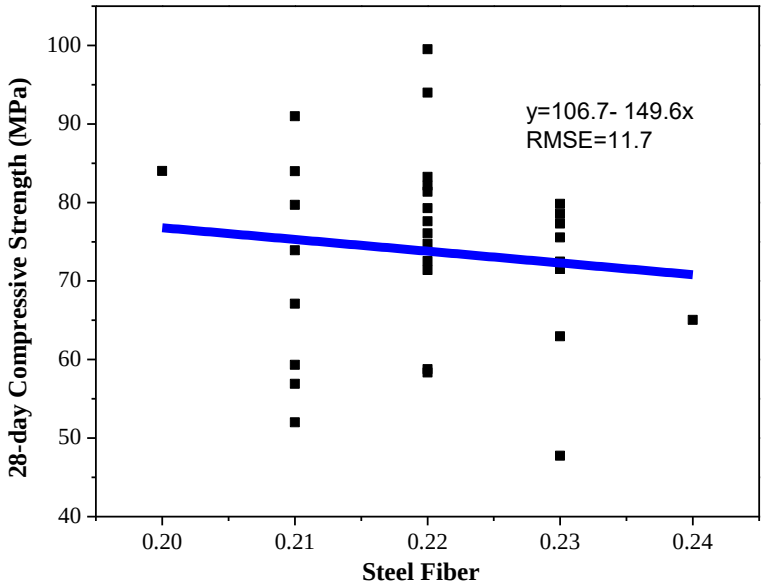

Figure 4.7. 28 day compressive strength vs. steel fiber volume fraction.

4.2.1 Model Fitting

A Least Squares technique in model regression and ANOVA (Analysis of Variance) was used in this step.

These analyses were carried out using the statistical software, Design-Expert, in this project. The sequential model sum of squares in 28 day compressive strength is illustrated in Table 4-2. The terms in Table 4-2 are explained as follows:

Linear - linear model as shown in equation (2.10).

2FI - two factor interaction model as shown in equation (2.11) without quadratic terms.

Quadratic - quadratic model as shown in equation (2.11).

Cubic - cubic model.

Residual – the difference between the observed value and the estimated value of a response.

Sum of Squares – sum of the squared deviations from the mean for each model.

Df – degree of freedom for the selected model. In statistics, the number of degrees of freedom is the number of values in the final calculation of a statistic that are free to vary.

Mean Square – for each model, it is the sum of squares divided by the degrees of freedom. This is used to calculated the F Value for the models.

F Value – it is used to test the significance of adding new model terms to those terms already in the model.

P-value – a small p-value (here p-value ≤ 0.05) indicates that adding corresponding terms has improved the model.

Table 4.2. Sequential model sum of squares for 28 day compressive strength.

Source	Sum of Squares	df	Mean Square	F Value	p-value Prob > F
Mean vs Total	168829.80	1	168829.80		
Linear vs Mean	1612.92	5	322.58	2.99	0.0301
2FI vs Linear	1132.06	10	113.21	1.08	0.4307
Quadratic vs 2FI	627.20	5	125.44	1.33	0.3259
Cubic vs Quadratic	467.31	5	93.46	0.99	0.5056
Residual	473.53	5	94.71		
Total	173142.82	31	5585.25		

The sum of squares values in Table 4.2 were calculated according to equations (2.27), (2.31) and (2.32) using Design Expert Version 9.0 software. F values can be calculated according to Figure 4.8.

The widely accepted significance level of 0.05 was adopted in this project. The significance level of a statistical hypothesis test is the fixed probability of wrongly rejecting the null hypothesis H_0, if it is, in fact, true. It is evident that a linear model is the best choice from Table 4.2, because the

p-value = 0.0301 of the linear model was less than 0.05, whereas the others were all greater. than 0.05. In this case, the p-value is the probability that the order terms are modeling noise rather that helping explain the trend in the response. Mean squares and F values in Table 4.2 were obtained according to Table 4.3.

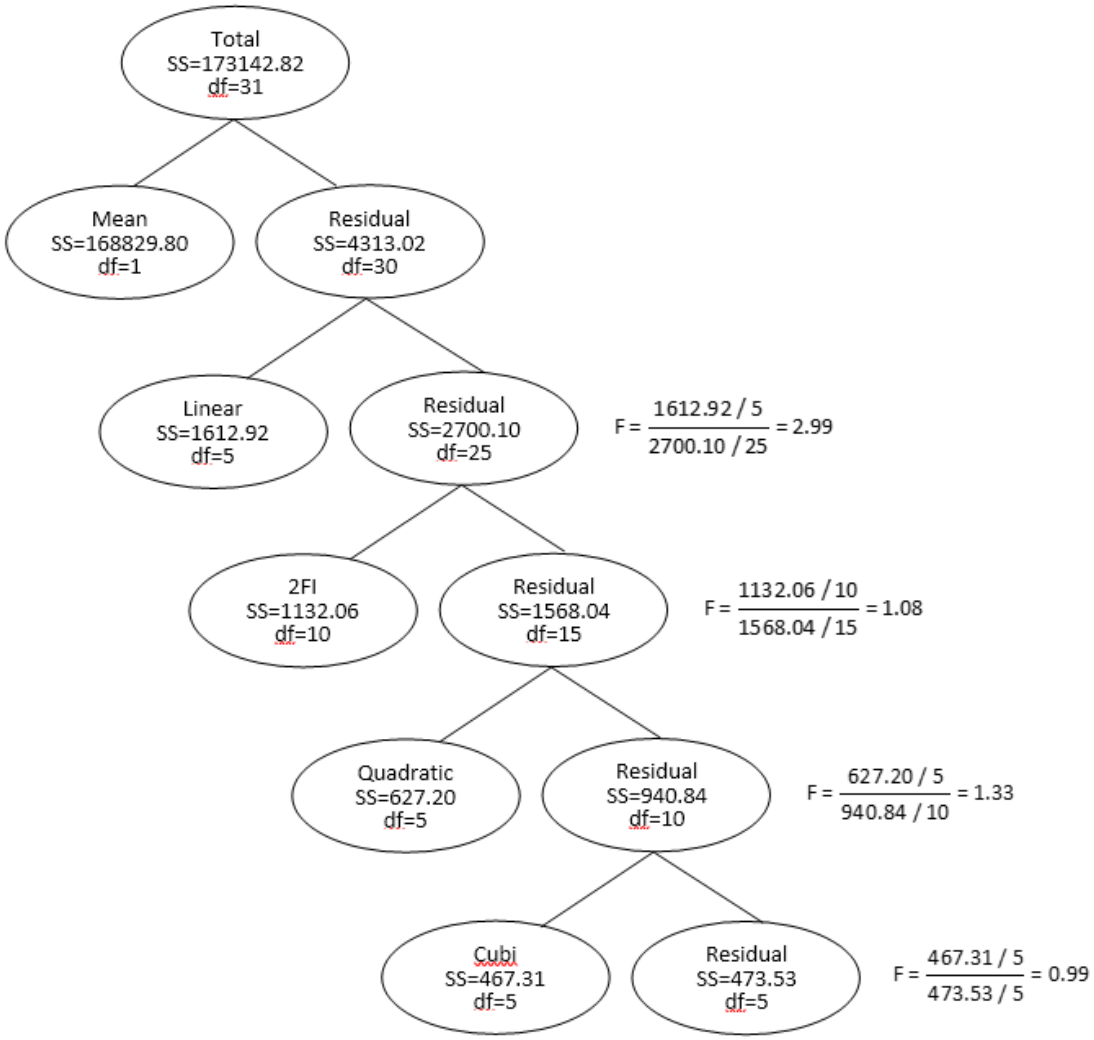

Figure 4.8. Calculations for sequential model sum of squares in Table 4-2.

Table 4.3. ANOVA for significance of Regression.

Source of Variation	Sum of Squares	df	Mean Square	F
Regression	SS_R	k	$MS_R = SS_R / k$	MS_R / MS_E
Error or residual	SS_E	$n-k-1$	$MS_E = SS_E / (n-k-1)$	
Total	SS_T	$n-1$		

Table 4.4 shows "Lack of Fit" test results in which the residual error is compared with pure error from replicated design points. A lack of fit error significantly larger than the pure error indicates that something remains in the residuals that can be a more appropriate model. If there is significant lack of fit (low probability value of p-value of 0.10 or smaller), then great care must be taken about using the model as a response predictor. Table 4.4 shows that the linear model had an insignificant lack of fit (P-value was 0.5888 which is the smallest one.).

Table 4.4. Lack of Fit Tests for 28 day compressive strength.

Source	Sum of Squares	df	Mean Square	F Value	p-value Prob > F
Linear	2254.40	21	107.35	0.96	0.5888
2FI	1122.35	11	102.03	0.92	0.5926
Quadratic	495.15	6	82.52	0.74	0.6471
Cubic	27.83	1	27.83	0.25	0.6435
Pure Error	445.69	4	111.42		

The residual sum of squares SS_E can be partitioned into two components:

$$SS_E = SS_{PE} + SS_{LOF} \tag{4.4}$$

where SS_{PE} is the pure error sum of squares and SS_{LOF} is the lack of fit sum of squares. In this case, the pure error sum of squares SS_{PE} can be calculated using the following formula (Montgomery 2013):

$$SS_{PE} = \sum_{j=1}^{5} (y_j - \bar{y})^2 \tag{4.5}$$

where y_j is the 28 day compressive strength at center points and $\bar{y}$ is the average value of the five 28 day compressive strengths at center points (design #5, #7, #10, #23 and #27 in Table 4.1). the mean value $\bar{y}$ can be calculated as:

$$\bar{y} = \frac{1}{5}(79.267 + 81.367 + 77.6 + 71.4 + 99.5) = 81.8268. \tag{4.6}$$

The pure error sum of squares is then:

$$\begin{aligned} SS_{PE} = {} & (79.267 - 81.8268)^2 + (81.367 - 81.8268)^2 + (77.6 - 81.8268)^2 + \\ & (71.4 - 81.8268)^2 + (99.5 - 81.8268)^2 = 445.69 \end{aligned}. \tag{4.7}$$

The lack of fit sum of squares in Table 4.4 can be calculated according to Figure 4.9 and Table 4.2.

The ANOVA results for this linear model is shown in Table 4.5. Such tests are useful in determining the value of each regression variable in the regression model. The model might be more effective with the inclusion of additional variables or perhaps with the deletion of one or more of the variables already in the model.

Table 4.5. ANOVA for 28 day compressive strength.

Source	Sum of Squares	df	Mean Square	F Value	p-value Prob > F
Model	1611.90	4	402.97	3.88	0.0134
A-Water	975.80	1	975.80	9.39	0.0050
B-Silica Fume	99.09	1	99.09	0.95	0.3378
C-Silica Flour	483.30	1	483.30	4.65	0.0404
E-Steel Fiber	53.70	1	53.70	0.52	0.4786
Residual	2701.12	26	103.89		
Lack of Fit	2255.43	22	102.52	0.92	0.6127
Pure Error	445.69	4	111.42		
Cor Total	4313.02	30			

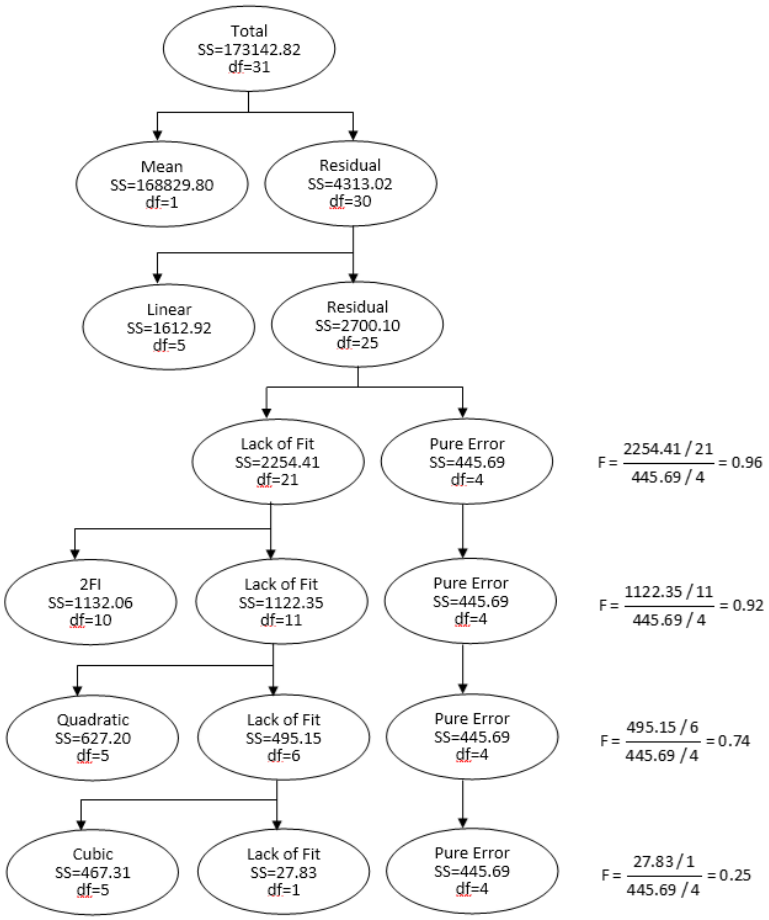

Figure 4.9. Calculations for lack of fit results in Table 4.4.

The variable D-Sand was not included in this table because its p-value = 0.9231 was too large. Though B-Silica Fume and E-Steel Fiber are also insignificant factors (p-value > 0.1) in this model, these two factors were included because more comparison to 7 day compressive strength can be made. The equation for the 7 day compressive strength includes B and E as shown in the following section. From Table 4-5, the model F-value of 3.88 implies the model is significant. There is only 1.34% chance that an F-value this large could occur due to noise. The "Lack of Fit F-value" of 0.92 implies the Lack of Fit is not significant relative to the pure error. There is a 61.27% chance that a "Lack of Fit F-value" this large could occur due to noise. Non-significant lack of fit is good, i.e. Lacof Fit p-value > 0.5.

For 28 day compressive strength, the fitted model can be expressed in two ways: one is the equation in terms of coded factors and the other one is the equation in terms of actual factors. The conversion from actual units to coded units can be obtained using the following equation:

$$X_{Coded} = \frac{X_{Actual} - \left(X_{Low} + X_{Hi}\right)/2}{\left(X_{Hi} - X_{Low}\right)/2} \tag{4.8}$$

where X_{Low} and X_{Hi} are the low level and high level of that factor and X_{Actual} is that factor's value in actual unit in CCD design. The final fitted equations are:

$$\hat{Y}_{28\,Com.} = 73.80 - 6.38 * A + 2.03 * B + 4.49 * C - 1.50 * E \tag{4.9}$$

in terms of coded factors where $\hat{Y}_{28\,Com.}$ is 28 day compressive strength and

$$\hat{Y}_{28\,Com.} = 211.10850 - 637.63889 * A + 67.73148 * B + 99.72222 * C - 149.58333 * E \tag{4.10}$$

in terms of actual factors. These confirmed the linear model (equation (4.3)) described in foregoing paragraph.

Both of these equations can be used to make predictions about the 28 day compressive strength for given levels of each factor. The coded equation has an advantage over the actual equation when

identifying the relative impact of the factors by comparing the factor coefficients. The actual equation should not be used to determine the relative impact of each factor because the coefficients are scaled to accommodate the units of each. However, the actual equation is an intuitive equation from which the 28 day compressive strength can be calculated directly.

The adequacy of this fitted model can be validated quantitatively by calculating statistical measures such as PRESS (Predicted Residual Sum of Squares) and adequate precision. These are shown in Table 4-6. The PRESS is a measure of how well a particular model fits each point in the design (the smaller the PRESS, the better the fit). The coefficients for the model are calculated with one point excluded. The new model's prediction is subtracted from the "deleted" observation to find the predicted residual. This is done for each data point. The smaller the PRESS is, the better the fit will be. In this case, this can be confirmed by comparing PRESS between models with and without D-Sand factor. The Press of 3797.94 without the D-Sand factor is better than that of 4085.67 with the D-Sand factor. The Adjusted R-squared value is a measure of the amount of variation about the mean explained by the model. In addition, the Predicted R-squared value is a measure of how well the model predicts a response value. The difference between Adjusted R-squared and Predicted R-squared should be within approximately 0.20. If they are not, there may be a problem with either the data or the model. In this study, the "Pred R-Squared" (Predicted R-Squared) of 0.1194 is in reasonable agreement with the "Adj R-Squared" (Adjusted R-Squared) of 0.2774, i.e. the difference is less than 0.2. An "Adeq Precision" (Adequate Precision) value of 7.032 is also acceptable because the ratio 7.032 is greater than the minimum desirable value of 4. Adequate precision is a measure of the range in predicted response relative to its associated error, in other words a signal to noise ratio.

Table 4.6. Summary statistics for 28 day compressive strength.

Std. Dev. (MPa)	10.19	R-Squared	0.3737
Mean (MPa)	73.80	Adj R-Squared	0.2774
C.V. %	13.81	Pred R-Squared	0.1194
PRESS	3797.94	Adeq Precision	7.032

4.2.2 Model Diagnostics

In the analysis of model fitting, ANOVA was used. However, there are three assumptions for ANOVA:

i) Independence of observations

ii) Normality – distribution of the residuals are normal

iii) Equality (or homogeneity) of variances – the variance of data in groups, i.e. a constant σ^2.

The first assumption can be tested by using a plot of residuals in a time sequence. The independence assumption can be validated if the there is no obvious pattern on the plot. Figure 4-10 shows the plot of residuals in a time sequence (as represented by the run number). Figure 4-10 is evidently structureless as there is no any observable pattern. This supports the validity of the independence assumption of observations. If there was a trend on the plot, this would be a serious problem and it is difficult to correct. As a result, it is important to prevent this problem when the data are collected. Proper randomization of the experiments is an important step in obtaining independence.

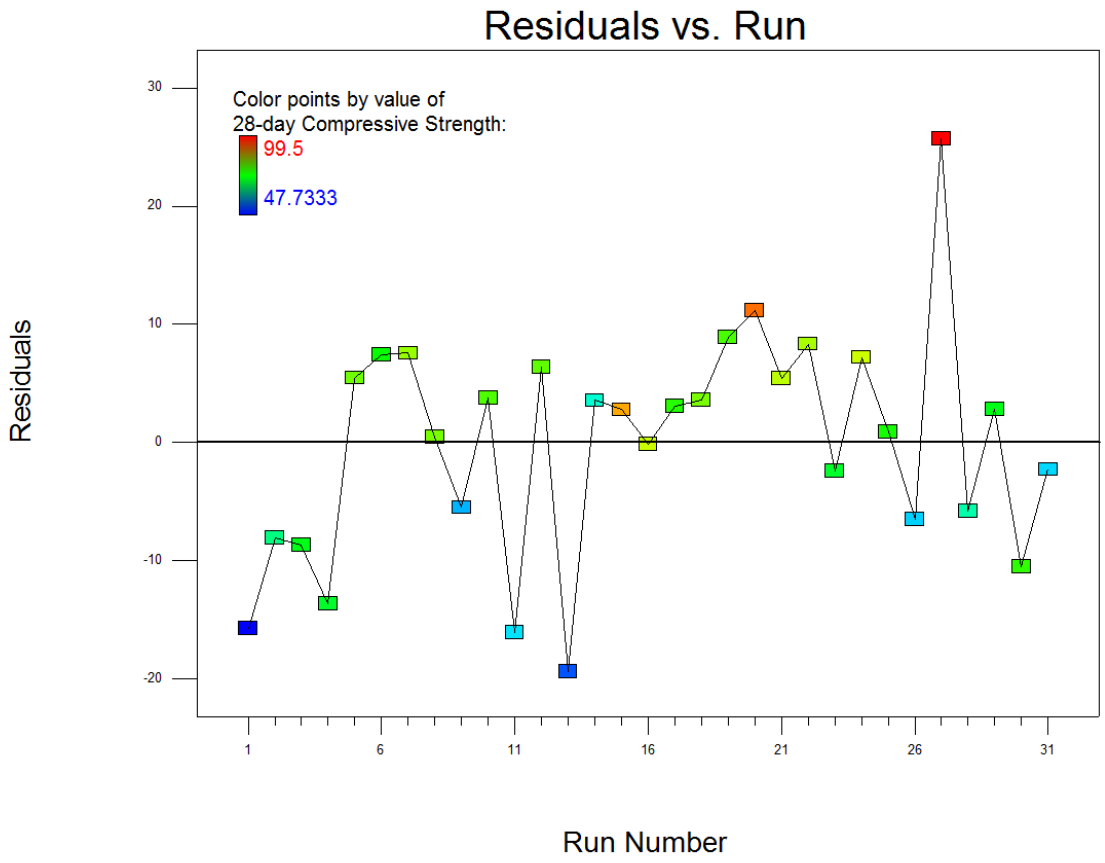

Figure 4.10. Plot of residuals vs. run for 28 day compressive strength.

The normality assumption can be tested by constructing a normal probability plot of the residuals. If the underlying error distribution is normal, this plot will resemble a straight line. The normal plot of residuals is shown in Figure 4.11. From Figure 4.11, it is clear that data points representing the 28 day compressive strength are approximately linearly varying, though there are some minor departures. In general, moderate departures from normality are of little concern. This shows the validity of normality assumption. The normal probability was calculated according to the following formula:

$$Normal\ \ probability = \frac{1}{n}(j - 0.5),\ \ j = 1, 2, 3, \cdots n \tag{4.11}$$

where *n* is the number of design, here *n* is 31, and *j* is the *j*th design.

The assumption of equality of variances was tested by plotting residuals versus fitted or predicted values. The plot should be randomly scattered and structureless if the assumption is true. Figure 4.12 shows the plot of residuals versus predicted values. Since there is no obvious pattern or trend on Figure 4.12, this suggests that the assumption of constant variances was validated.

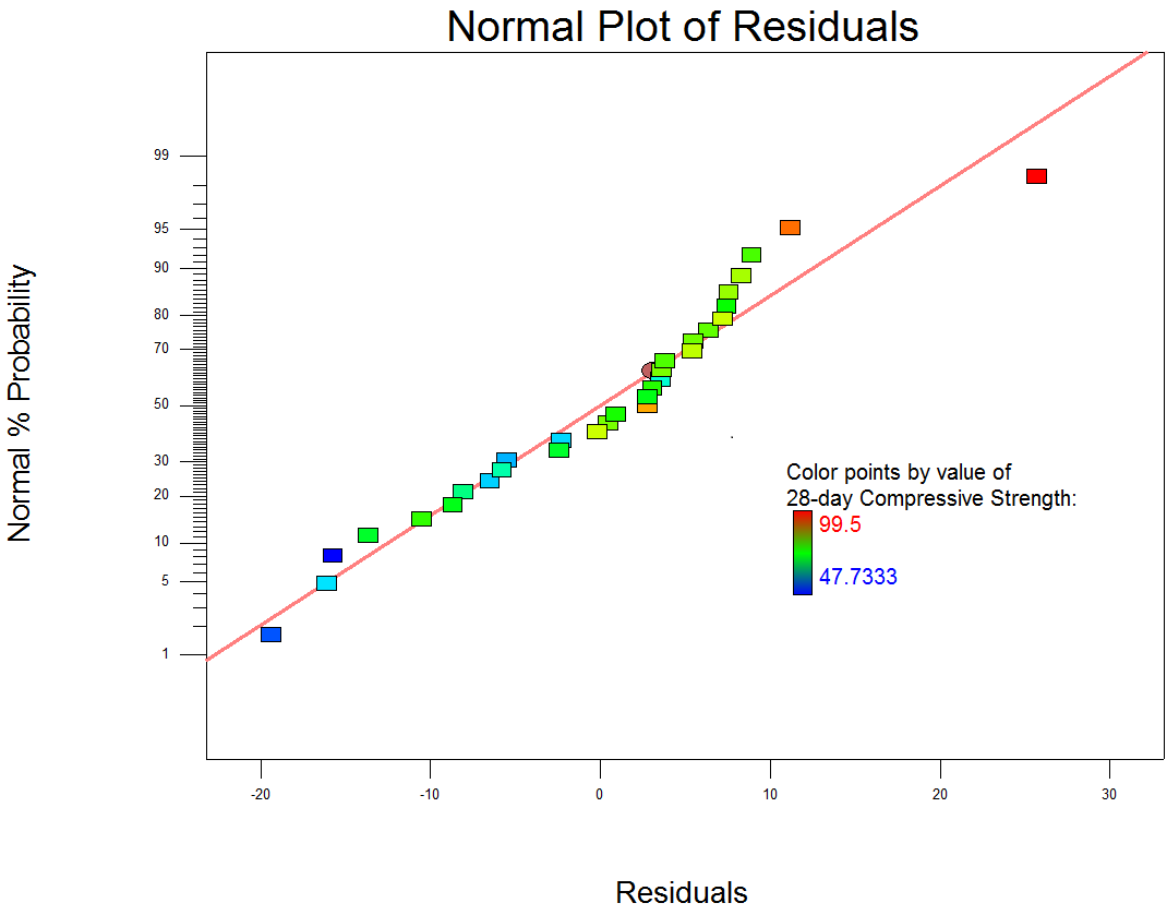

Figure 4.11. Normal probability plot of residuals for 28 day compressive strength.

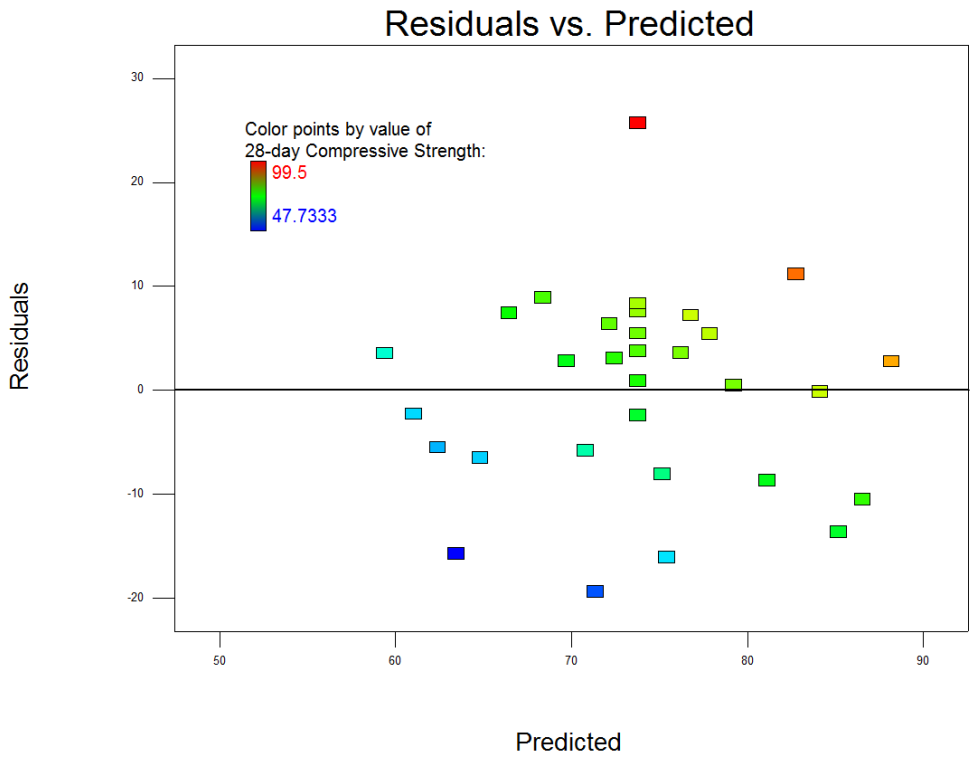

Figure 4.12. Plot of residuals vs. predicted values for 28 day compressive strength.

To confirm the assumption of constant variances, the plot of externally studentized residuals versus predicted values is shown in Figure 4.13. As for Figure 4.13, this figure shows random scatter and a lack of structure. Besides this, Figure 4.13 can also help the experimenter detect outliers in the data. If there are points outside the red lines which were generated by calculating a t distribution with significance level of 0.05, this means that data points are not fit well by the current model. Either the observed value was wrong or the model is wrong. Usually, typographical errors are the most common causes of outliers. If typographical errors are not the reason for the discrepancy, further investigation must be conducted on those points.

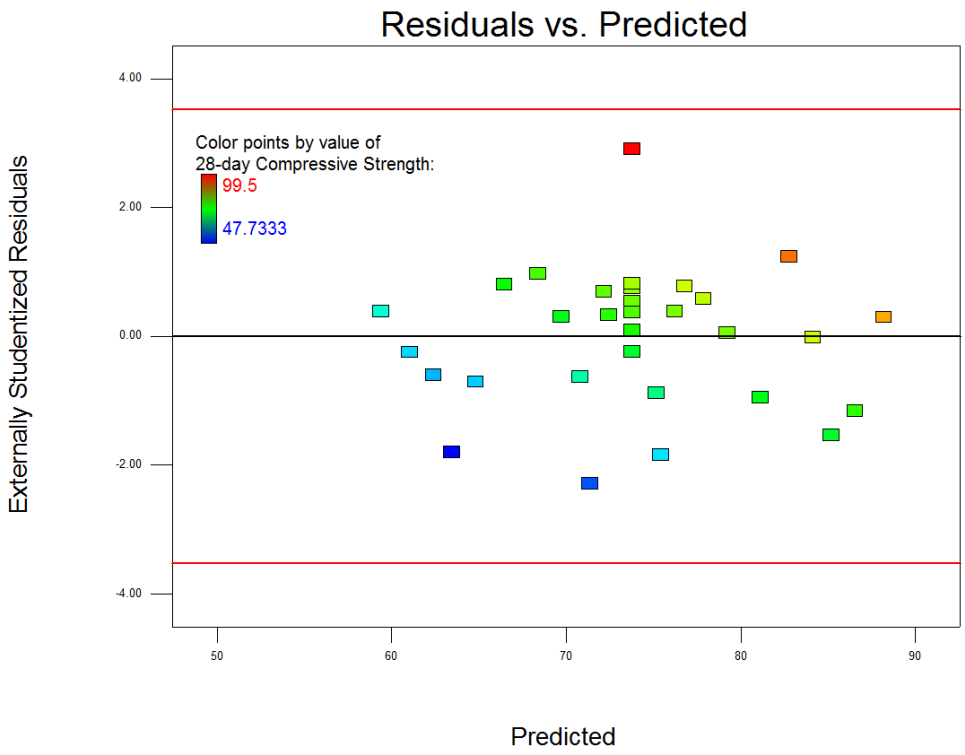

Figure 4.13. Plot of externally studentized residuals vs. predicted values for 28 day compressive strength.

From Figure 4.10 to 4.13, no statistical problems were found. This linear model (equation (4.5) or equation (4.6)) therefore satisfies the three assumptions of ANOVA. After validation, a 3D response surface was obtained as illustrated in Figure 4.14, shown here with a fixed C-Silica Flour mass ratio of 0.16 and E-Steel Fiber mass ratio of 0.22 set at their middle levels since only three variables can be represented on this 3-dimensional graph. From this figure, the relationships between 28 day compressive strength, A-Water, and B-Silica Fume can be observed. It is evident that the 28 day compressive strength increases with decreasing A-Water (or, more specifically, with the W/C ratio) and increasing B-Silica Fume mass ratios for the levels of silica flour and steel fiber selected for this plot. However, there is no information on C-Silica Flour and E-Steel Fiber on Figure 4.14. Next, a special perturbation plot was constructed as shown in Figure 4.15 with all

the variables at their middle levels for mass ratios, i.e. A-Water = 0.21, B-Silica Fume = 0.20, C-Silica Flour = 0.16, and E-Steel Fiber = 0.22.

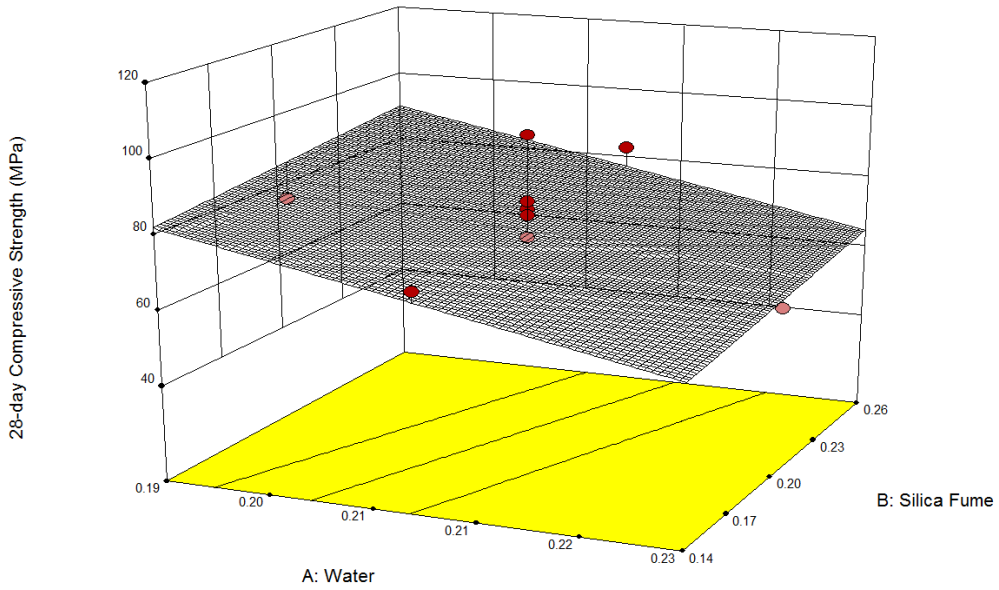

Figure 4.14. Response surface of 28 day compressive strength.

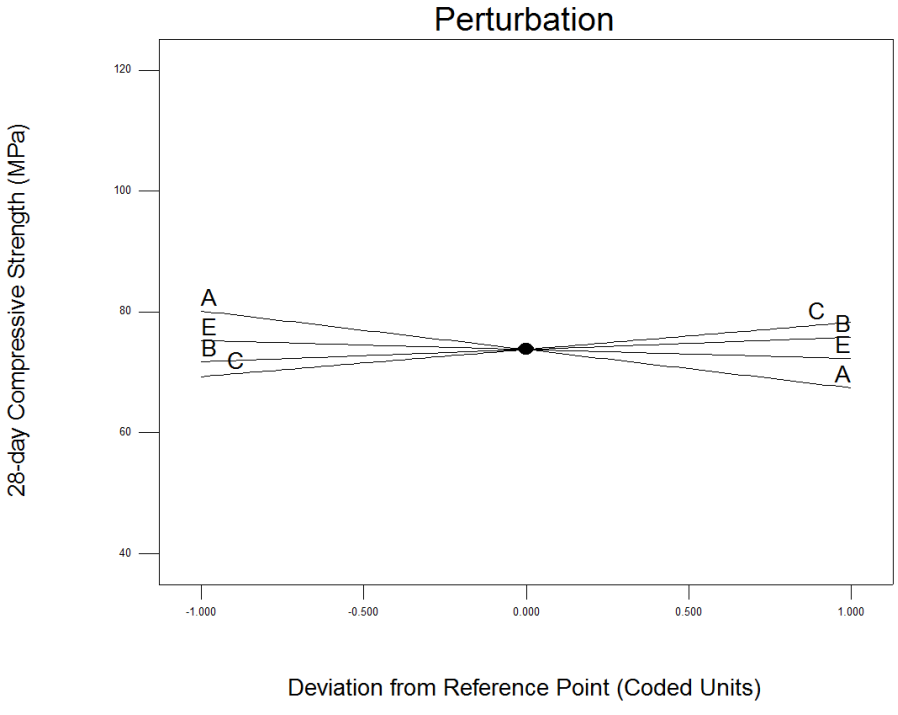

Figure 4.15. Perturbation plot of 28 day compressive strength.

The perturbation plot helps to compare the effect of all the factors at a particular point in the design space. The response is plotted by changing only one factor over its range while holding all the other factors constant. A steep slope or curvature in a factor shows that the response is sensitive to that factor. A relatively flat line shows insensitivity to change in that particular factor. From Figure 4.15, it can be observed that E-Steel Fiber has the least effect on the model, A –Water is the most effective factor, C-Silica Flour is the second-most influential, and B-Silica Fume is the third most effective factor at their center points. This fact can also be verified through checking the absolute values of coefficients of the coded fitted equation as described before.

4.3 7 day Compressive Strength

7 day compressive strength is usually used to monitor early concrete compressive strength gain. For normal concrete, it is often estimated to be about 75% of the 28 day strength (Kosmatka et al. 2003). However, Neville (Neville 1996) suggests that if the 28 day compressive strength is to be estimated at 7 day, a relationship between the 28 day and 7 day strengths has to be established experimentally for the given concrete. There is no reliable relationship between these two strengths. Regardless of the reliability of the estimate for 28 day compressive strength, 7 day strength test results are useful to contractors and concrete producers as an early warning signal. If a low 7 day compressive strength occurs, suitable steps can be taken promptly to adjust batch quantities and improve the quality of concrete.

A standard deviation bar plot is illustrated in Figure 4.16. From this figure, the uncertainty of tested 7 day compressive strength is seen to be acceptable similar with 28 day compressive strength. The observed maximum 7 day compressive strength was 62 MPa at design #30 and the minimum value was 36 MPa at design #1 which is also the minimum 28 day strength design.

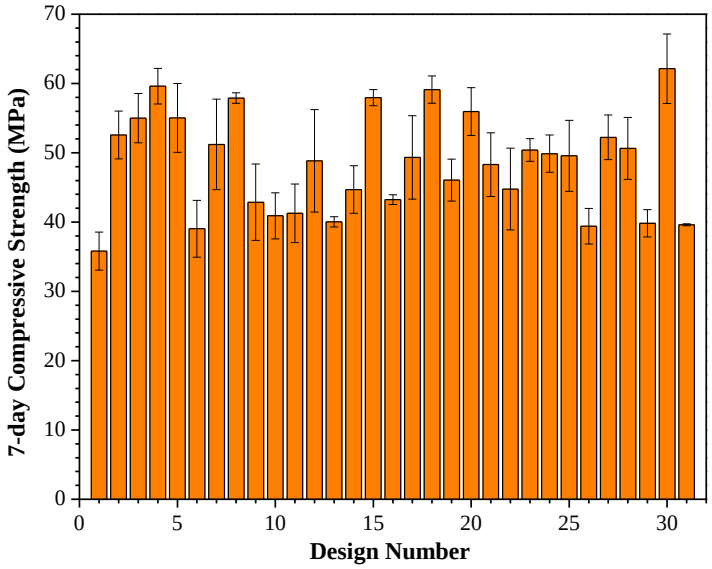

Figure 4.16. 7 day compressive strength with error bars.

Relationships among 7 day compressive strength and related factors could be obtained from scatter plots. Scatter plots of 7 day compressive strength vs. W/C, silica fume, silica flour, sand and steel fiber are shown in Figures 4.17 to 4.21, respectively.

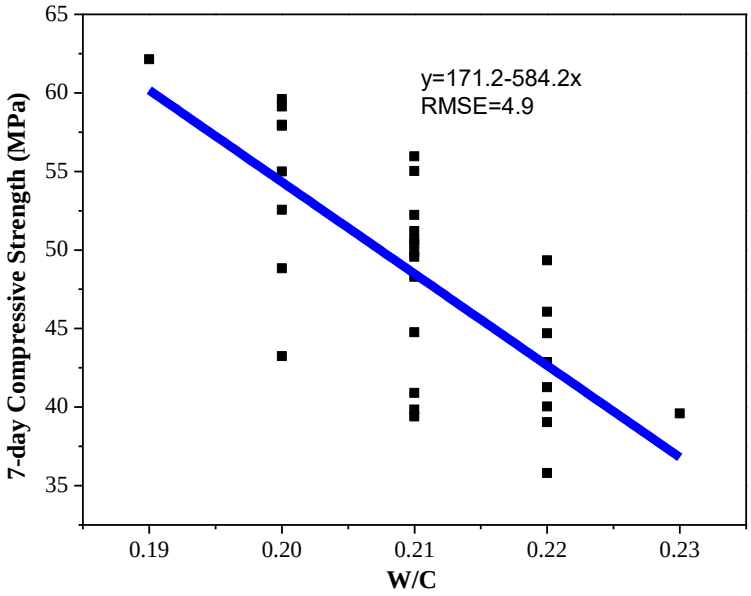

Figure 4.17. 7 day compressive strength vs. W/C ratio.

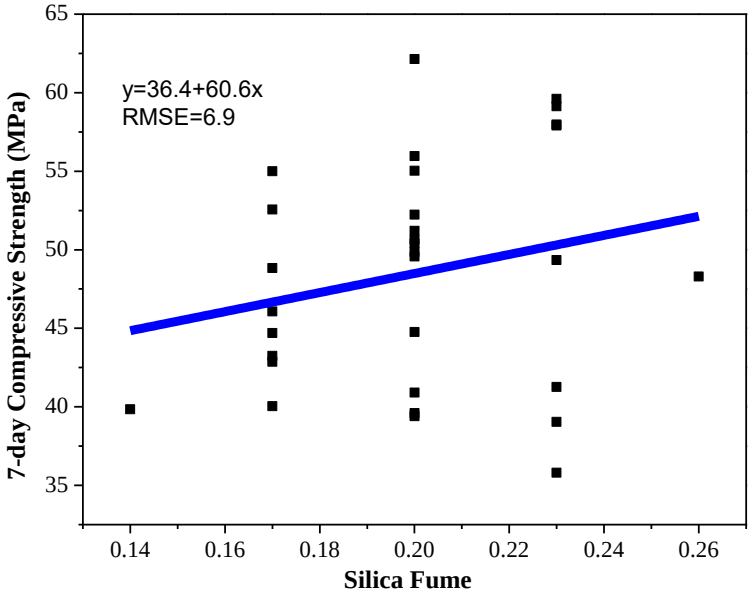

Figure 4.18. 7 day compressive strength vs. silica fume.

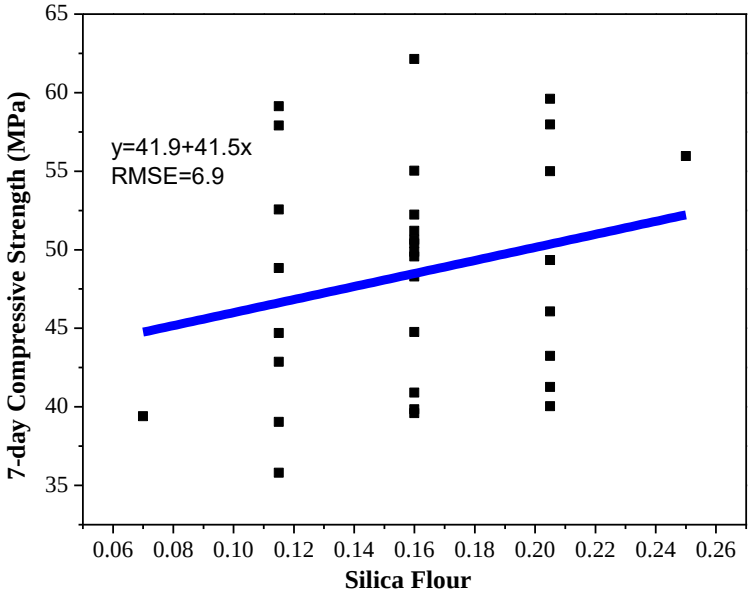

Figure 4.19. 7 day compressive strength vs. silica flour.

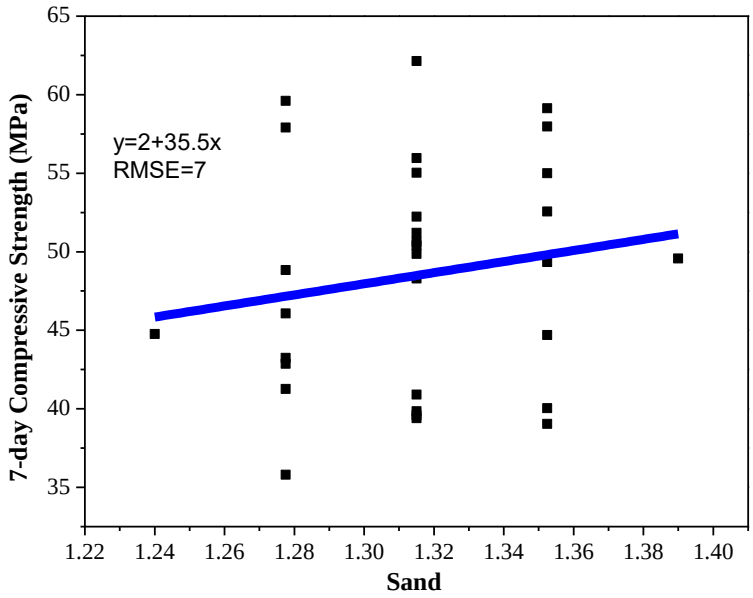

Figure 4.20. 7 day compressive strength vs. sand.

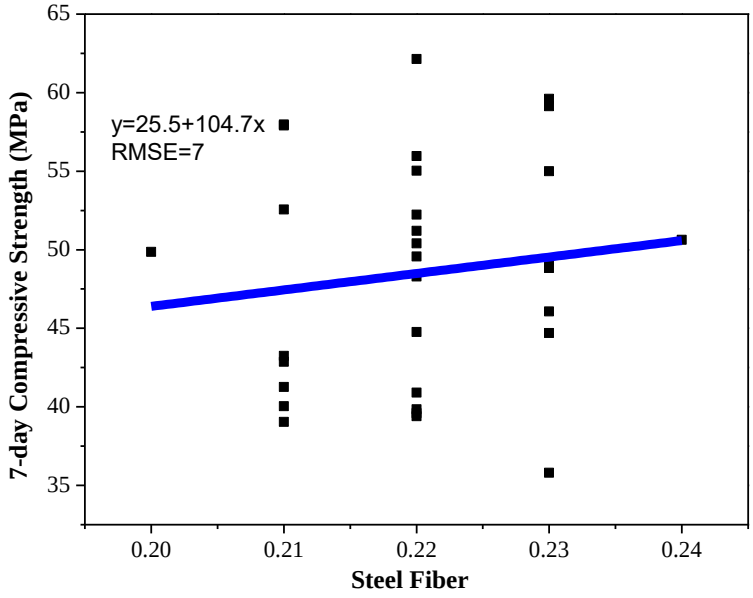

Figure 4.21. 7 day compressive strength vs. steel fiber.

From these plots, the general impression is that the 7 day compressive strength increases with decreasing W/C ratio, and increasing silica fume, silica flour, sand and steel fiber. The linear equation can be deduced as:

$$Y_{7\,Com.} = a_0 - aA + bB + cC + dD + eE \tag{4.12}$$

where a_0 is the intercept of the function, and *a* , *b*, *c*, *d*, and *e* are positive or zero values. And *A*, *B*, *C*, *D*, *E* are denoted as W/C, silica fume, silica flour, sand and steel fiber, respectively.

Figure 4.22 shows the ratio of 7 day to 28 day compressive strength. Only some of the results reveal that the 7 day compressive strength is about 75% of 28 day compressive strength. The ratio varies from 51.5% to 83.3% with the average ratio of 66.5% (denoted by the blue line in Figure 4-22). The 28 day compressive strength can be calculated by dividing 7 day compressive strength by the ratio of 7 day to 28 day compressive strength. If the ratio is taken to the maximum value, the minimum 28 day compressive strength will be estimated. Though there is no unique relationship between 7 day and 28 day compressive strength, 28 day compressive strength still can be estimated from the 83.3% ratio. The 7 day compressive strength is then still a useful, conservative indicator of 28 day compressive strength.

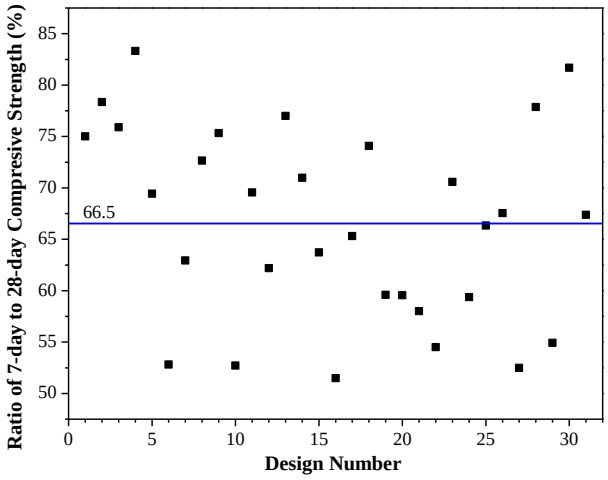

Figure 4.22. Ratio of 7 day to 28 day compressive strength.

4.3.1 Model Fitting

The ANOVA for significance of regression in 7 day compressive strength is shown in Table 4-7. All the explanations of terms in Section can be found in Section 4.2.1.

Table 4.7. Sequential model sum of squares for 7 day compressive strength.

Source	Sum of Squares	df	Mean Square	F Value	p-value Prob > F
Mean vs Total	72887.42	1	72887.42		
Linear vs Mean	1050.53	5	210.11	10.43	< 0.0001
2FI vs Linear	243.72	10	24.37	1.41	0.2666
Quadratic vs 2FI	69.67	5	13.93	0.73	0.6155
Cubic vs Quadratic	72.66	5	14.53	0.62	0.6949
Residual	117.58	5	23.52		
Total	74441.58	31	2401.34		

The linear model is seen to be the best choice from Table 4-7, because the p-value of linear model is less than 0.05, whereas the others are all greater than 0.05. Lack of Fit Tests is shown in Table 4.8., indicating that the linear model has an insignificant lack of fit (the p-value is 0.7753).

Table 4.8. Lack of Fit Tests for 7 day compressive strength.

Source	Sum of Squares	df	Mean Square	F Value	p-value Prob > F
Linear	388.90	21	18.52	0.65	0.7753
2FI	145.19	11	13.20	0.46	0.8607
Quadratic	75.52	6	12.59	0.44	0.8243
Cubic	2.86	1	2.86	0.100	0.7679
Pure Error	114.72	4	28.68		

The ANOVA for this linear model is shown in Table 4-9. Though the D-Sand (p-value = 0.1605) and E-Steel Fiber (p-value = 0.2639) are insignificant factors (p-value > 0.1) in this model, these two factors were kept to investigate the relationships among response and these factors. The model

F-value of 10.43 implies the model is significant. The chance that an F-value this large could occur due to noise is < 0.0001, which is very small. The "Lack of Fit F-value" of 0.65 implies the Lack of Fit is not significant relative to the pure error. There is a 77.53% chance that a "Lack of Fit F-value" this large could occur due to noise.

The final fitted equations for 7 day compressive strength are:

$$\hat{Y}_{7\,Com.} = 48.49 - 5.84 * A + 1.82 * B + 1.87 * C + 1.32 * D + 1.05 * E \tag{4.13}$$

in terms of coded factors, where $\hat{Y}_{7\,Com.}$ is the 7 day compressive strength, and

Table 4.9. ANOVA for 7 day compressive strength.

Source	Sum of Squares	df	Mean Square	F Value	p-value Prob > F
Model	1050.53	5	210.11	10.43	< 0.0001
A-Water	819.00	1	819.00	40.66	< 0.0001
B-Silica Fume	79.45	1	79.45	3.94	0.0581
C-Silica Flour	83.63	1	83.63	4.15	0.0523
D-Sand	42.13	1	42.13	2.09	0.1605
E-Steel Fiber	26.32	1	26.32	1.31	0.2639
Residual	503.63	25	20.15		
Lack of Fit	388.90	21	18.52	0.65	0.7753
Pure Error	114.72	4	28.68		
Cor Total	1554.16	30			

$$\hat{Y}_{7\,Com.} = 82.89536 - 584.16667 * A + 60.64815 * B + 41.48148 * C + 35.33333 * D + 104.72222 * \mathrm{E} \tag{4.14}$$

in terms of actual factors. From the coded equation, it can be concluded that the order of impacts of factors is A>C>B>D>E from comparing the coefficients of the factors.

A summary statistic table is shown in Table 4-10. The "Pred R-Squared" (Predicted R-Squared) value of 0.5043 is in reasonable agreement with the "Adj R-Squared" (Adjusted R-Squared) value of 0.6111, i.e. the difference is less than 0.2. In addition, the "Adeq Precision" (Adequate Precision) value of 11.943 is desirable because the ratio is greater than 4.

Table 4.10. Summary statistics for 7 day compressive strength.

Std. Dev.	4.49	R-Squared	0.6759
Mean	48.49	Adj R-Squared	0.6111
C.V. %	9.26	Pred R-Squared	0.5043
PRESS	770.42	Adeq Precision	11.943

4.3.2 Model Diagnostics

The plot of residuals in time sequence is shown in Figure 4.23. There is no pattern on this figure. This shows the validity of independence assumption of observations.

The normal plot of residuals is shown in Figure 4.24. The data points of 7 day compressive strength are approximately linear though there are some minor departures. This shows the validity of normal assumption.

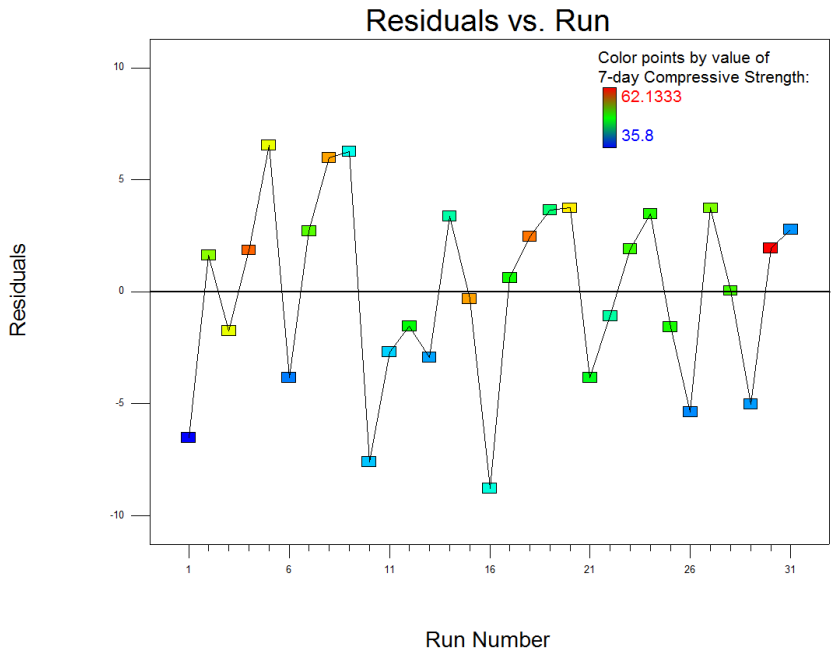

Figure 4.23. Plot of residuals vs. run for 7 day compressive strength.

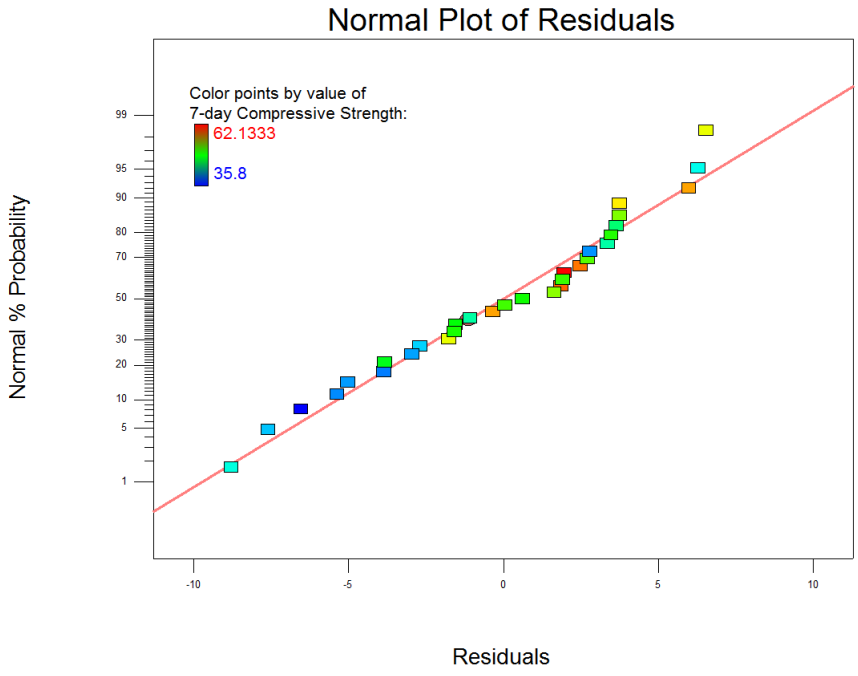

Figure 4.24. Normal probability plot of residuals for 7 day compressive strength.

The plot of residuals versus predicted values and the plot of externally studentized residuals versus predicted values are illustrated in Figure 4.25 and 4.26. There are no patterns or trends on Figure 4.25 and 4.26. As a result, the assumption of constant variances appears to be validated. Therefore, this linear model satisfies the 3 assumptions of ANOVA.

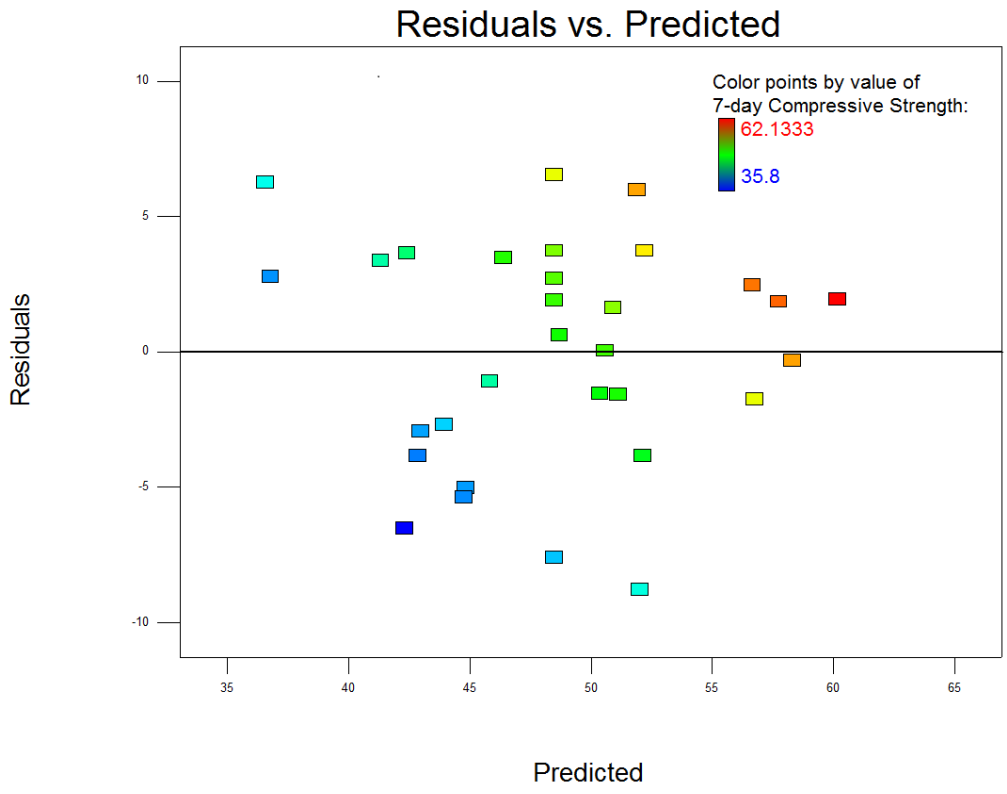

Figure 4.25. Plot of residuals vs. predicted values for 7 day compressive strength.

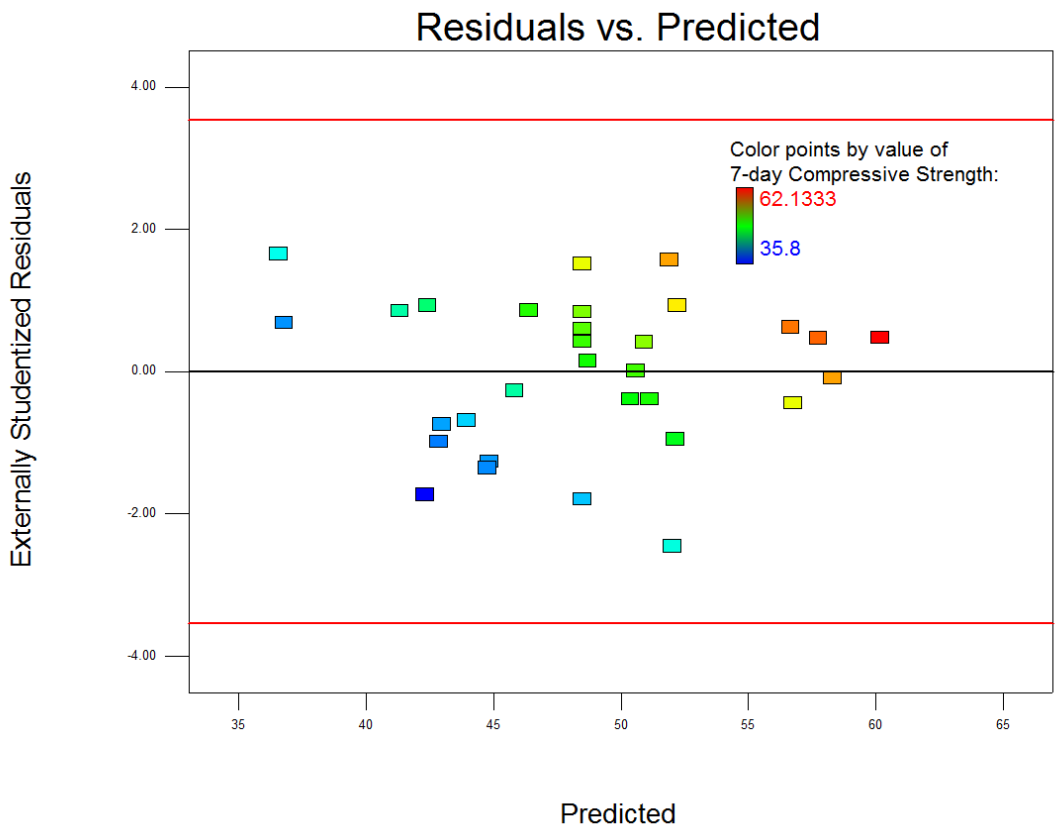

Figure 4.26. Plot of externally studentized residuals vs. predicted values for 7 day compressive strength.

4.4 28 day Splitting Tensile Strength

The 28 day splitting strength is used to deduce flexural strength of concrete because it is usually lower than flexural strength (ASTM C496 / C496M-11 2004). A standard deviation bar plot is illustrated in Figure 4.27. The uncertainty of tested 28 day splitting tensile strength is acceptable, similar as 28 day compressive strength. The observed maximum 28 day splitting tensile strength is 30.3 MPa at design #5 and the minimum value of that is 18.6 MPa at design #30.

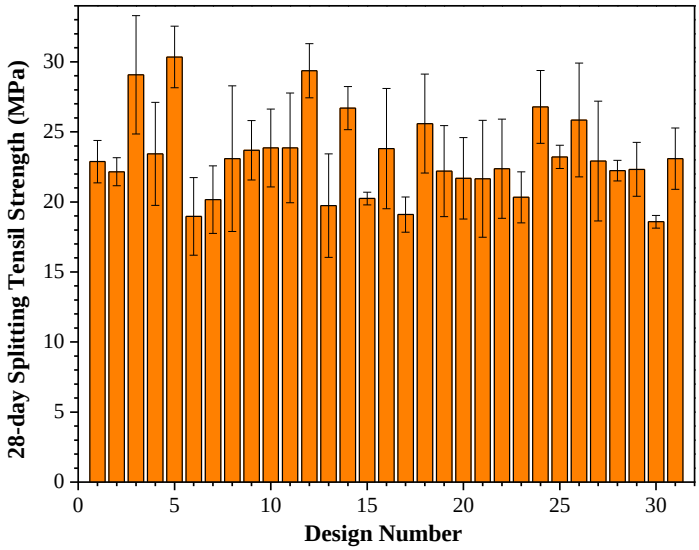

Figure 4.27. 28 day splitting tensile strength with error bars.

4.4.1 Model Fitting

The summary statistics table for splitting tensile strength is shown in Table 4.11.

Table 4.11. Summary statistics for 28 day splitting tensile strength.

Source	Sequential p-value	Lack of Fit p-value	Adjusted R-Square	Predicted R-Square
Linear	0.3620	0.9202	0.0240	-0.1924
2FI	0.8703	0.8344	-0.2251	-4.9765
Quadratic	0.9404	0.6386	-0.6475	-7.2028
Cubic	0.4763	0.7172	-0.6015	-10.0404

The value of predicted R-squared for linear model (equation (2.8)) is negative number -0.1924. This means that overall mean is a better model. As a result, the fitted model is:

$$\hat{Y}_{28\,splitting} = 23.2 \tag{4.15}$$

where $\hat{Y}_{28\,splitting}$ is the estimated 28 day splitting tensile strength.

4.5 Air Content for Hardened Concrete

Air content can be used to estimate the resistance to freezing and thawing. Because only one slab was used for each batch, there is no error bar plot. The air content for this project is illustrated in Figure 4.28 with maximum value of 6.9% at design #2 and the minimum value of 1.8% at design #7.

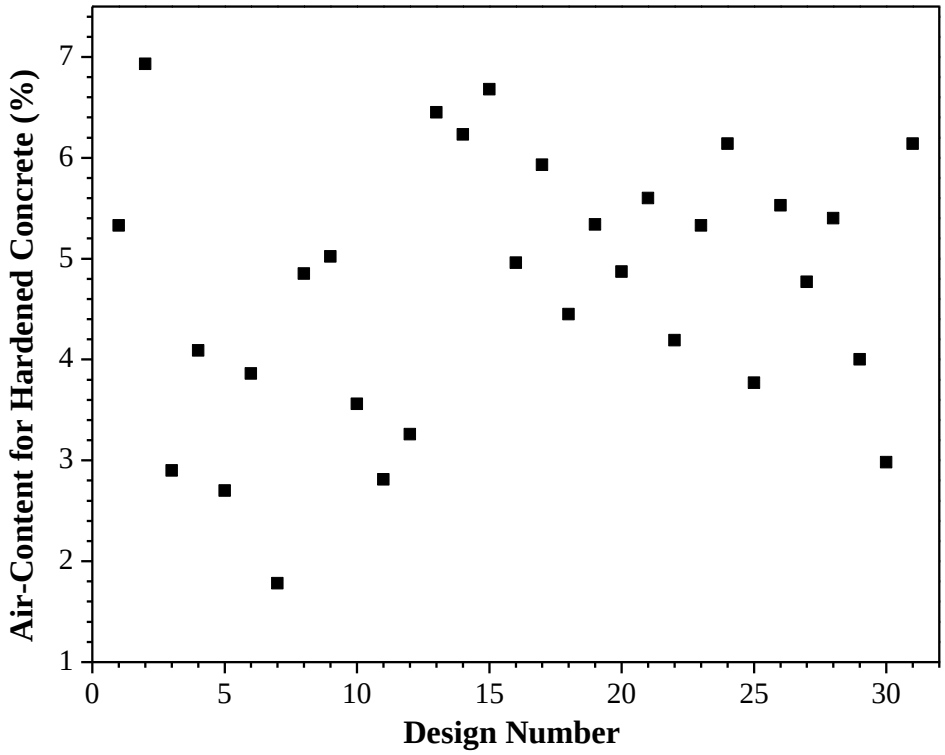

Figure 4.28. Air content for hardened concrete.

4.5.1 Model Fitting

Table 4.12 shows the ANOVA for significance of regression in air content for hardened concrete.

Table 4.12. Sequential model sum of squares for air content of hardened concrete.

Source	Sum of Squares	df	Mean Square	F Value	p-value Prob > F
Mean vs Total	686.20	1	686.20		
Linear vs Mean	6.95	5	1.39	0.78	0.5768
2FI vs Linear	19.96	10	2.00	1.20	0.3616
Quadratic vs 2FI	10.35	5	2.07	1.42	0.2959
Cubic vs Quadratic	5.83	5	1.17	0.67	0.6646
Residual	8.71	5	1.74		
Total	738.00	31	23.81		

In this case, the quadratic model is the best choice from Table 4-12 though the p-value of 0.2959 is insignificant. That is because this p-value is lower than those for the remaining models. The purpose for model fitting is to search for the most suitable model for the data.

Table 4.13 illustrates the ANOVA for this quadratic model. Though E-Steel Fiber (p-value = 0.3096) is seen to be an insignificant factor (p-value > 0.1) in this model, it was retained to support a hierarchy for the quadratic model. The model F value of 4.50 implies the model is significant. The chance that an F-value this large could occur due to noise is 0.68%. The "Lack of Fit F-value" of 0.47 implies the Lack of Fit is not significant relative to the pure error. There is a 88.58% chance that a "Lack of Fit F-value" this large could occur due to noise.

A summary statistics table is illustrated in Table 4.14. The "Pred R-Squared" (Predicted R-Squared) value of 0.2120 is in reasonable agreement with the "Adj R-Squared" (Adjusted R-Squared) value of 0.3179, i.e. the difference is less than 0.2. The "Adeq Precision" (Adequate Precision) value of 7.266 is desirable because the ratio is greater than 4.

Table 4.13. ANOVA for quadratic model of air content.

Source	Sum of Squares	df	Mean Square	F Value	p-value Prob > F
Model	21.18	4	5.29	4.50	0.0068
A-Water	3.50	1	3.50	2.97	0.0964
E-Steel Fiber	1.27	1	1.27	1.07	0.3096
AE	11.24	1	11.24	9.54	0.0047
E^2	5.17	1	5.17	4.39	0.0460
Residual	30.62	26	1.18		
Lack of Fit	22.14	22	1.01	0.47	0.8858
Pure Error	8.48	4	2.12		
Cor Total	51.80	30			

Table 4.14. Summary statistics for air content of hardened concrete.

Std. Dev.	1.09	R-Squared	0.4089
Mean	4.70	Adj R-Squared	0.3179
C.V. %	23.07	Pred R-Squared	0.2120
PRESS	40.82	Adeq Precision	7.266

4.5.2 Model Diagnostics

Figure 4.29 shows the plot of residuals in time. There is no concern about the validity of independence assumption of observations.

The normal plot of residuals is shown in Figure 4.30. The linear data pattern supports the validity of the normal assumption.

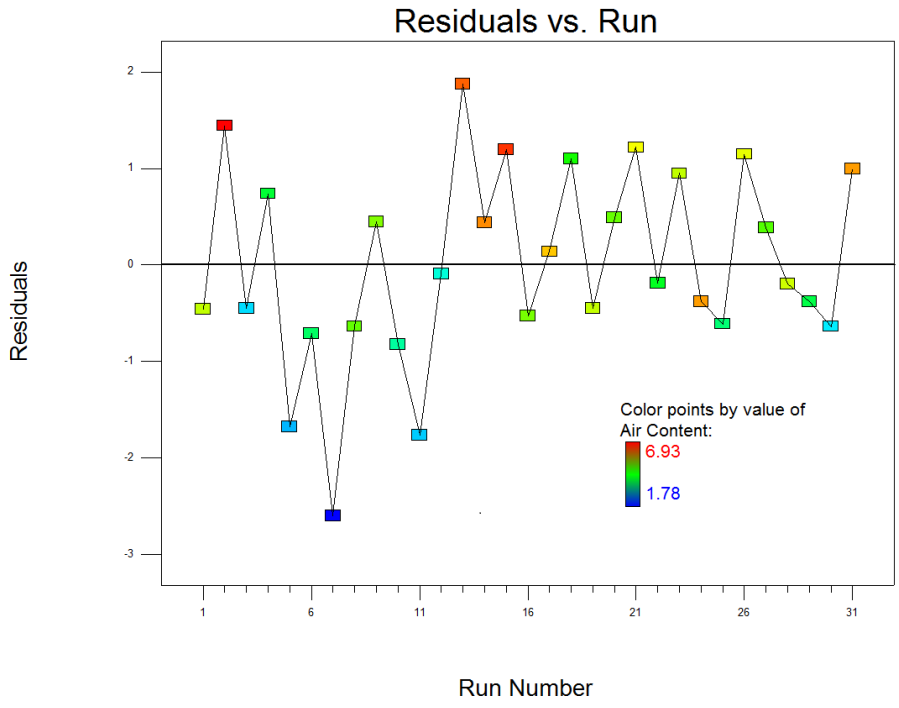

Figure 4.29. Plot of residuals vs. run for air content of hardened concrete.

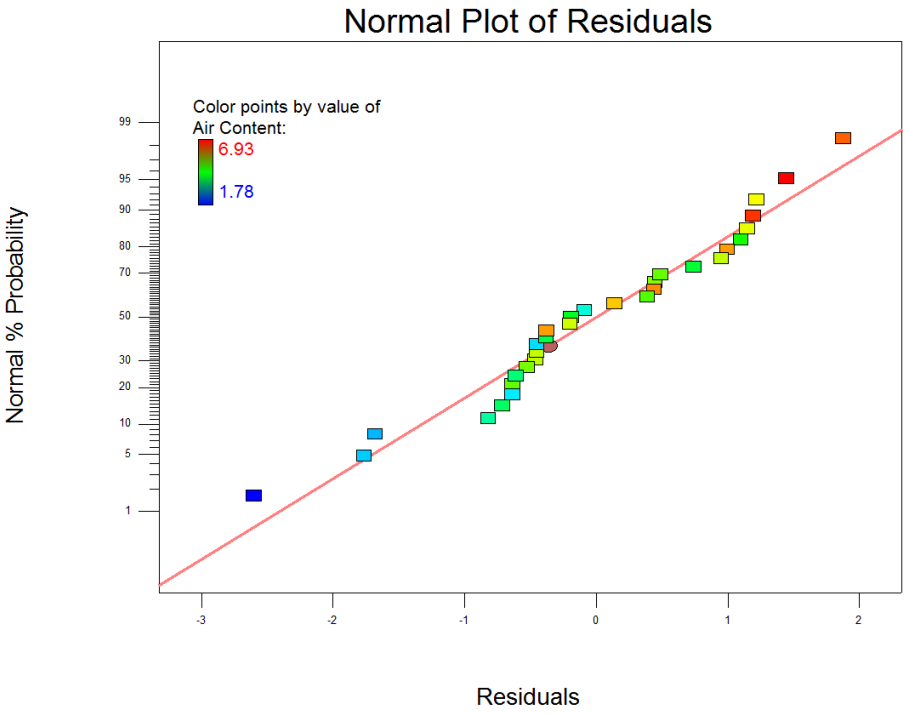

Figure 4.30. Normal probability plot of residuals for air content of hardened concrete.

Figure 4.31 and 4.32 show the plot of residuals versus predicted values and the plot of externally studentized residuals versus predicted values, respectively. Structureless patterns suggest the validation of the assumption of constant variances. This quadratic model therefore satisfies the three assumptions of ANOVA.

Figure 4.33 shows the response surface for air content of hardened concrete. Air content can be found on response surface.

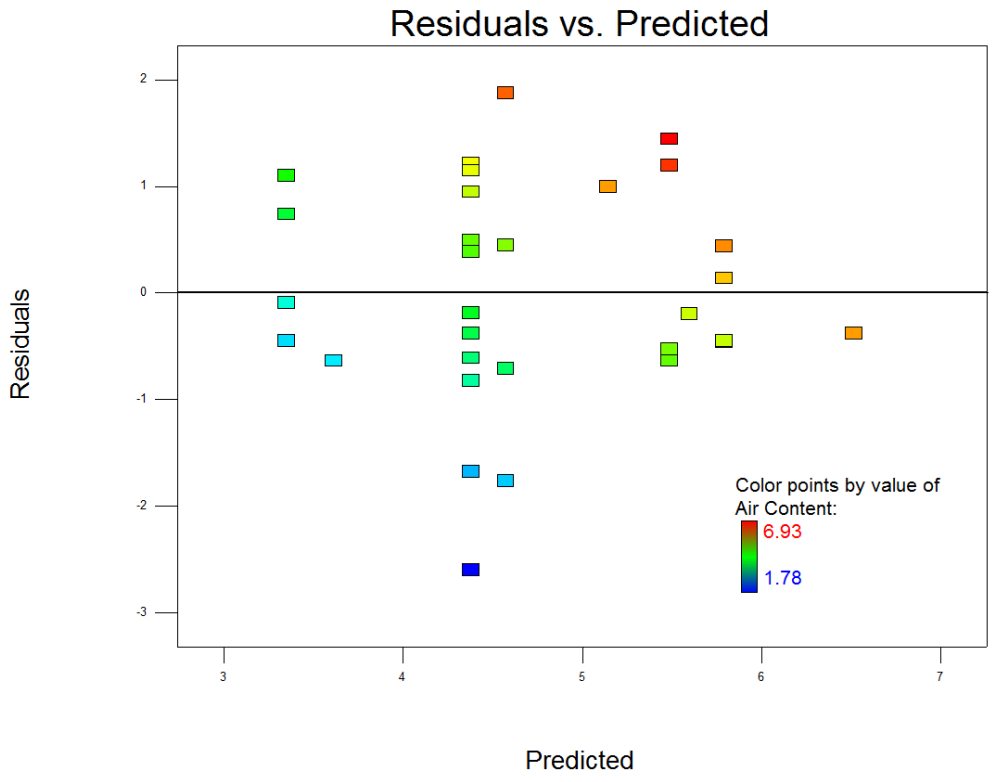

Figure 4.31. Plot of residuals vs. predicted values for air content of hardened concrete.

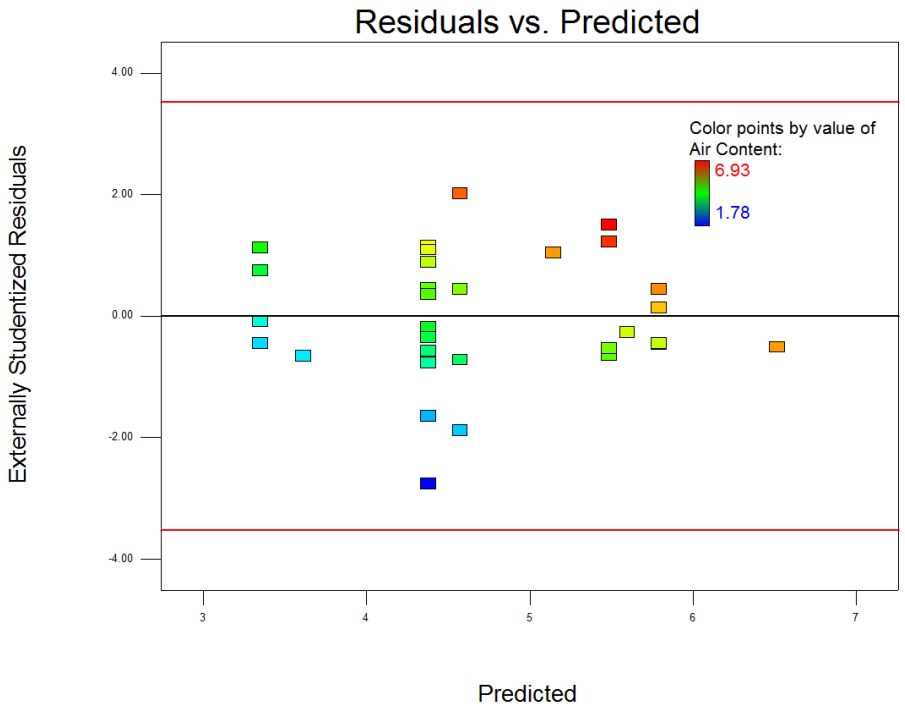

Figure 4.32. Plot of externally studentized residuals vs. predicted values for air content of hardened concrete.

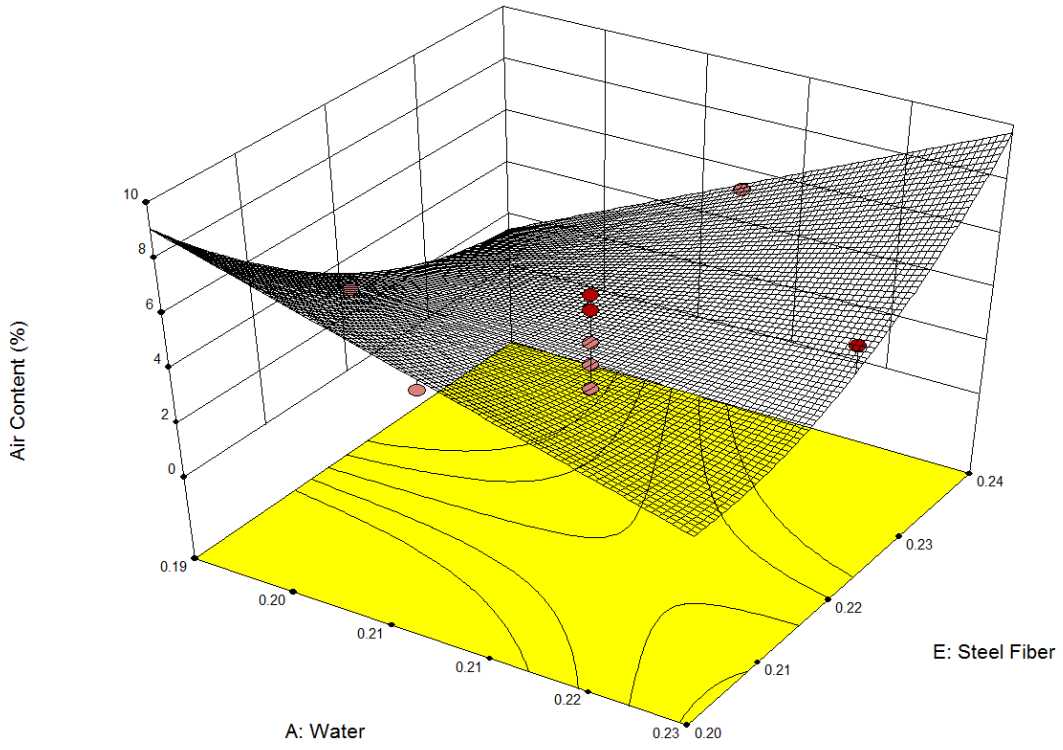

Figure 4.33. Response surface for air content of hardened concrete.

4.6 Concrete Cost

The estimated cost of the concrete mix designs is illustrated in Figure 4.34, based on the price of materials purchased from local distributors. Superplasticizer was sponsored by CHRYSO company in Rockwall, Texas. Because the costs of water and superplasticizer were unknown, the costs for these materials were not included in the final costs (dollars/m^3). It should be noted that the concrete costs cited here cannot be used for commercial purposes. Rather, they are only an indicator of the relative cost among the designs. Table 4.15 shows the prices and specific gravities of materials.

Table 4.15. Prices and specific gravities of materials.

	Cement	Silica Fume	Silica Flour	Sand	Steel Fiber
Price (dollars/kg)	0.85	1.508	2.227	0.397	5.49
Specific Gravity	3.15	2.2	2.65	2.65	7.85

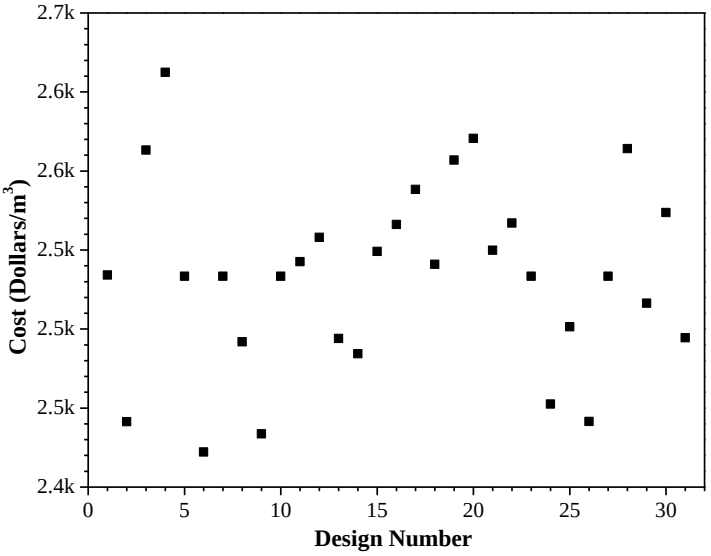

Figure 4.34. Concrete cost.

Letting *A*, *B*, *C*, *D* and *E* denote the ratios to cement (by mass) of water, silica fume, silica flour, sand and steel fiber, respectively, the concrete price (dollars) based on 1 kg of cement included is therefore given by:

$$\text{Concrete Price} = 0.85 + 1.508 * \text{B} + 2.227 * \text{C} + 0.397 * \text{D} + 5.49 * \text{E} \tag{4.16}$$

and the volume (m^3) for that concrete is:

$$\text{Concrete Volume} = \frac{1}{3150} + \frac{\text{A}}{1000} + \frac{\text{B}}{2200} + \frac{\text{C}}{2650} + \frac{\text{D}}{2650} + \frac{\text{E}}{7850} + \frac{75}{10^6} \ . \tag{4.17}$$

Combining these two expressions, the unit cost (dollars/m^3) can be derived in terms of price/volume as:

$$Cost = \frac{0.85 + 1.508 * B + 2.227 * C + 0.397 * D + 5.49 * E}{\frac{1}{3150} + \frac{A}{1000} + \frac{B}{2200} + \frac{C}{2650} + \frac{D}{2650} + \frac{E}{7850} + \frac{75}{10^6}} \ . \tag{4.18}$$

This equation cannot be input into the Design-Expert software to do the optimization due to the limitation of the software (only a polynomial model is accepted). However, a fitted equation can be obtained using a similar analysis to that of air content. The final fitted model (in actual factors with cost unit of dollars/m^3) is:

$$\begin{aligned} Cost = {} & 2361.9 - 3341.7 * A + 494.9 * B + 1710.7 * C - 718.3 * D + 6833.7 * E \\ & + 528.2 * AB - 172.2 * AC + 961.5 * AD - 2886.2 * AE \\ & - 431.7 * BC + 80.7 * BD - 1472.6 * BE \\ & - 160.8 * CD - 1307.6 * CE - 1142.1 * DE \\ & + 1551.5 * A^2 - 99.2 * B^2 - 293.9 * C^2 + 129.2 * D^2 - 403.1 * E^2 \end{aligned} \tag{4.19}$$

The model can be confirmed by the plot of predicted values versus actual values as shown in Figure 4.35. It can be seen that the predicted points are exactly on the 45 degree line. This means the predicted values of costs are exactly the same as the calculated values.

4.7 Multiple Responses Optimization

The purpose of optimization is to best meet a set of specifications. Best specifications may mean maximizing, minimizing, or targeting a response or responses. In this project, multiple responses were involved simultaneously in the optimization problem. The responses involved are 7 day compressive strength, 28 day compressive strength, 28 day splitting tensile strength, air content for hardened concrete and concrete cost (dollars/m^3). Since multiple responses were involved, graphical optimization was not adopted. Alternatively, numerical optimization was employed. So far, all the fitted models for these responses were obtained in preceding descriptions. However, the fitted model of 28 day splitting tensile strength was found to be a constant.

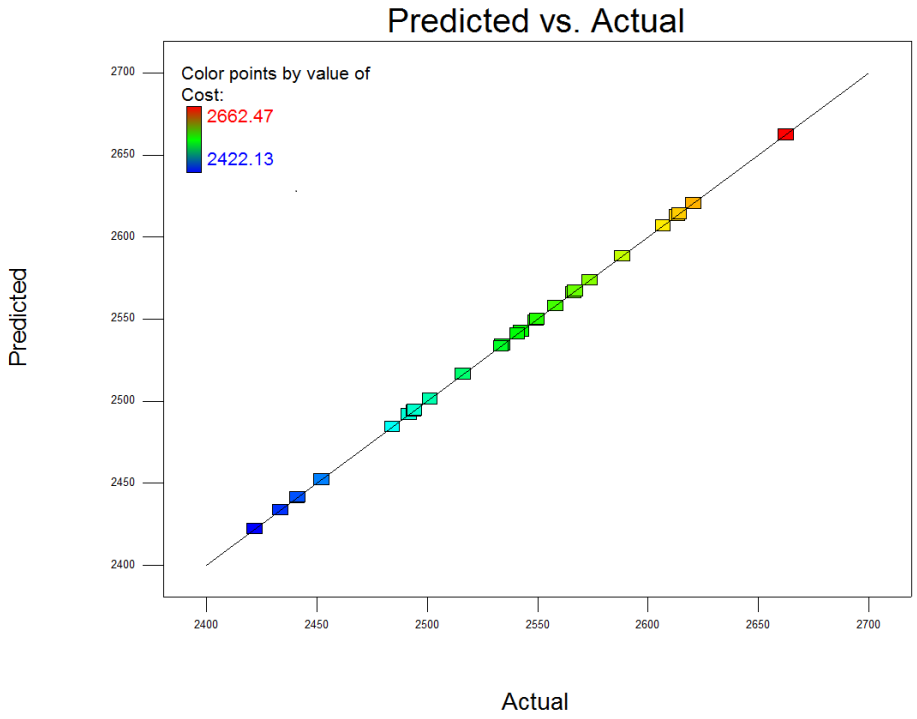

Figure 4.35. Cost plot of predicted vs. actual.

Therefore this model was set as "none" during the optimization procedure. The desirability functions described in Section 2.7.5 were used to perform the optimization. Two scenarios that can

cover the two classes of materials being sought in this study (HPC and VHPC/UHPC) have been considered. In scenario 1, the goal was to see whether it would be possible to produce an UHPC with the specified strengths using the mix ingredients and manufacturing procedures at hand regardless of cost and freezing/thawing durability. This scenario would provide a quick way to answer the purely technical question as to whether it is possible to make UHPC (with 28 day compressive strengths higher than 150 MPa) or VHPC (with 28 day compressive strengths higher than 100 MPa). The second scenario which includes cost and air content, was used to generate a cost effective concrete mix having a good resistance to freeze/thaw cycles within the realm of possible outcomes. The two scenarios are summarized in Table 4.16.

Table 4.16. Two optimization scenarios.

1st Scenario

	7 day Compressive Strength	28 day Compressive Strength	Air Content	Cost
Criteria	Max	Max	None	None
Importance	3	5	None	None

2nd Scenario

	7 day Compressive Strength	28 day Compressive Strength	Air Content	Cost
Criteria	Max	Max	Target (6%)	Min
Importance	3	4	3	5

The first optimization mainly focuses on the 28 day compressive strength and the second mainly focuses on minimum concrete cost. In the desirability function $D(X)$, each response can be assigned an importance relative to the other responses. Importance (r_i) varies from the lowest

importance of 1 to the highest importance of 5. If varying degrees of importance are assigned to the different responses, the desirability function is:

$$D = \left(d_1^{r_1} \times d_2^{r_2} \times \cdots \times d_n^{r_n}\right)^{\frac{1}{\sum r_i}} = \left(\prod_{i=1}^{n} d_i^{r_i}\right)^{\frac{1}{\sum r_i}} \tag{4.20}$$

where *n* is the number of responses in the optimization. If all the importance values are the same, the desirability function reduces to the normal form

$$D = \left(d_1 \times d_2 \times \cdots \times d_n\right)^{\frac{1}{n}} = \left(\prod_{i=1}^{n} d_i\right)^{\frac{1}{n}} \tag{4.21}$$

The desirability functions used in first and second scenario are shown in Figure 4.36 and Figure 4.37, respectively. In Figure 4.36 and Figure 4.37, the lowest level means zero in desirability function which indicates that one or more responses fall outside desirable limits, and the highest level means one in desirability function which represents the ideal case. After optimizations through the Design-Expert Version 9.0 software, the solutions are shown in Table 4-16.

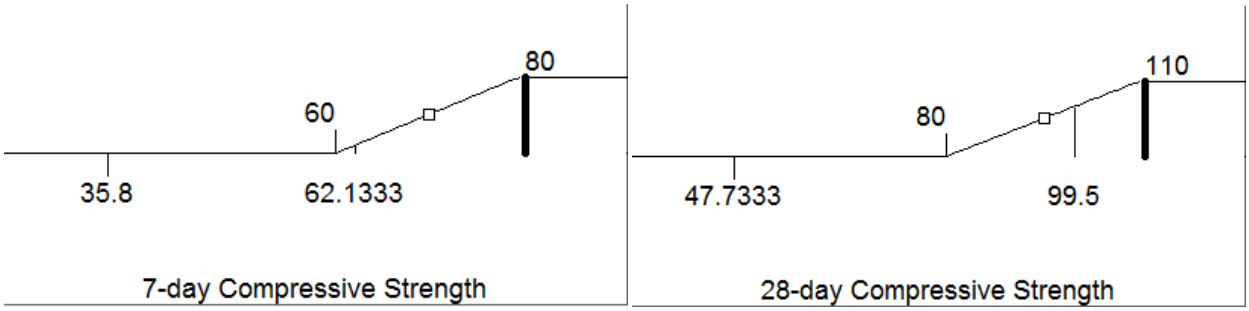

Figure 4.36. Desirability functions for first scenario.

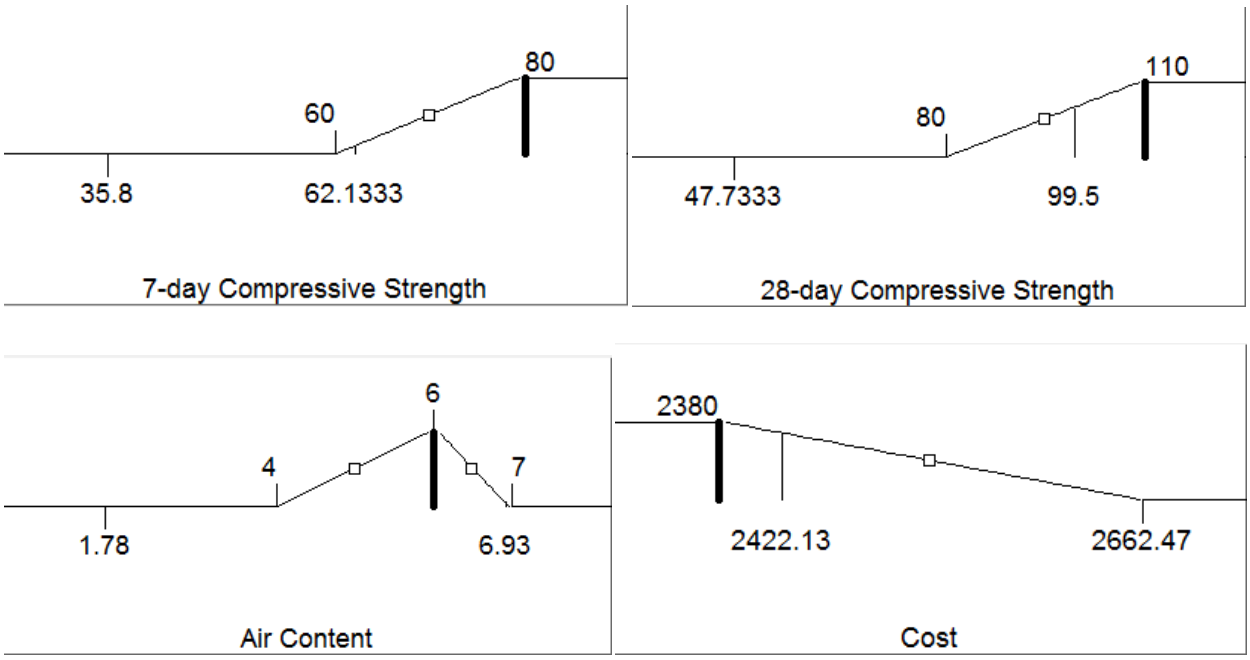

Figure 4.37. Desirability functions for second scenario.

Table 4.17. Optimization results.

1st Scenario				
Water	Silica Fume	Silica Flour	Sand	Steel Fiber
0.19	0.26	0.25	1.364	0.201
7 day Compressive Strength (MPa)		28 day Compressive Strength (MPa)		
67.3		102.4		

2nd Scenario				
Water	Silica Fume	Silica Flour	Sand	Steel Fiber
0.192	0.26	0.073	1.39	0.209
7 day Compressive Strength (MPa)	28 day Compressive Strength (MPa)	Air Content (%)		Cost (dollars/m^3)
60.3	82	6.00		2423.3

The splitting tensile strength can be estimated from the overall mean, i.e. 23.2 MPa. Since the flexural strength is larger than the splitting tensile strength, it can be deduced that the 28 day flexural strength is greater than 23.2 MPa which satisfies the goals for HPC and VHPC/UHPC.

The 28 day compressive strengths of 102.4 MPa and 82 MPa for the first and second scenarios are both over the 70 MPa mark for HPC. Hence, the goals for HPC were satisfied.

The result from second scenario gives a mixture which satisfies HPC specifications at the lowest cost. The goal of 28 day flexural strength of UHPC was also obtained. The optimized maximum 28 day compressive strength of 102.4 MPa is barely within the range of VHPC, and far below the minimum 150 MPa for UHPC. Given that compressive strength is not the only criterion for calling a concrete VHPC (a relatively low compressive strength with very high durability and low permeability is also considered to be VHPC), it would be possible to produce VHPC with relatively low compressive strengths. On the other hand, results of the analysis clearly show that it would be impossible to produce UHPC, with 28 day compressive strengths greater than 150 MPa, using the mix ingredients and fabrication processes adopted in this study.

Although the optimal design of the first scenario should be tested to verify whether a 28 day compressive strength of 102.4 MPa can be achieved or not, this task was not carried out. This is because that there is very little benefit to choose the optimal design over that of design #27. At about 2%, the strength gain is very marginal and within the experimental error of design #27 as shown in Figure 4.2.

5. Conclusions and Recommendations

5.1 Conclusions

The main research goal of this project was to determine whether HPC and VHPC/UHPC can be obtained using ingredients locally available in Saskatchewan with the following properties:

a) High Performance Concrete (HPC)

- Compressive strength at 28 day: 70 to 100 MPa
- Splitting tensile strength at 28 day: over 20 MPa
- Air-content in hardened concrete: 4 to 6%
- Flow cone spread values: 270 to 330 mm

b) Very/Ultra High Performance Concrete (VHPC/UHPC)

- Compressive strength at 28 day: over 100 MPa for VHPC, over 150 MPa for UHPC
- Splitting tensile strength at 28 day: over 20 MPa
- Air-content in hardened concrete: 4 to 6%
- Flow cone spread values: 270 to 330 mm

Basic theories and equations were presented on how to improve the compressive strength of concrete. Placing, consolidation and curing of concrete were also discussed. Several mixture proportioning methods were compared including ACI 211.1, ACI 363, De Larrard, and Mehta & Aitcin simplified methods. None of them was deemed to be suitable for this project because too many experiments would have been needed for the case of seven parameters considered in this study (water, cement, silica fume, silica flour, sand, steel fiber, and superplasticizer).

The response surface methodology (RSM) was introduced and adopted in this project because it can deal with multiple factor experimental designs, analysis of model fitting, and optimization of responses simultaneously. The number of experiments designed with RSM can be relatively low, which is economical and time saving for the experimenter.

The goal for developing a HPC material with the specified properties was successful. The optimal mix was obtained through the optimization of multiple responses. This optimization includes minimum cost, maximum 7 and 28 day compressive strength and targeting 6% of air content of hardened concrete. The optimal mix had the following properties with the cost of $\$2423.3/m^3$:

- Compressive strength at 28 day:	82 MPa	(specs: 70 to 100 MPa)
- Splitting tensile strength at 28 day:	23 MPa	(specs: over 20 MPa)
- Air-content in hardened concrete:	6%	(specs: 4 to 6%)
- Flow cone spread values:	274 mm	(specs: 270 to 330 mm)

The goal for making a VHPC material with the specified 28 day compressive strength, 28 day splitting tensile strength and flow cone spread value was successful through the optimization of maximum 7 and 28 day compressive strength regardless of air content and cost. The optimal mix had the following properties:

- Compressive strength at 28 day:	102.4 MPa	(specs: over 100 MPa)
- Splitting tensile strength at 28 day:	23 MPa	(specs: over 20 MPa)
- Flow cone spread values:	274 mm	(specs: 270 to 330 mm)

Results of the analysis clearly show that it would be impossible to produce UHPC, with 28 day compressive strengths greater than 150 MPa, using the mix ingredients and fabrication processes adopted in this study.

From these conclusions, it was observed that the highest optimization result for 28 day compressive strength was 102.4 MPa. It was concluded that it would be very difficult to increase this strength using the current material and experimental methods. As a result, different materials or new methods would have to be investigated for making UHPC, this will be introduced in section

5.2. Also, it was concluded based on observations from this project that a high energy mixer should be used to improve results; more mixing energy would help to disperse all of the components, potentially increasing the workability.

5.2 Recommendations for Future Work

Given that special fabrication processes, such as curing techniques where steam and/or stresses are applied, can dramatically improve the strength of concrete, it is recommended to try such techniques in future studies to see if it is possible to produce high strength VHPC and UHPC using materials locally available in Saskatchewan.

Durability tests, including the carbonation depth test (DE LA RILEM 1988), chloride ion penetration test (ASTM C1202-12 2012), and abrasion resistance test (ASTM C944 / C944M-12 2012) may be conducted in the future to evaluate the durability of mixtures.

Being a general method, the RSM approach is not limited to the materials used in this project in searching for HPC and VHPC/UHPC mixtures. Hence, other materials may also be tested using RSM such as metakaolin instead of silica fume. Other researchers were able to make UHPC using metakaolin as substitution of silica fume (Tafraoui et al. 2009).

Besides the RSM method, material selection is also critical for proportioning HPC and VHPC/UHPC. Compaction is the key to HPC and VHPC/UHPC. Future work can focus on the issue of optimizing the packing density of concrete ingredients. The larger the packing density, the higher the compressive strength. Procedures of how to optimize the packing density of the various particles of different grain sizes have been presented in the literature (Naaman and Wille 2010). In this scenario, the grain size distribution (GSD) of sand becomes more important. Since special GSD sands are not readily available for purchase, and may have to be specially ordered, searching

for a sand with an optimized GSD could lead to dramatic improvements in the manufacturing of high performance concrete.

List of References

ACI Committee 211 (1991). "Standard Practice for Selecting Proportions for Normal, Heavyweight and Mass Concrete." American Concrete Institute, Farmington Hills, MI.

ACI Committee 363 (1992). "State-of-the-Art Report on High Strength Concrete." American Concrete Institute, Farmington Hills, MI.

Acker, P., and Behloul, M. (2004). "Ductal® Technology: A Large Spectrum of Properties, A Wide Range of Applications." FIB Symposium, Avignon, France.

Aïtcin, P. C. (1989). "From gigapascals to nanometres: Advances in cement manufacture and use." *Proceedings of the Engineering Foundation Conference, Missouri, 1988, New York: Engineering Foundation*, 105-130.

Aïtcin, P. C. (2004). *High-Performance Concrete*, Routledge, New York.

Aïtcin, P. C., and Mehta, P. K. (1990). "Effect of Coarse Aggregate Characteristics on Mechanical Properties of High-Strength Concrete." *ACI Materials Journal*, 87(2), 103-107.

ASTM C230 / C230M-14 (2014). "Standard Specification for Flow Table for Use in Tests of Hydraulic Cement." ASTM International, West Conshohocken, PA.

ASTM C231 / C231M-14 (2014). "Standard Test Method for Air Content of Freshly Mixed Concrete by the Pressure Method." ASTM International, West Conshohocken, PA.

ASTM C496 / C496M-11 (2004). "Standard Test Method for Splitting Tensile Strength of Cylindrical Concrete Specimens." ASTM International, West Conshohocken, PA.

ASTM C944 / C944M-12 (2012). "Standard Test Method for Abrasion Resistance of Concrete or Mortar Surfaces by the Rotating-Cutter Method." ASTM International, West Conshohocken, PA.

ASTM C1202-12 (2012). "Standard Test Method for Electrical Indication of Concrete's Ability to Resist Chloride Ion Penetration." ASTM International, West Conshohocken, PA.

Bache, H. H. (1981). "Densified Cement/Ultra-Fine Particle-Based Materials." *Second International Conference on Superplasticiers in Concrete*, Aalborg Cement, Ottawa, Canada.

Bickley, J. A., and Fung, R. (2006). "Optimizing the Economics of High Performance Concrete." *The 2006 National Concrete Bridge Conference*Reno Nevada, United States of America.

Box, G. E. P. (1952). "MULTI-FACTOR DESIGNS OF FIRST ORDER." *Biometrika*, 39, 49-57.

Box, G. E. P., and Hunter, J. S. (1957). "Multi-Factor Experimental Designs for Exploring Response Surfaces." *The Annals of Mathematical Statistics*, 28(1), 195-241.

Box, G. E. P., Hunter, J. S., and Hunter, W. G. (2005). *Statistics for Experimenters: Design, Innovation, and Discovery, Second Edition*, John Wiley & Sons, Hoboken, New Jersey, United States of America.

Box, G. E. P., and Wilson, K. B. (1951). "On the Experimental Attainment of Optimum Conditions." *Journal of the Royal Statistical Society. Series B (Methodological)*, 13(1), 1-45.

Brühwiler, E., and Denarié, E. (2008). "Rehabilitation of concrete structures using Ultra-High Performance Fibre Reinforced Concrete." *UHPC-2008: The Second International Symposium on Ultra High Performance Concrete*Kassel, Germany.

Chatterji, S., and Gudmundsson, H. (1977). "Characterization of entrained air bubble systems in concretes by means of an image analysing microscope." *Cement and Concrete Research*, 7(4), 423-428.

DE LA RILEM, R. (1988). "CPC-18 Measurement of hardened concrete carbonation depth."

De Larrard, F. (1990). "A Method for Proportioning High-Strength Concrete Mixtures." *Cement, concrete and aggregates*, 12(1), 47-52.

De Larrard, F., and Belloc, A. (1997). "The Influence of Aggregate on the Compressive Strength of Normal and High-Strength Concrete." *ACI Materials Journal*, 94(5), 417-426.

del Castillo, E. (2007). *Process Optimization: A Statistical Approach*, Springer US.

Derringer, G. C., and Suich, R. (1980). "Simultaneous Optimization of Several Response Variables." *Journal of Quality Technology*, 12(4), 214-219.

Féret, R. (1892). "Sur la compacité des mortiers hydrauliques. Mémoires et documents relatifs àl'art des constructions et au service de l'ingénieur." *Annales des Ponts et Chaussées*, 4, 5-161.

FHWA (2006). "Material Property Characterization of Ultra-High Performance Concrete."

FHWA (2011). "Ultra-High Performance Concrete."

FHWA (2013). "Ultra-High Performance Concrete: A State-of-the-Art Report for the Bridge Community."

Freedman, S. (1971). "High-Strength Concrete." *Modern Concrete*, 34, 15-22.

Garas, V. Y. (2009). "MULTI-SCALE INVESTIGATION OF TENSILE CREEP OF ULTRAHIGH PERFORMANCE CONCRETE FOR BRIDGE APPLICATIONS " Doctor of Philosophy, Georgia Institute of Technology, Atlanta, GA.

Graybeal, B. A. (2005). "CHARACTERIZATION OF THE BEHAVIOR OF ULTRA-HIGH PERFORMANCE CONCRETE." Doctor of Philosophy, University of Maryland.

Graybeal, B. A. (2014). "Ultra-high-performance concrete connections for precast concrete bridge decks." *PCI Journal*, 59(4), 48-62.

Habel, K., Charron, J.-P., Braike, S., Hooton, R. D., Gauvreau, P., and Massicotte, B. (2008). "Ultra-high performance fibre reinforced concrete mix design in central Canada." *Canadian Journal of Civil Engineering*, 35(2), 217-224.

Harrington, E. (1965). "The desirability function." *Industrial quality control*, 21(10), 494-498.

Hartwell, D. R. (2011). "Laboratory testing of Ultra High Performance Concrete deck joints for use in accelerated bridge construction." Iowa State University.

Holschemacher, K., Weiße, D., and Klotz, S. (2005). "Bond of reinforcement in ultra high-strength concrete." *Special Publication*, 228, 513-528.

Jana, D. "A Round Robin Test on Measurements of Air Void Parameters in Hardened Concrete by Various Automated Image Analyses and ASTM C 457 Methods." *Proc., Proceedings of the 29th Conference on Cement Microscopy, International Cement Microscopy Association*.

Kosmatka, H., Kerkhoff, B., and Panarese, W. (2003). *Design and Control of Concrete Mixtures FOURTEENTH EDITION*, Portland Cement Association, United States of America.

Kumar Mehta, P., and Aitcin, P.-C. (1990). "Principles underlying production of high-performance concrete." *Cement, concrete and aggregates*, 12(2), 70-78.

Laurencot, J., Pleau, R., and Pigeon, M. "The microscopical determination of air voids characteristics in hardened concrete: Development of an automatic system using image analysis techniques applied to micro-computers." *Proc., Proceedings of 14th International Conference on Cement Microscopy*.

Lawler, J. S., Connolly, J. D., Krauss, P. D., and Tracy, S. L. (2007). "Guidelines for Concrete Mixtures Containing Supplementary Cementitious Materials to Enhance Durability of Bridge Decks." *NCHRP Report 566*.

Mehta, P. K., and Aïtcin, P. C. (1990). "Principles Underlying Production of High-Performance Concrete." *Cement, Concrete and Aggregates*, 12(2), 70.

Melis, L. M., Meyer, A. H., and Fowler, D. W. (1985). "AN EVALUATION OF TENSILE STRENGTH TESTING." University of Texas at Austin, Austin, TX.

Montgomery, D. C. (2013). *Design and Analysis of Experiments, 8th Edition*, John Wiley & Sons, Inc.

Muñoz, C., and Ángel, M. (2012). "Compatibility of ultra high performance concrete as repair material : bond characterization with concrete under different loading scenarios." Master's Thesis, Michigan Technological University.

Naaman, A., and Wille, K. "Some correlation between high packing density, ultra-high performance, flow ability, and fiber reinforcement of a concrete matrix." *Proc., BAC2010—2nd Iberian congress on self compacting concrete, University of Minho—Guimaraes, Portugal, July*, 1-2.

Neville, A. (1996). "Properties of Concrete, Fourth and Final Edition Standards." Pearson, Prentice Hall.

Orange, G., Dugat, J., and Acker, P. (1999). "A new generation of UHP concrete: DUCTAL® damage resistance and micromechanical analysis." *Procedings of the 3rd Internat RILEM Workshop, HPFRCC3*, 101-111.

Perry, V. H., and Zakariasen, D. (2004). "First Use of Ultra-High Performance Concrete for an Innovative Train Station Canopy." *Concrete Technology Today*, 25(2), 2-8.

Peterson, K., Carlson, J., and Anzalone, J. (2012). "Bubble Counter, http://wiki.misti.mtu.edu/index.php?title=BubbleCounter:Index."

Peterson, K. W., Swartz, R. A., Sutter, L. L., and Van Dam, T. J. (2001). "Hardened concrete air void analysis with a flatbed scanner." *Transportation Research Record: Journal of the Transportation Research Board*, 1775(1), 36-43.

Popovics, S. (1998). *Strength and Related Properties of Concrete: A Quantitative Approach*, John Wiley & Sons, Canada.

Reda, M., Shrive, N., and Gillott, J. (1999). "Microstructural investigation of innovative UHPC." *Cement and Concrete Research*, 29(3), 323-329.

ReliaSoft (2015). "Experiment Design & Analysis Reference."

Roberts, L., and Scali, M. "Factors affecting image analysis for measurement of air content in hardened concrete." *Proc., Proceedings of International Conference on Cement Microscopy*, 402-419.

Schmidt, M., and Fehling, E. (2005). "Ultra-high-performance concrete: research, development and application in Europe." *ACI Special publication*, 228, 51-78.

Shah, S. P., and Weiss, W. J. (1998). "Ultra high performance concrete: a look to the future." *International Journal of Civil and Structural Engineering*.

Shann, S. V. (2012). "Application of ultra high performance concrete (UHPC) as a thin-bonded overlay for concrete bridge decks." Master's Thesis, Michigan Technological University.

Simon, M., Lagergren, E., and Wathne, L. "Optimizing high-performance concrete mixtures using statistical response surface methods." *Proc., Proceedings of the 5th International Symposium on Utilization of High Strength/High-Performance Concrete, Norwegian Concrete Association, Oslo, Norway*, 1311-1321.

Simon, M. J. (2003). "Concrete Mixture Optimization Using Statistical Methods: Final Report." *FHWA-RD-03-060*.

Simon, M. J., Lagergren, E. S., and Snyder, K. A. "concrete mixture optimization using statistical mixture desighn methods." *Proc., High Performance Concrete International Symposium. Proceedings*, PCI/FHWA, 230-244.

Simon, M. J., Snyder, K. A., and Frohnsdorff, G. "Advances in concrete mixture optimisation." *Proc., Concrete Durability and Repair Technology Conference*, Thomas Telford Publishing, 21-32.

Stat-Ease (2014). "Design-Expert Software Version 9."

Tafraoui, A., Escadeillas, G., Lebaili, S., and Vidal, T. (2009). "Metakaolin in the formulation of UHPC." *Construction and Building Materials*, 23(2), 669-674.

Tang, M.-C. (2004). "High performance concrete - past, present and future." *Proceedings of the International Symposium on Ultra High Performance Concrete. Kassel, Germany*, 3-9.

Tayeh, B. A., Bakar, B. H. A., Johari, M. A. M., and Voo, Y. L. (2013). "Utilization of Ultra-high Performance Fibre Concrete (UHPFC) for Rehabilitation – A Review." *Procedia Engineering*, 54, 525-538.

Vandamme, M., and Ulm, F. J. (2009). "Nanogranular origin of concrete creep." *Proceedings of the National Academy of Sciences*, 106(26), 10552-10557.

Wille, K., Naaman, A. E., and Parra-Montesinos, G. J. (2011). "Ultra-High Performance Concrete with Compressive Strength Exceeding 150 MPa (22 ksi): A Simpler Way." *ACI Materials Journal*, 108(1).

Yazici, H. (2007). "The effect of curing conditions on compressive strength of ultra high strength concrete with high volume mineral admixtures." *Building and Environment*, 42(5), 2083-2089.

Yazıcı, H., Yardımcı, M. Y., Aydın, S., and Karabulut, A. Ş. (2009). "Mechanical properties of reactive powder concrete containing mineral admixtures under different curing regimes." *Construction and building materials*, 23(3), 1223-1231.

Zhang, Z., Ansari, F., and Vitillo, N. (2005). "Automated determination of entrained air-void parameters in hardened concrete." *ACI materials journal*, 102(1).